Electronic Supplementary Information for:

B–B Bond Activation and NHC Ring-expansion Reactions of Diboron(4) Compounds, and Accurate Molecular Structures of $B_2(NMe_2)_4$, B_2eg_2, B_2neop_2 and B_2pin_2

Martin Eck,[a] Sabrina Würtemberger-Pietsch,[a] Antonius Eichhorn,[a] Johannes H. J. Berthel,[a] Rüdiger Bertermann,[a] Ursula Paul,[a] Heidi Schneider,[a] Alexandra Friedrich,[a] Christian Kleeberg,*[b] Udo Radius,*[a] and Todd B. Marder*[a]

[a]*Institut für Anorganische Chemie and Institute for Sustainable Chemistry & Catalysis with Boron*
Julius-Maximilians-Universität Würzburg
Am Hubland, 97074 Würzburg (Germany)
E-mail: u.radius@uni-wuerzburg.de, todd.marder@uni-wuerzburg.de

[b]*Institut für Anorganische und Analytische Chemie*
Technische Universität Carolo-Wilhelmina zu Braunschweig
Hagenring 30, 38106 Braunschweig (Germany)
E-mail: ch.kleeberg@tu-braunschweig.de

Contents:

1 NMR spectroscopic data and HRMS data

1.1 Solution NMR spectra of compound **3** Bis(ethylene glycolato)diboron (B_2eg_2)

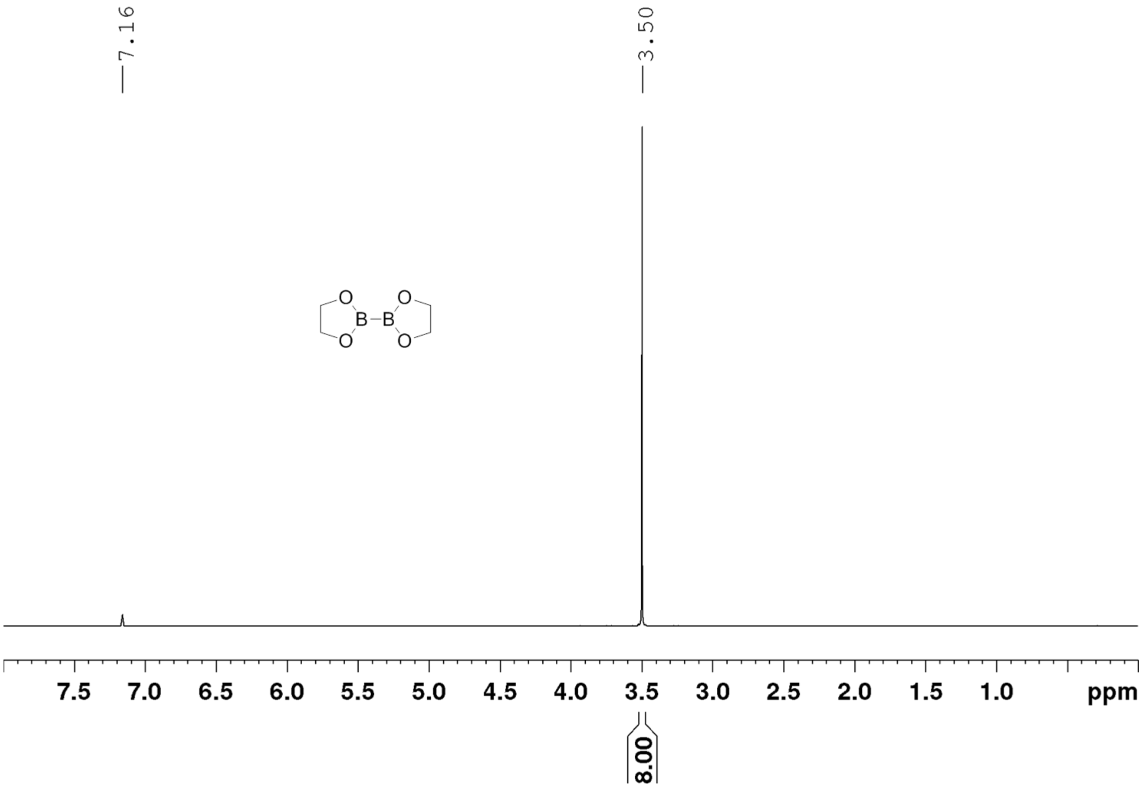

Figure S1: ^{1}H NMR spectrum of compound **3** in C_6D_6 (300 MHz, 25 °C).

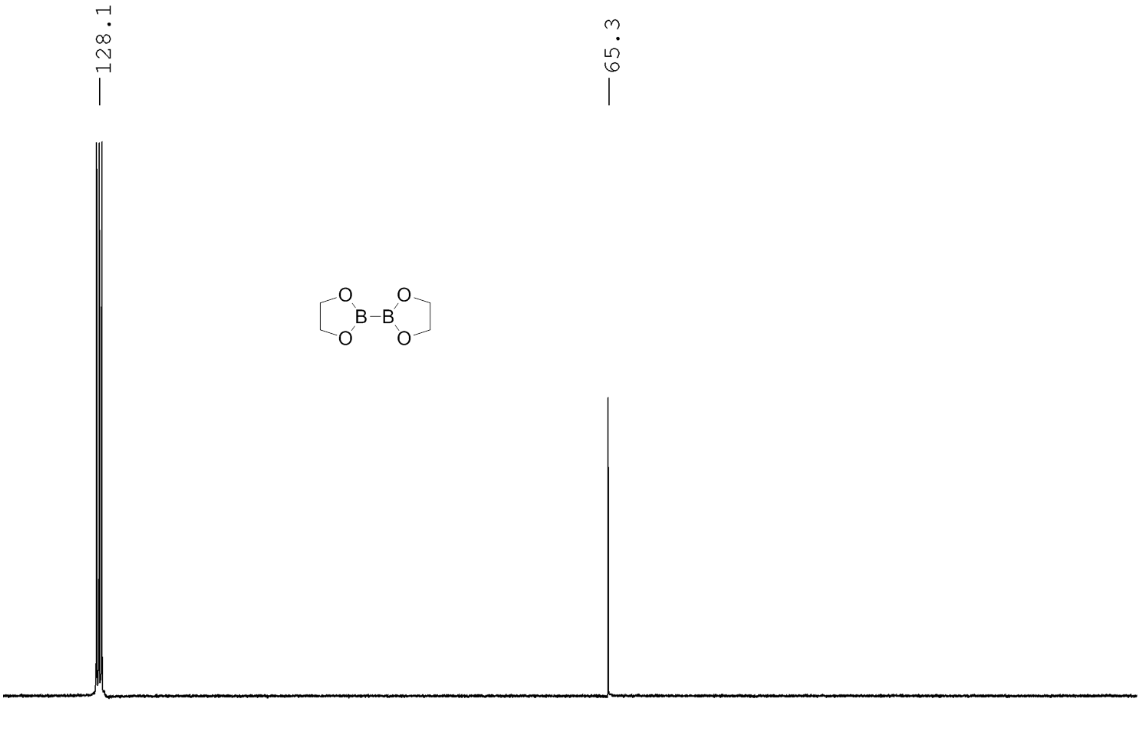

Figure S2: $^{13}C\{^1H\}$ NMR spectrum of compound **3** in C_6D_6 (75 MHz, 25 °C).

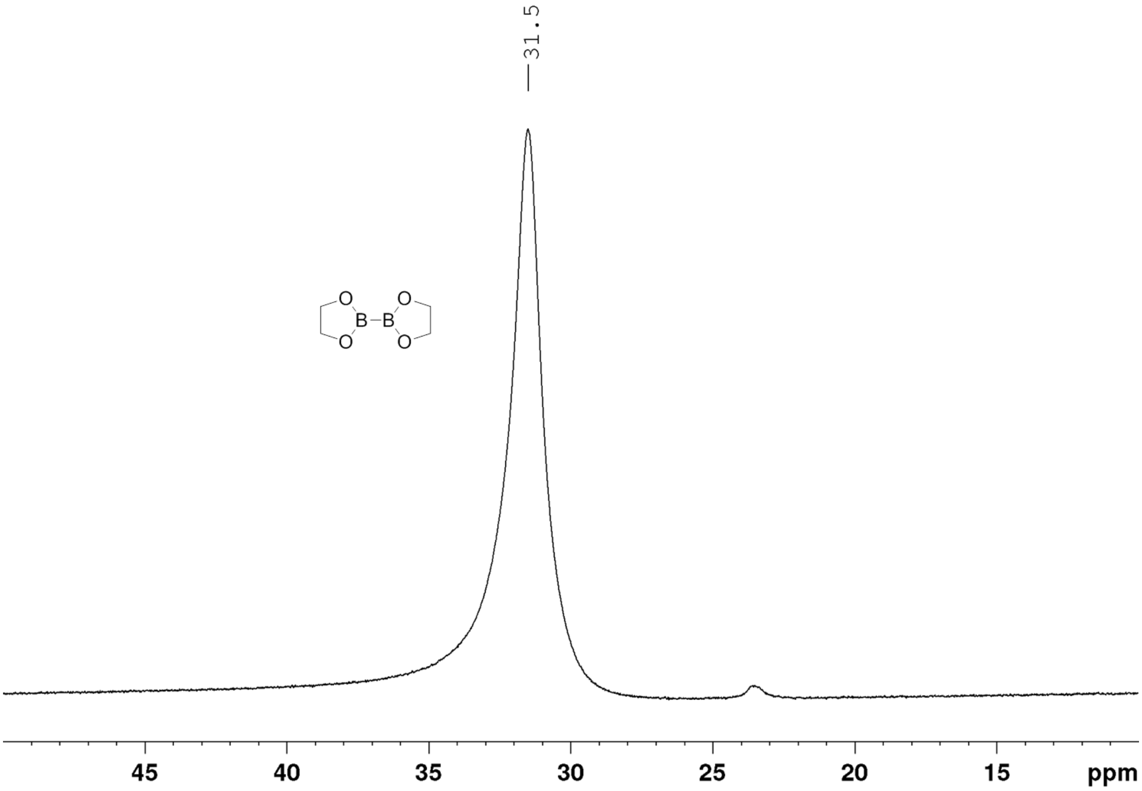

Figure S3: $^{11}\mathrm{B}\{^{1}\mathrm{H}\}$ NMR spectrum of compound **3** in C_6D_6 (96 MHz, 25 °C).

1.2 Solution NMR spectra of compound **6** mono-NHC adduct B_2pin_2•*i*Pr_2Im

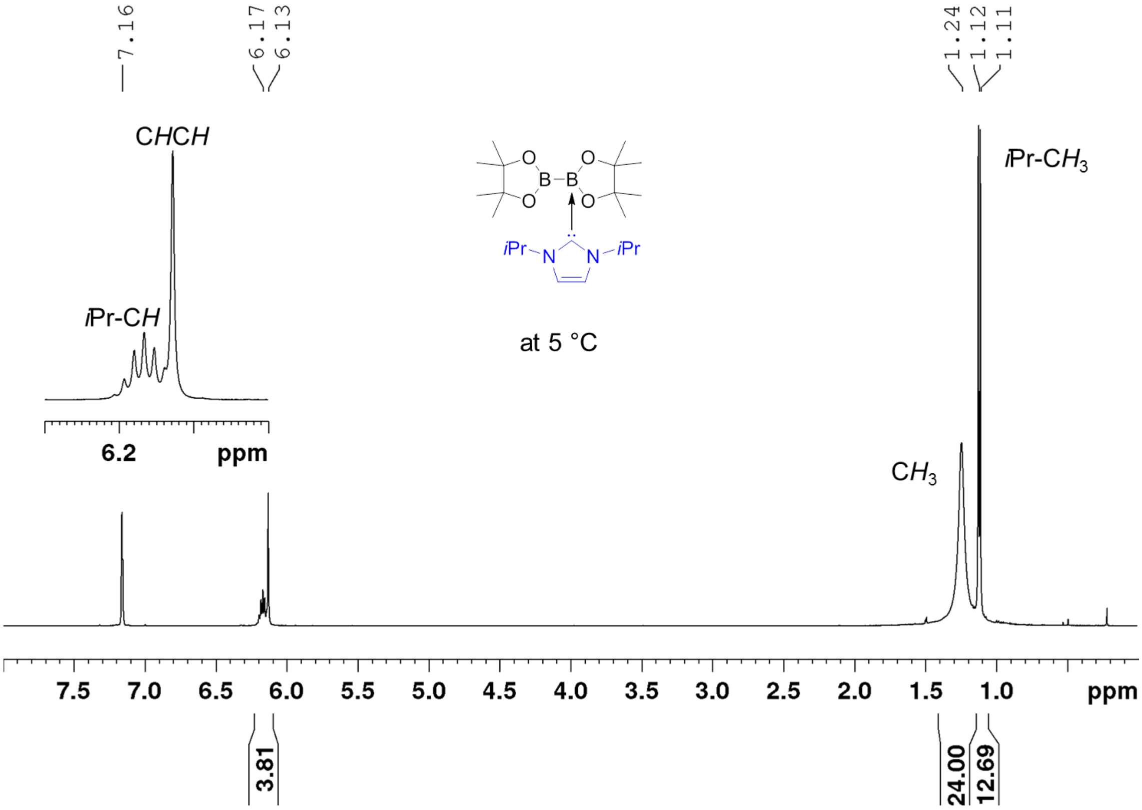

Figure S4: ^1H NMR spectrum of compound **6** in C_6D_6 (500 MHz, 5 °C).

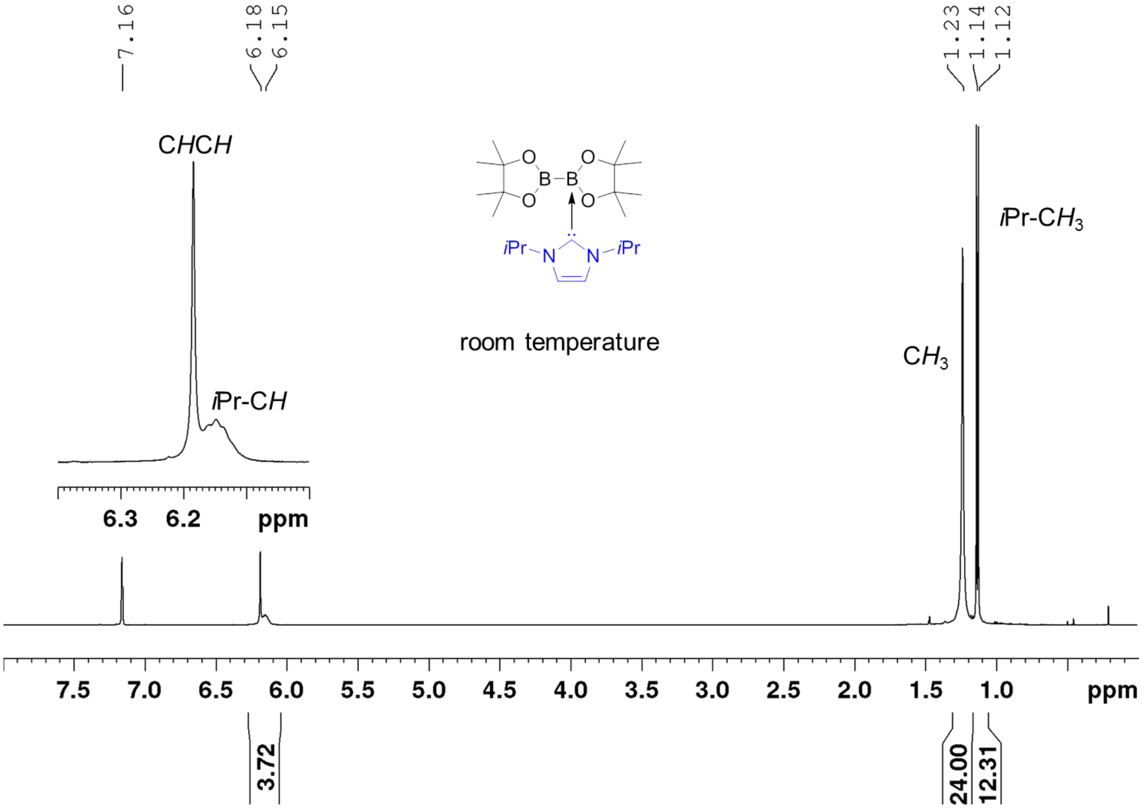

Figure S5: ^1H NMR spectrum of compound **6** in C_6D_6 (500 MHz, 25 °C).

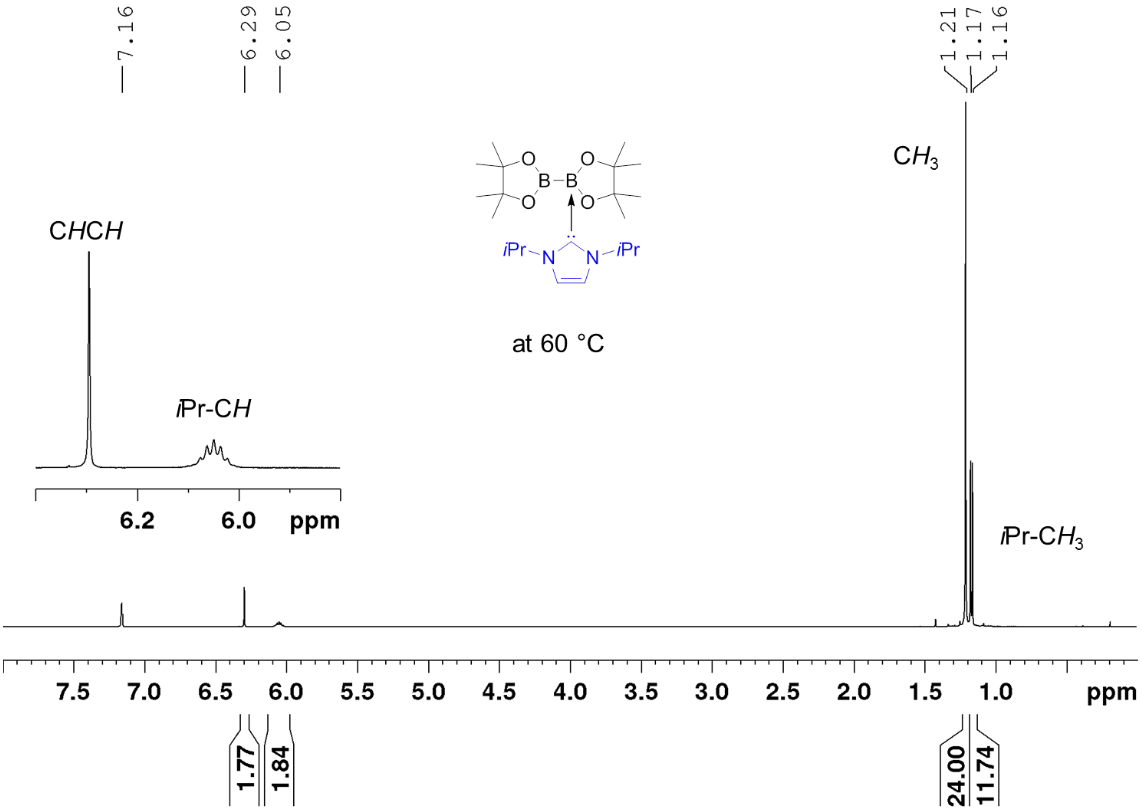

Figure S6: ^{1}H NMR spectrum of compound **6** in C_6D_6 (500 MHz, 60 °C).

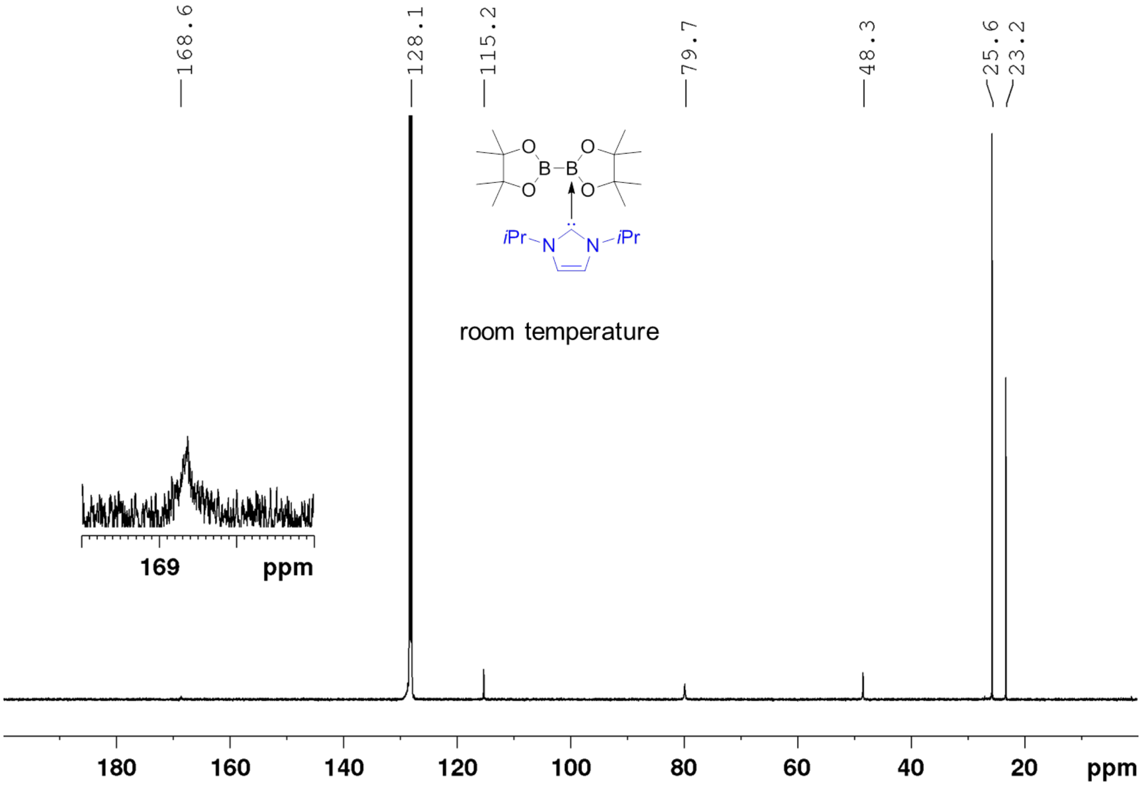

Figure S7: $^{13}C\{^1H\}$ NMR spectrum of compound **6** in C_6D_6 (125 MHz, 25 °C).

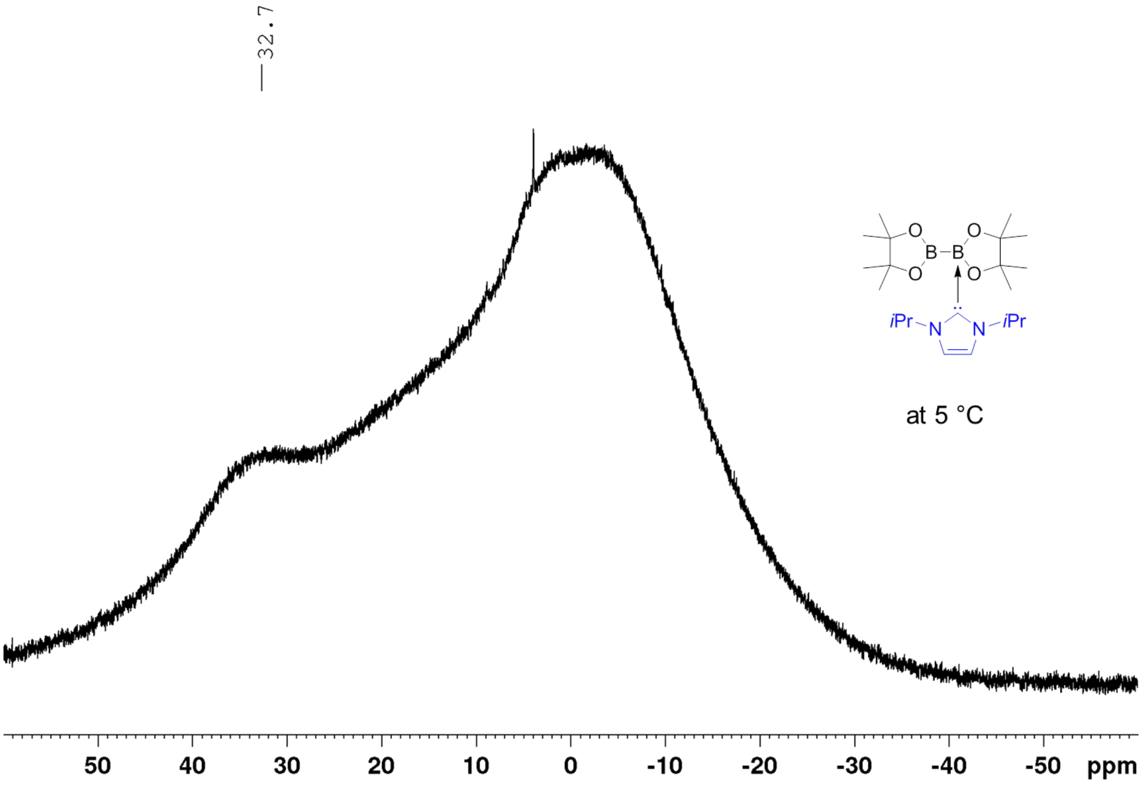

Figure S8: $^{11}B\{^{1}H\}$ NMR spectrum of compound **6** in C_6D_6 (160 MHz, 5 °C).

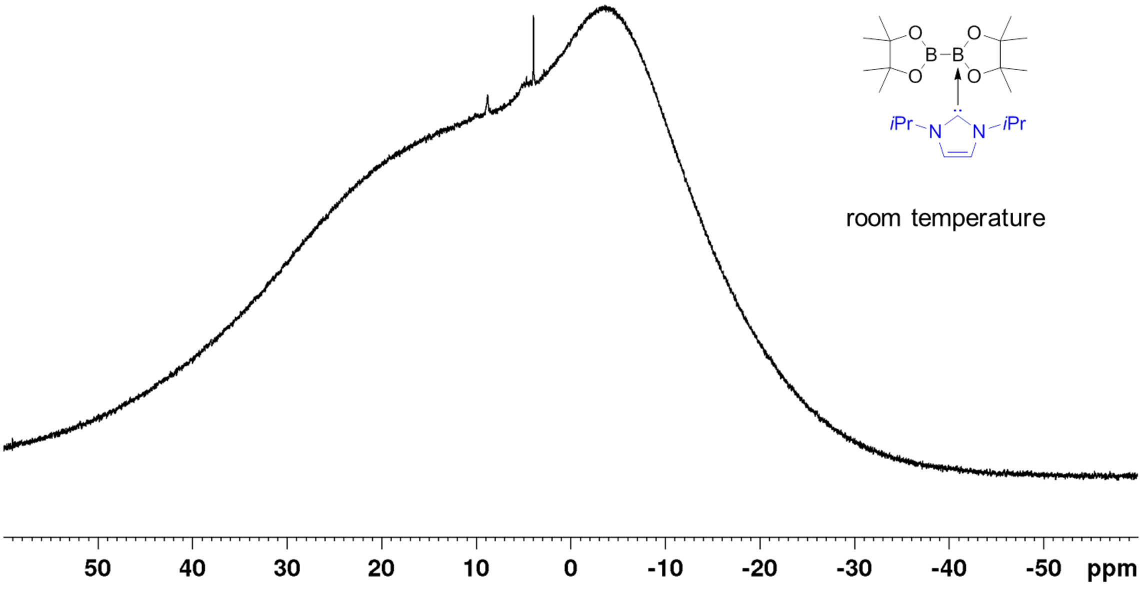

Figure S9: $^{11}B\{^{1}H\}$ NMR spectrum of compound **6** in C_6D_6 (160 MHz, 25 °C).

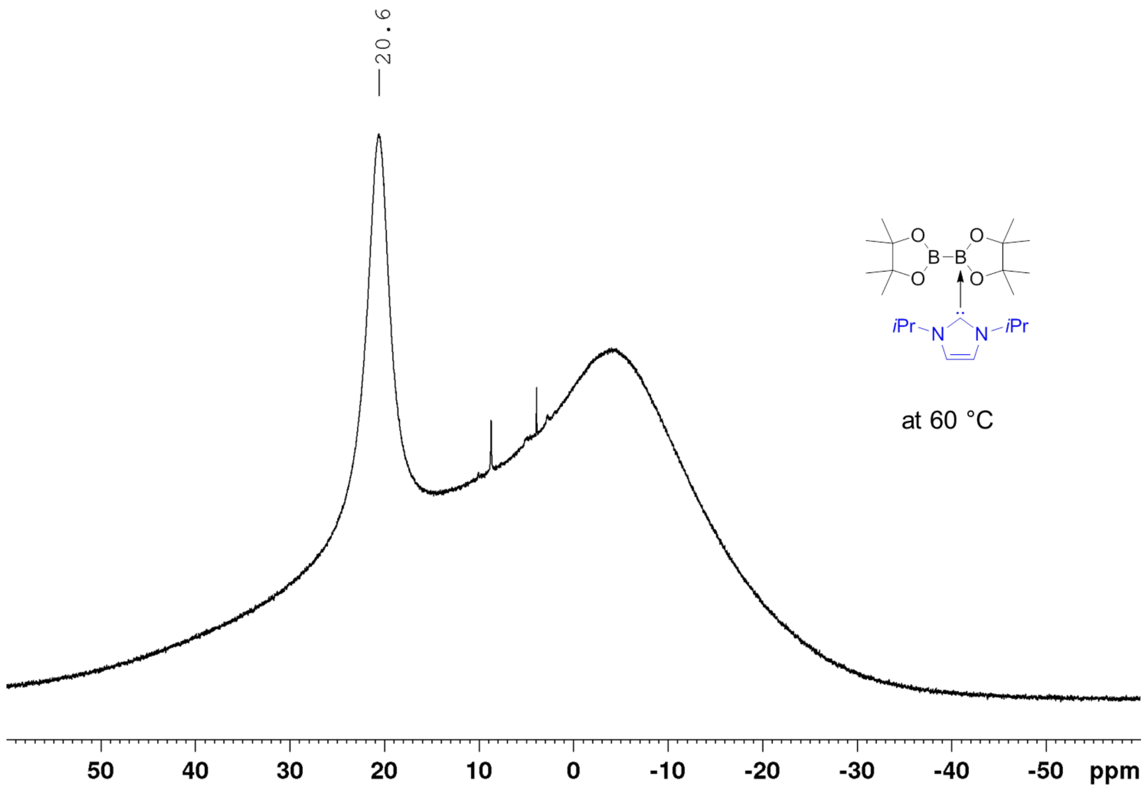

Figure S10: ^{11}B{^{1}H} NMR spectrum of compound **6** in C_6D_6 (160 MHz, 60 °C).

1.3 Solution NMR spectra of compound **7a** mono-NHC adduct B_2cat_2•$Dipp_2Im$

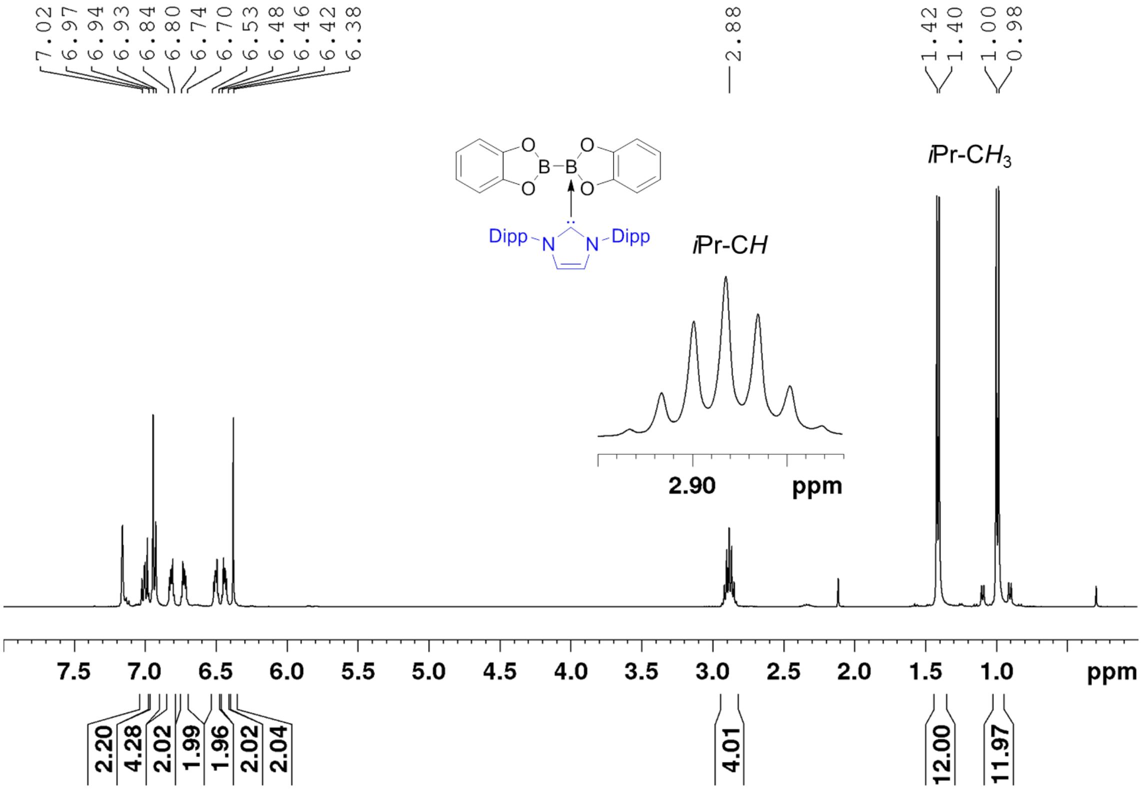

Figure S11: ^{1}H NMR spectrum of compound **7a** in C_6D_6 (400 MHz, 25 °C).

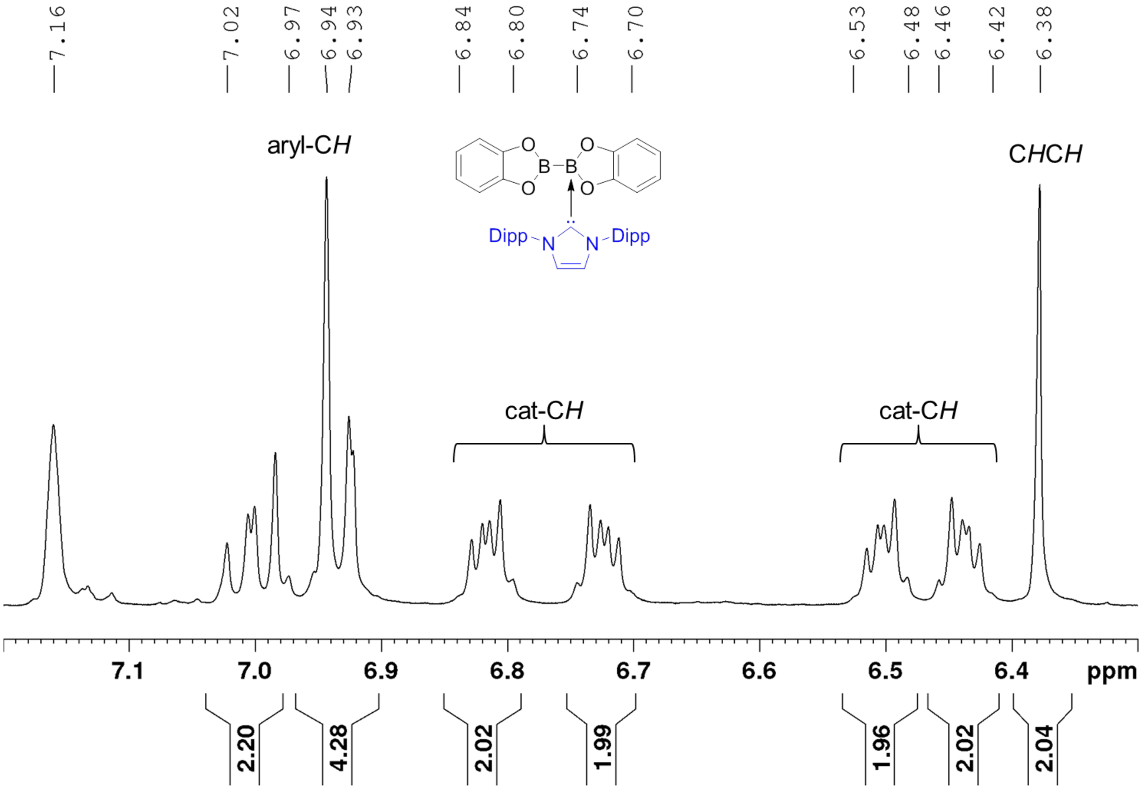

Figure S12: ^{1}H NMR spectrum of compound **7a** in C_6D_6 (400 MHz, 25 °C).

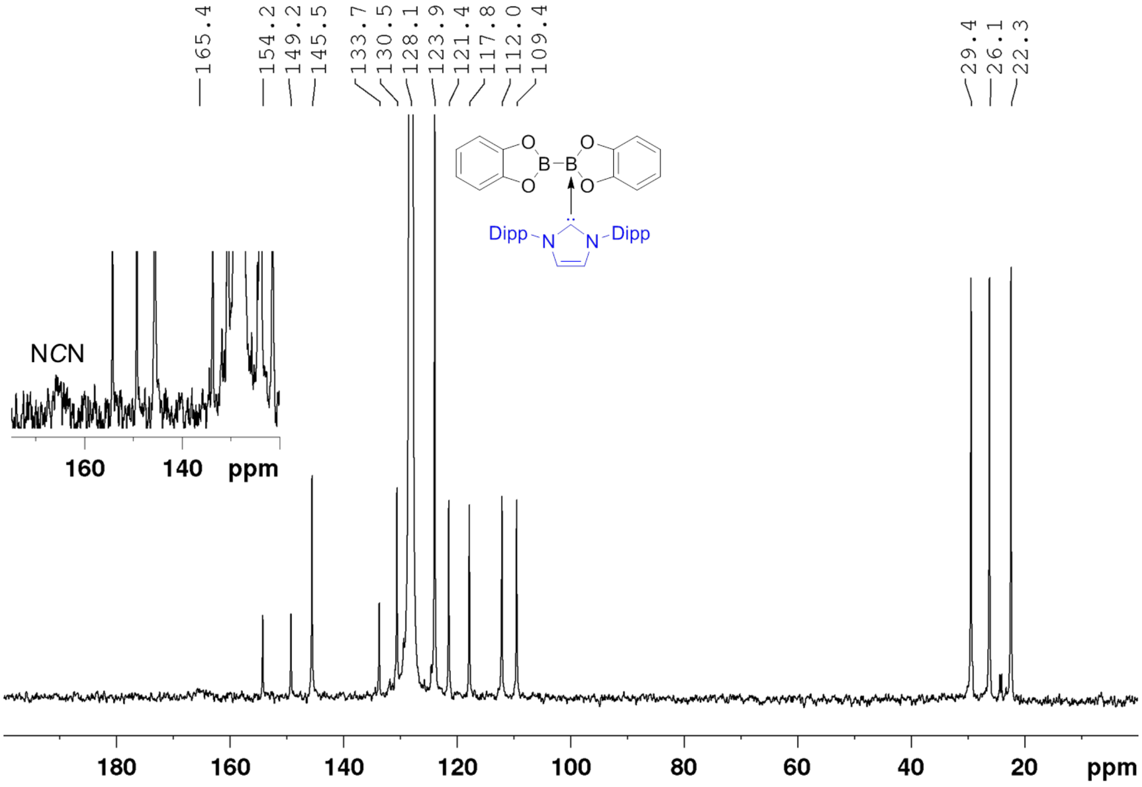

Figure S13: $^{13}C\{^{1}H\}$ NMR spectrum of compound **7a** in C_6D_6 (101 MHz, 25 °C).

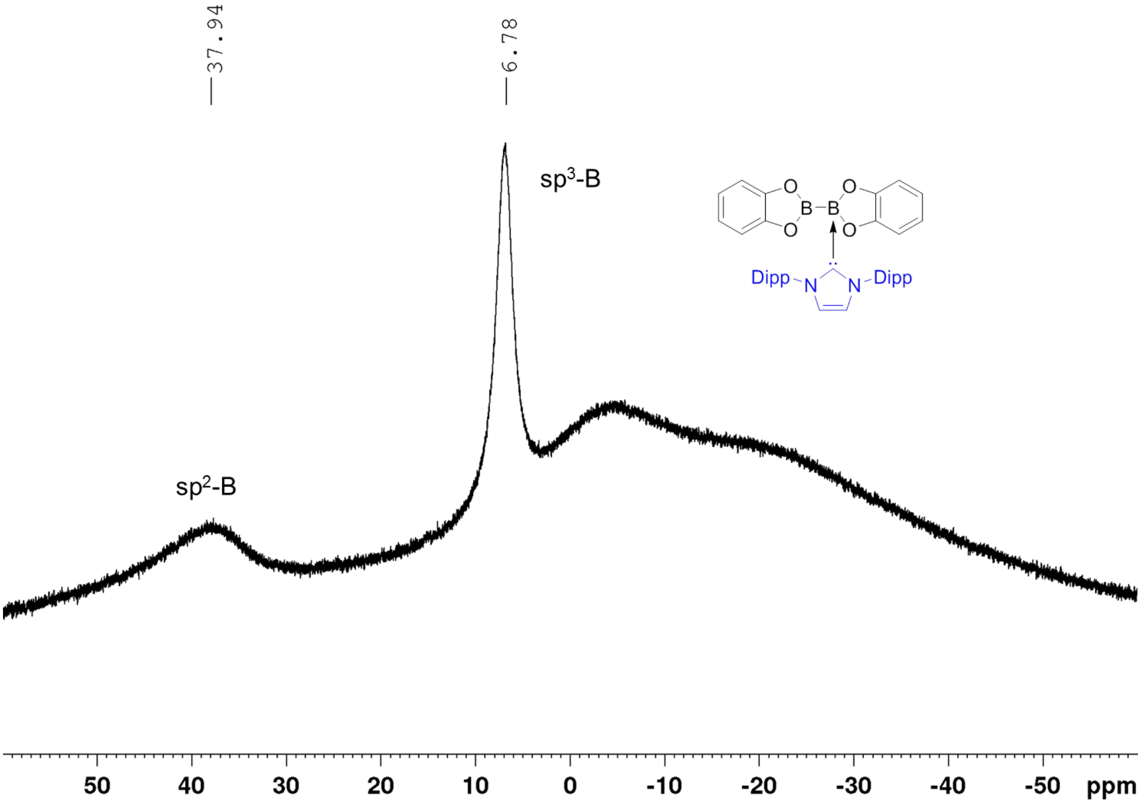

Figure S14: $^{11}B\{^{1}H\}$ NMR spectrum of compound **7a** in C_6D_6 (128 MHz, 25 °C).

1.4 Solution NMR spectra of compound **7b** mono-NHC adduct B_2cat_2•$Dipp_2SIm$

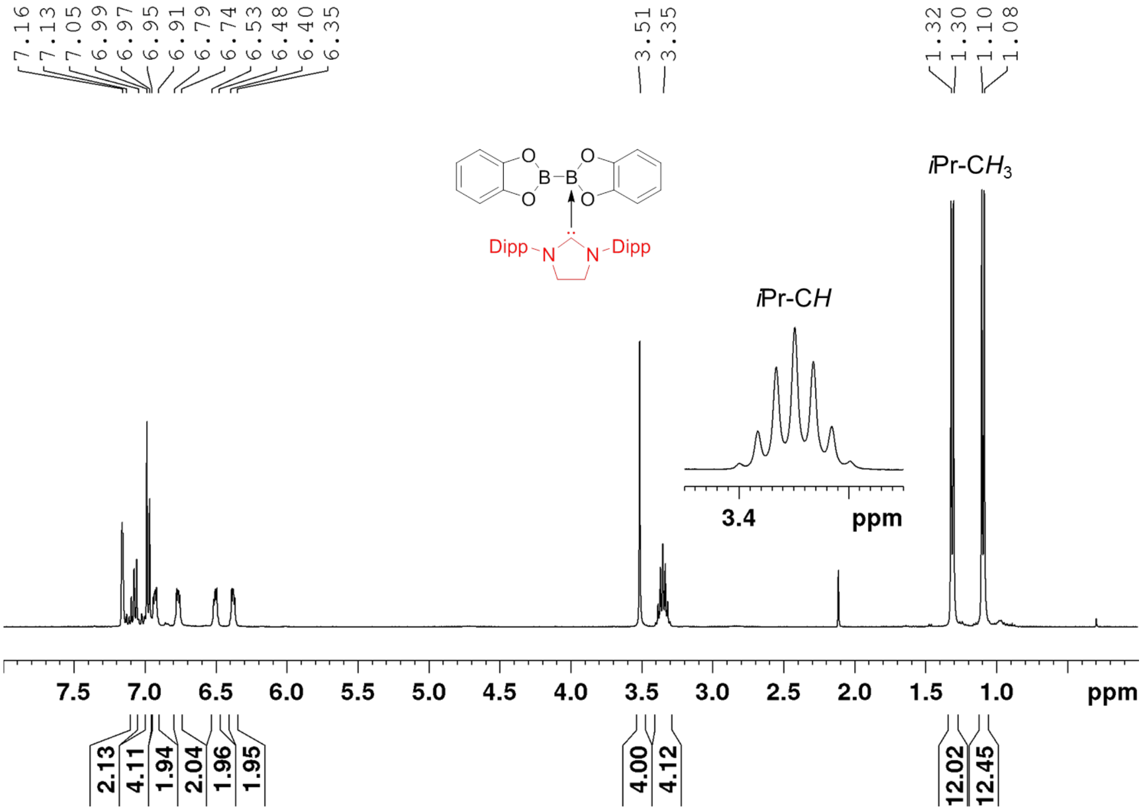

Figure S15: ^{1}H NMR spectrum of compound **7b** in C_6D_6 (400 MHz, 25 °C).

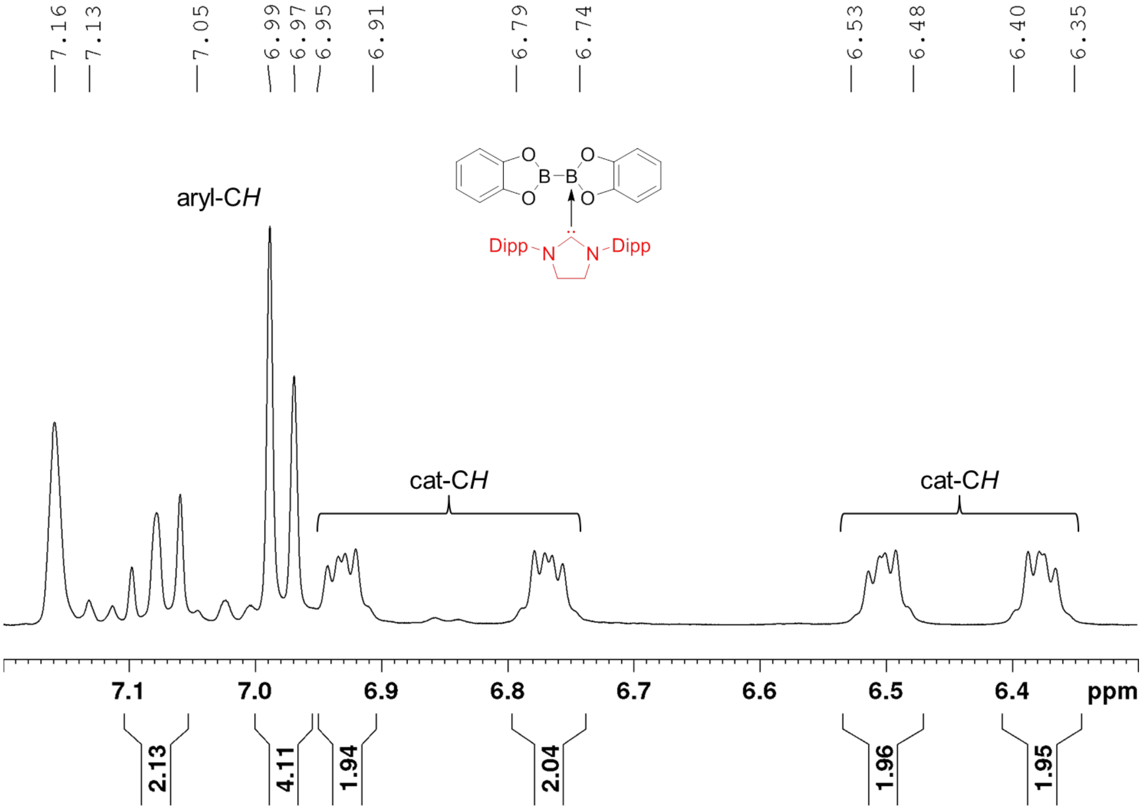

Figure S16: ^{1}H NMR spectrum of compound **7b** in C_6D_6 (400 MHz, 25 °C).

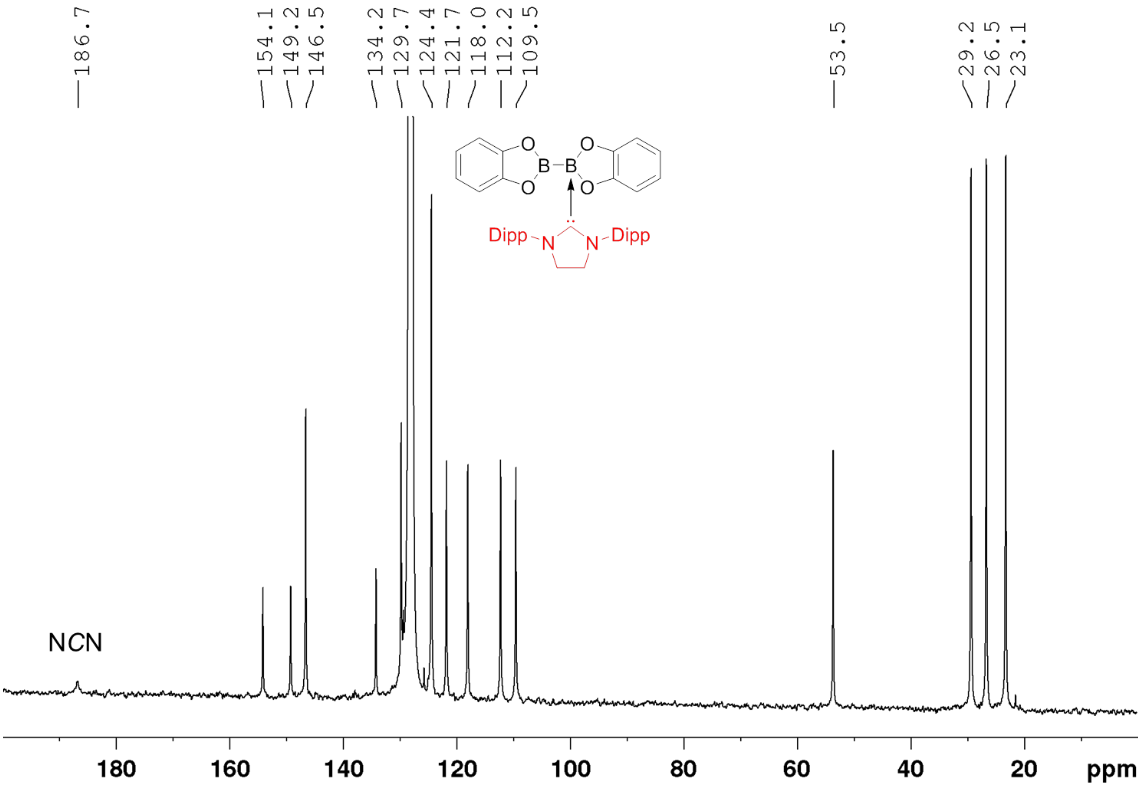

Figure S17: $^{13}C\{^{1}H\}$ NMR spectrum of compound **7b** in C_6D_6 (101 MHz, 25 °C).

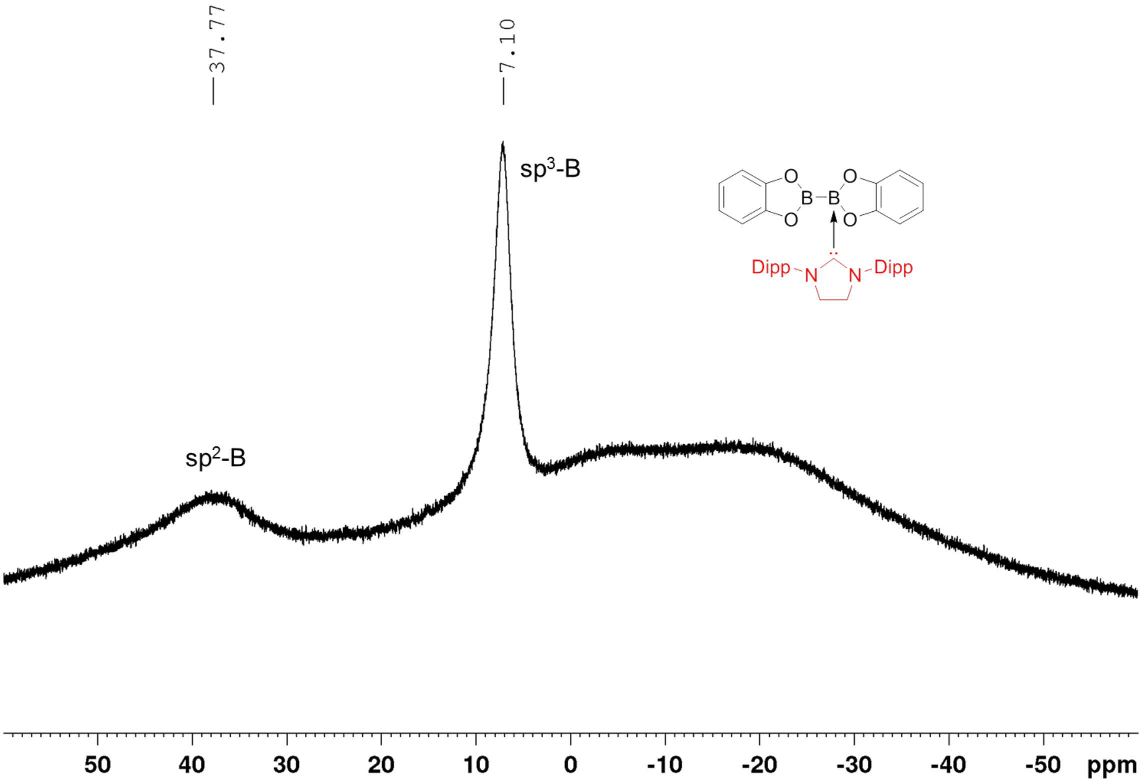

Figure S18: $^{11}B\{^{1}H\}$ NMR spectrum of compound **7b** in C_6D_6 (128 MHz, 25 °C).

1.5 Solution NMR spectra of compound **8** RER-B_2cat_2•Dipp_2SIm

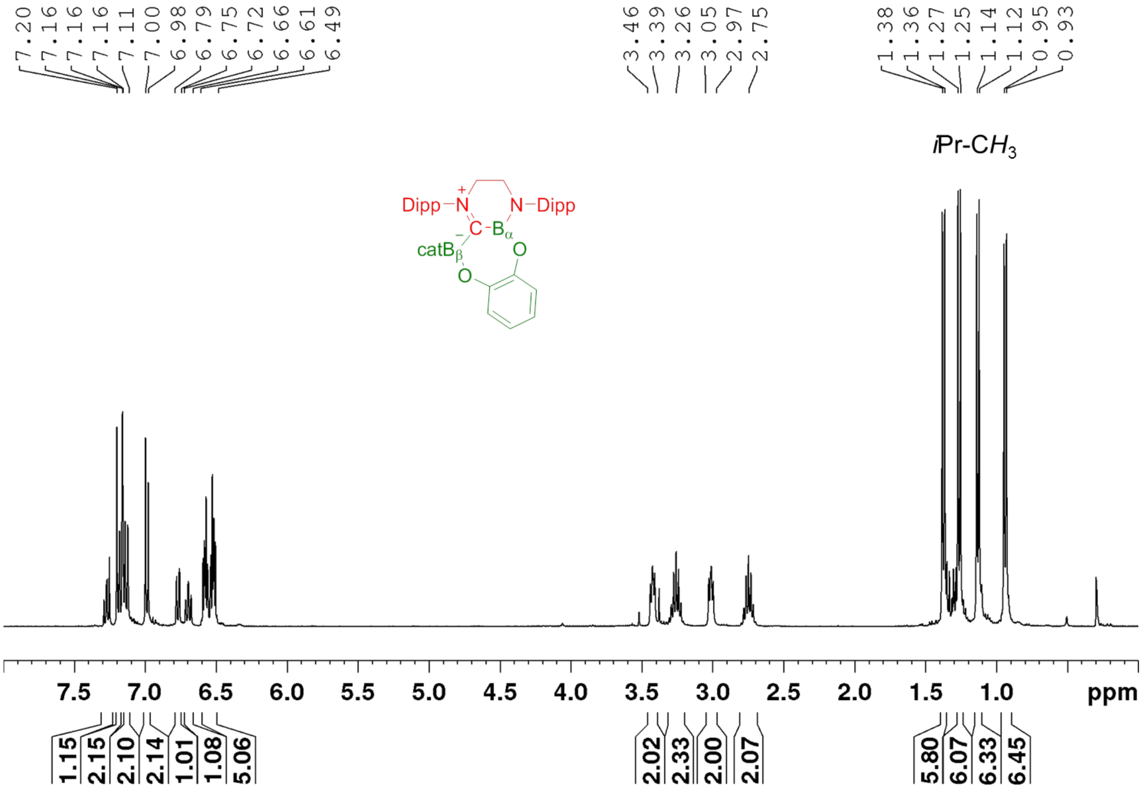

Figure S19: ^{1}H NMR spectrum of compound **8** in C_6D_6 (400 MHz, 25 °C).

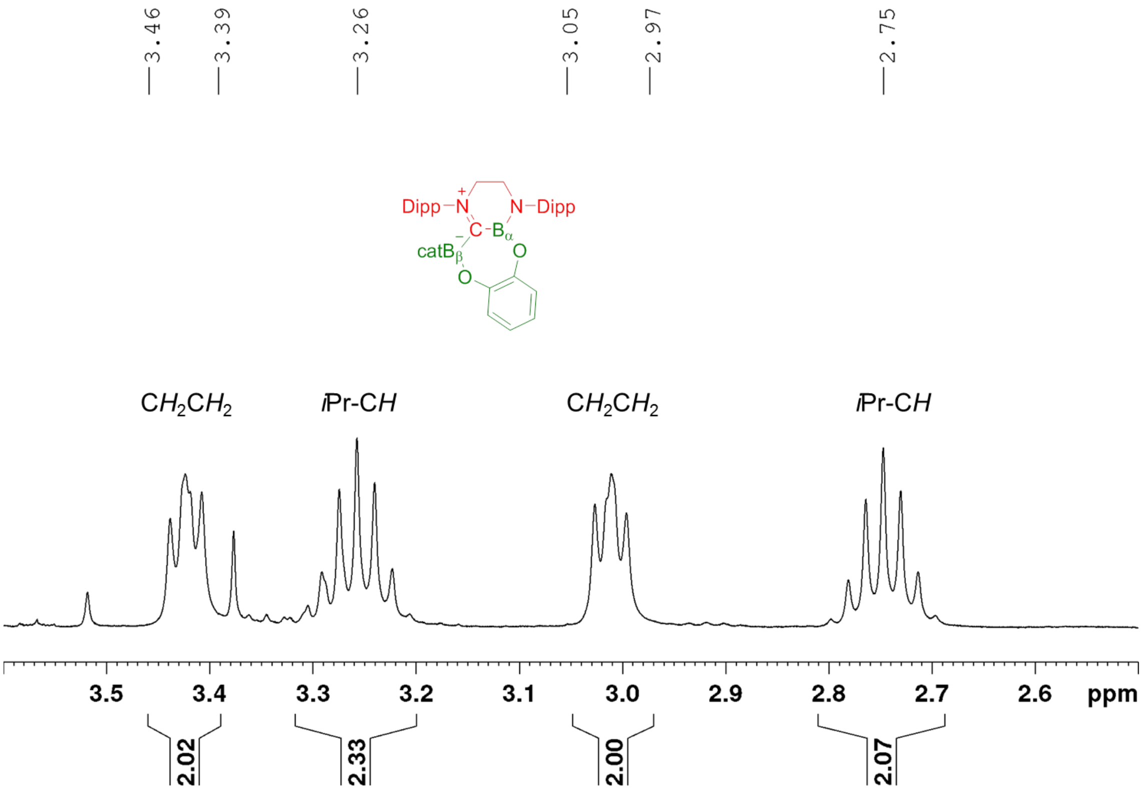

Figure S20: ^{1}H NMR spectrum of compound **8** in C_6D_6 (400 MHz, 25 °C).

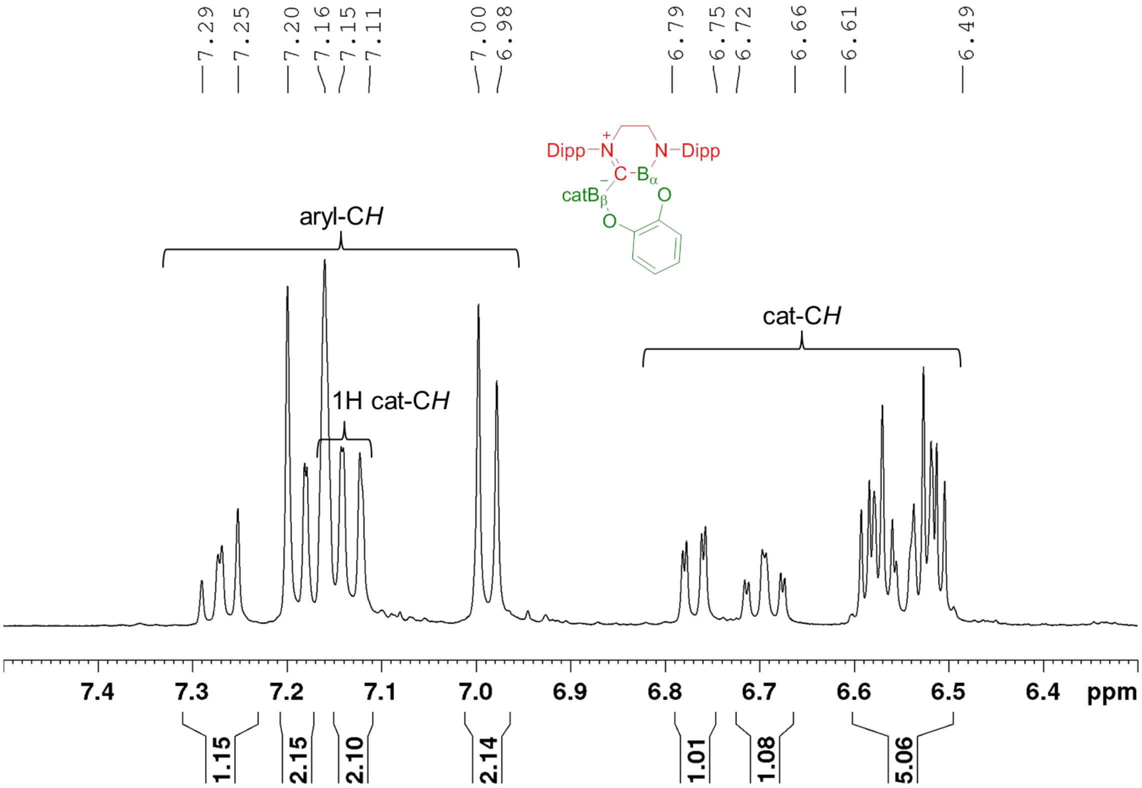

Figure S21: ^{1}H NMR spectrum of compound **8** in C_6D_6 (400 MHz, 25 °C).

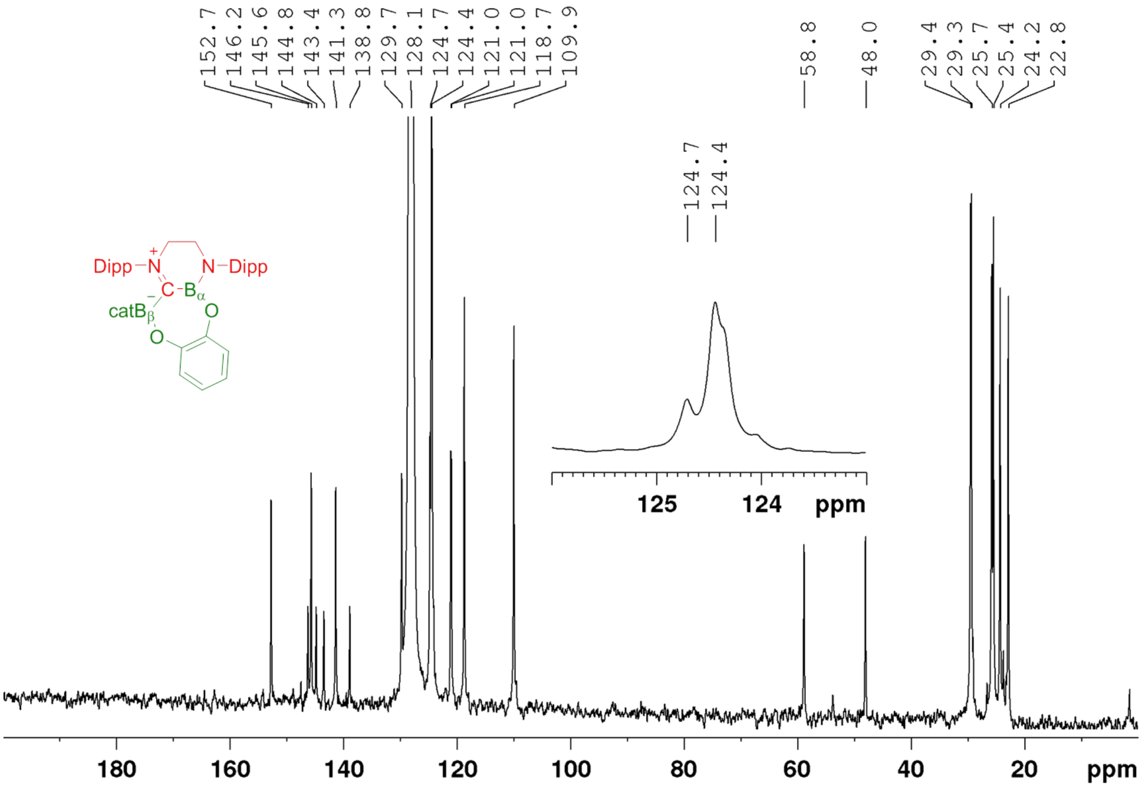

Figure S22: ^{13}C{^{1}H} NMR spectrum of compound **8** in C_6D_6 (101 MHz, 25 °C).

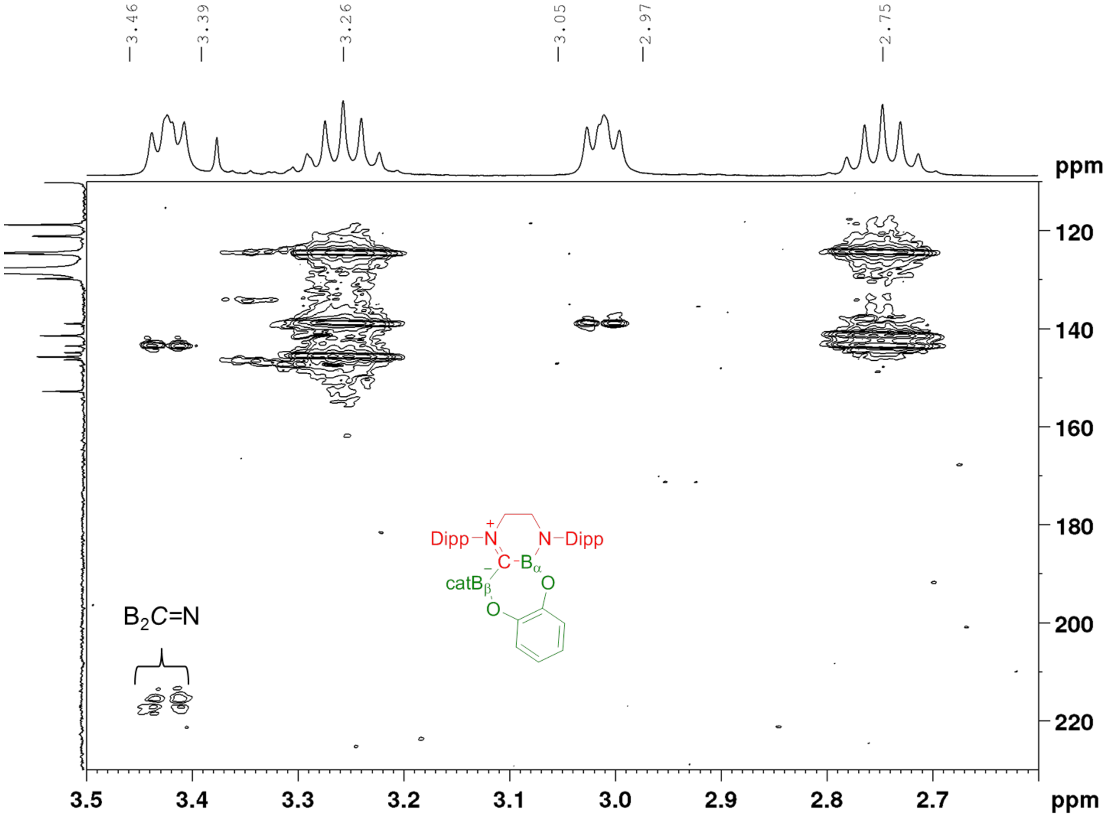

Figure S23: ^{13}C,^{1}H HMBC NMR spectrum of compound **8** in C_6D_6 (101 MHz, 25 °C).

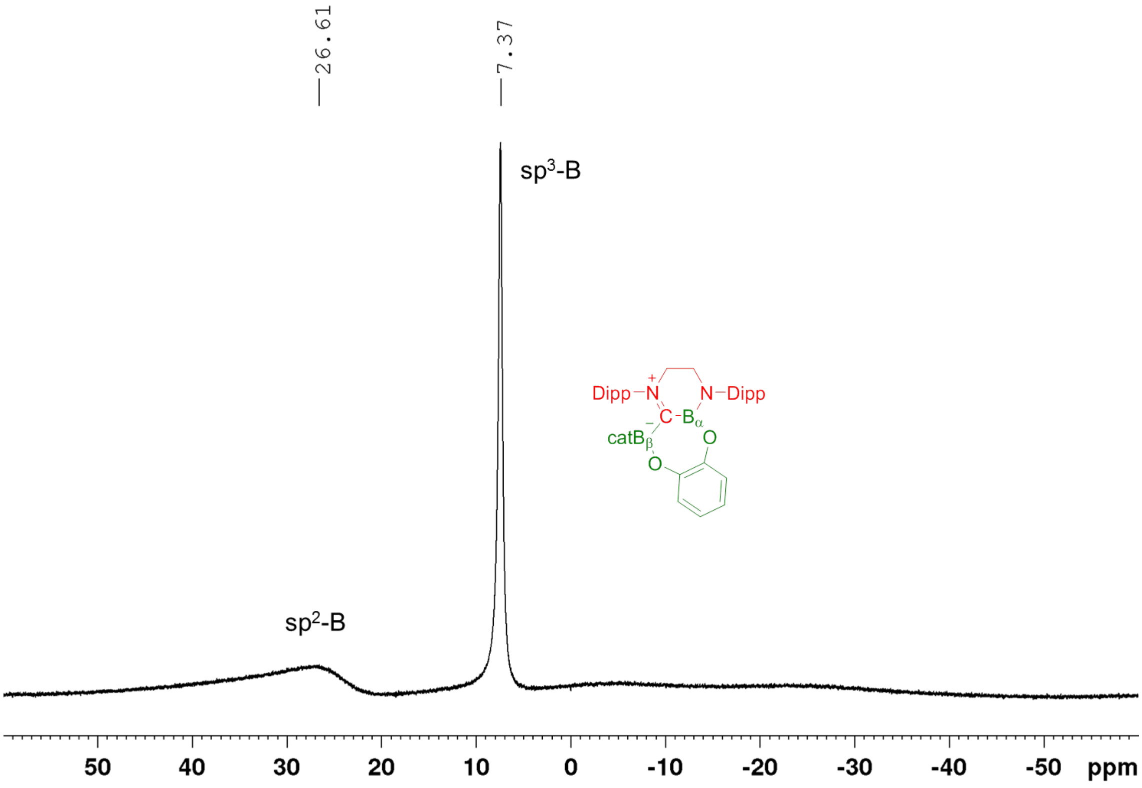

Figure S24: ^{11}B{^{1}H} NMR spectrum of compound **8** in C_6D_6 (128 MHz, 25 °C).

1.6 Solution NMR spectra of compound **9** RER-B$_2$cat$_2$•(*i*Pr$_2$Im)$_2$

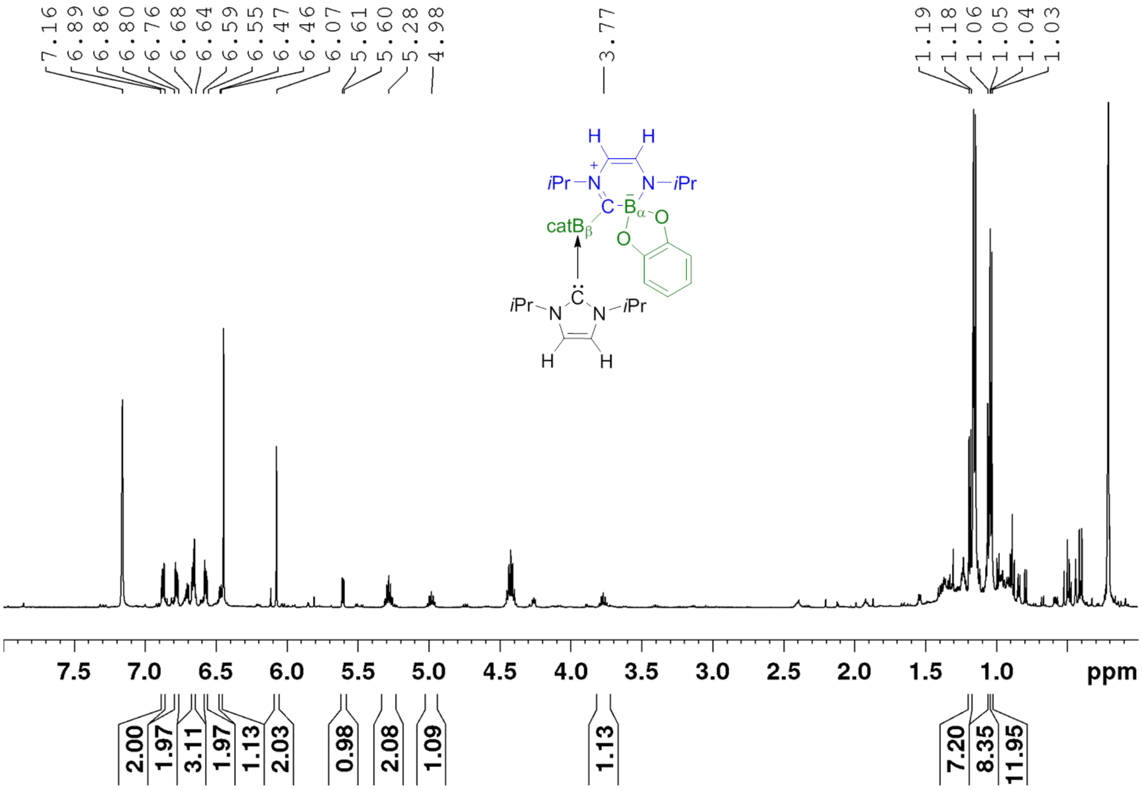

Figure S25: ^{1}H NMR spectrum of compound **9** in C$_6$D$_6$ (500 MHz, 25 °C).

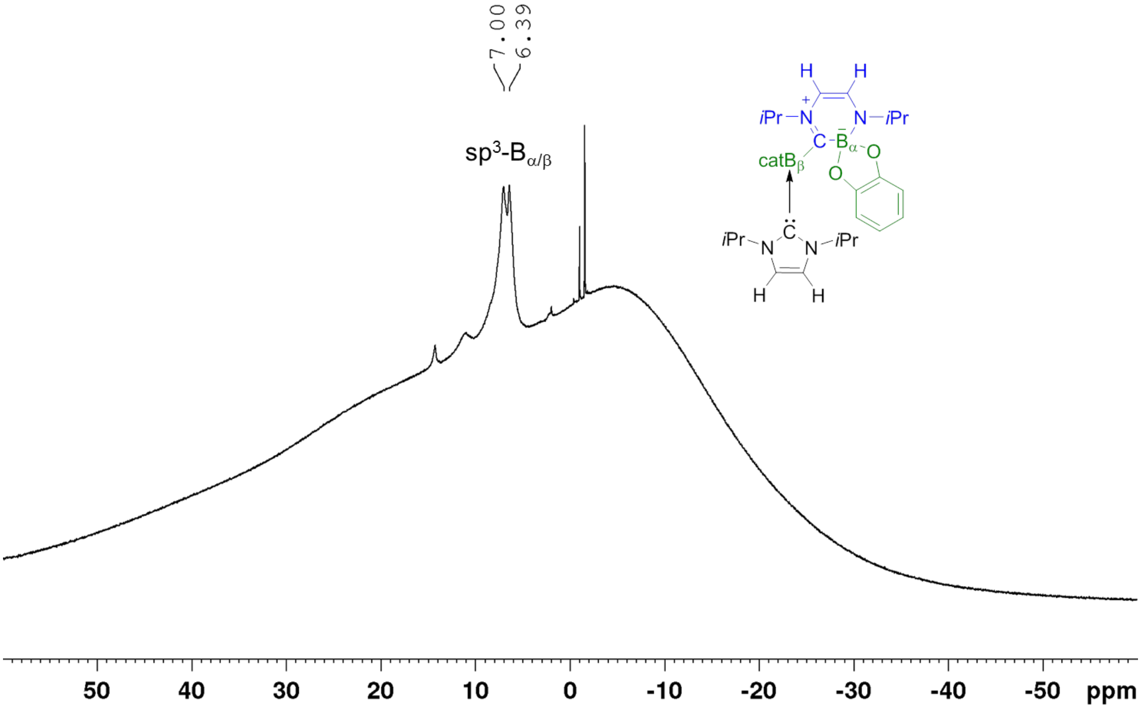

Figure S26: ^{11}B{^{1}H} NMR spectrum of compound **9** in C$_6$D$_6$ (160 MHz, 25 °C).

1.7 Compound **12** RER-B_2neop_2•$(Me_2Im)_2$

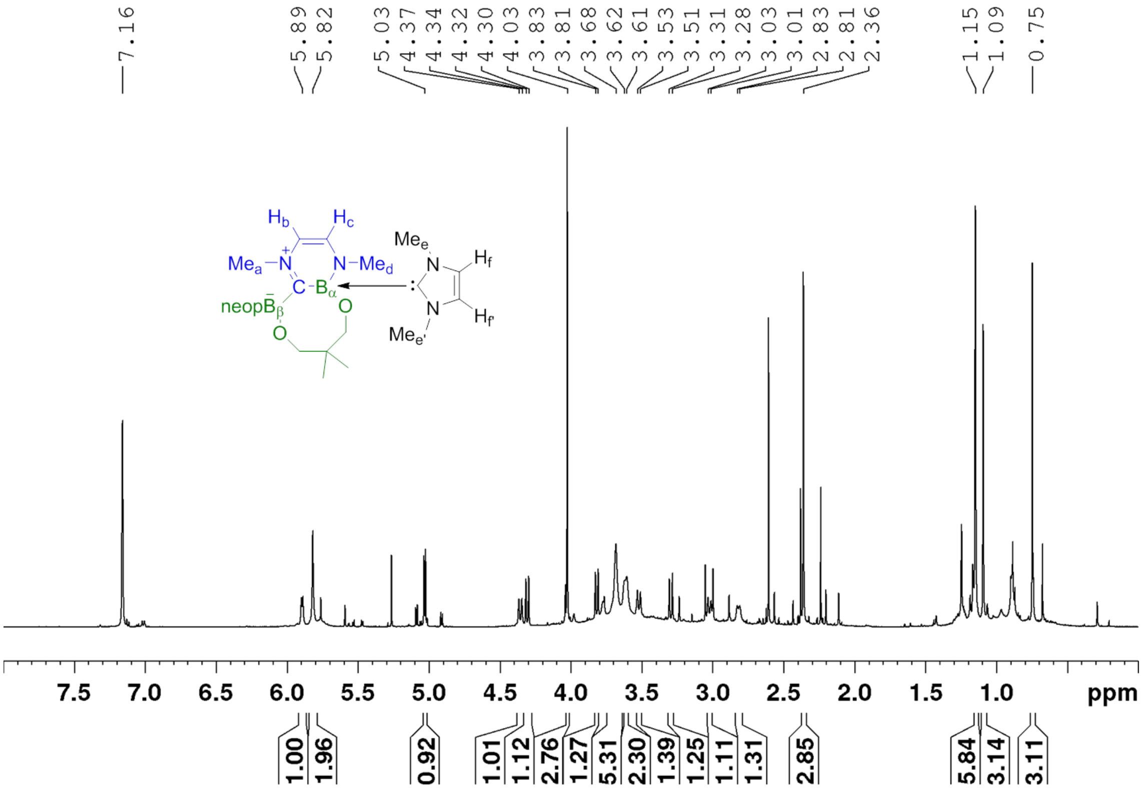

Figure S27: ^{1}H NMR spectrum of compound **12** in C_6D_6 (500 MHz, 25 °C).

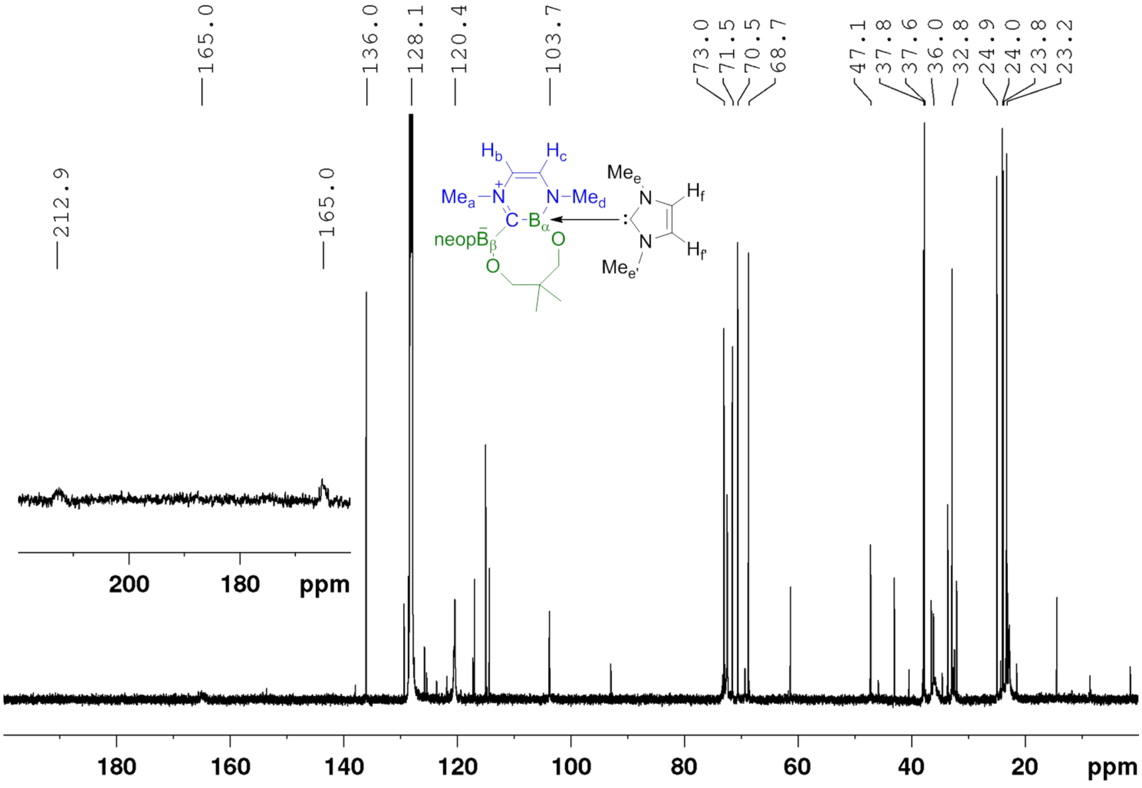

Figure S28: $^{13}C\{^1H\}$ NMR spectrum of compound **12** in C_6D_6 (125 MHz, 25 °C).

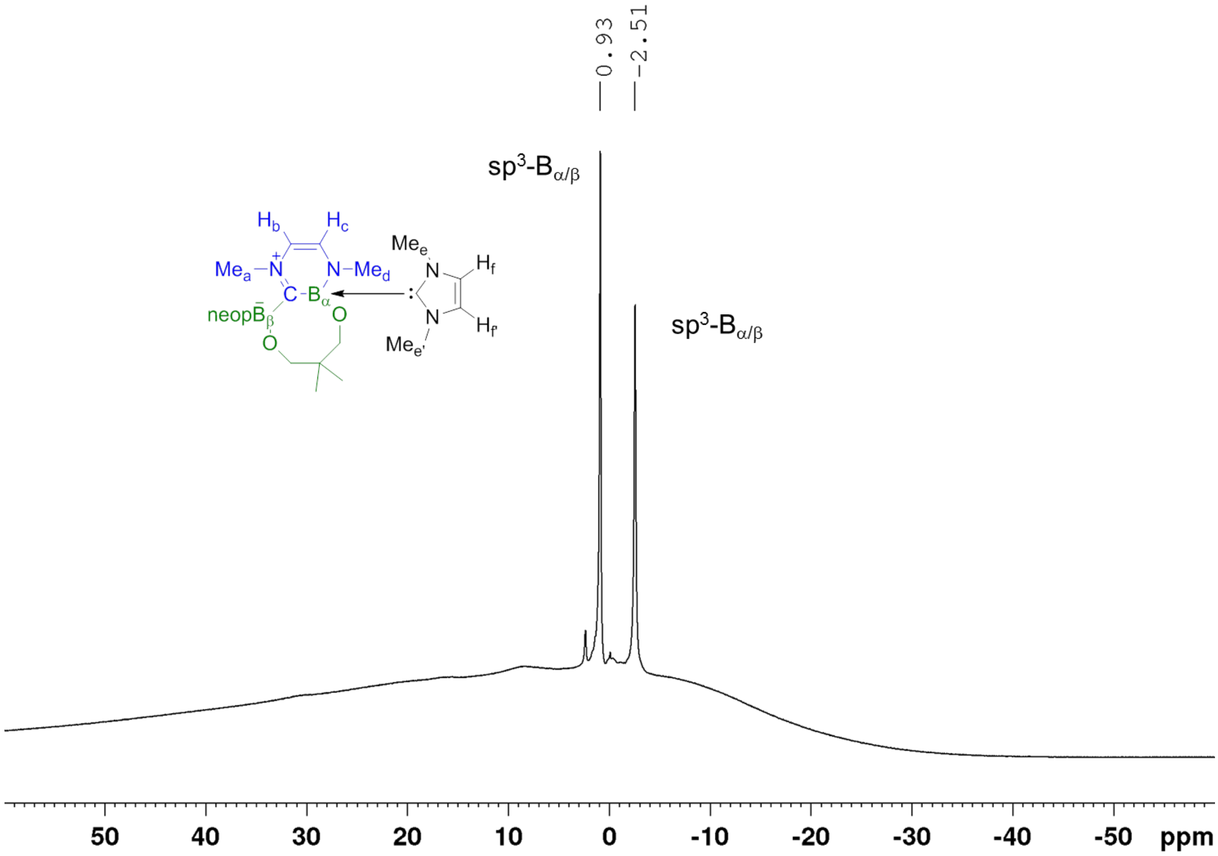

Figure S29: ^{11}B{^{1}H} NMR spectrum of compound **12** in C_6D_6 (160 MHz, 25 °C).

1.8 Solution NMR spectra of compound **13** RER-B$_2$neop$_2$•(Me$_2$Im^{Me})$_2$

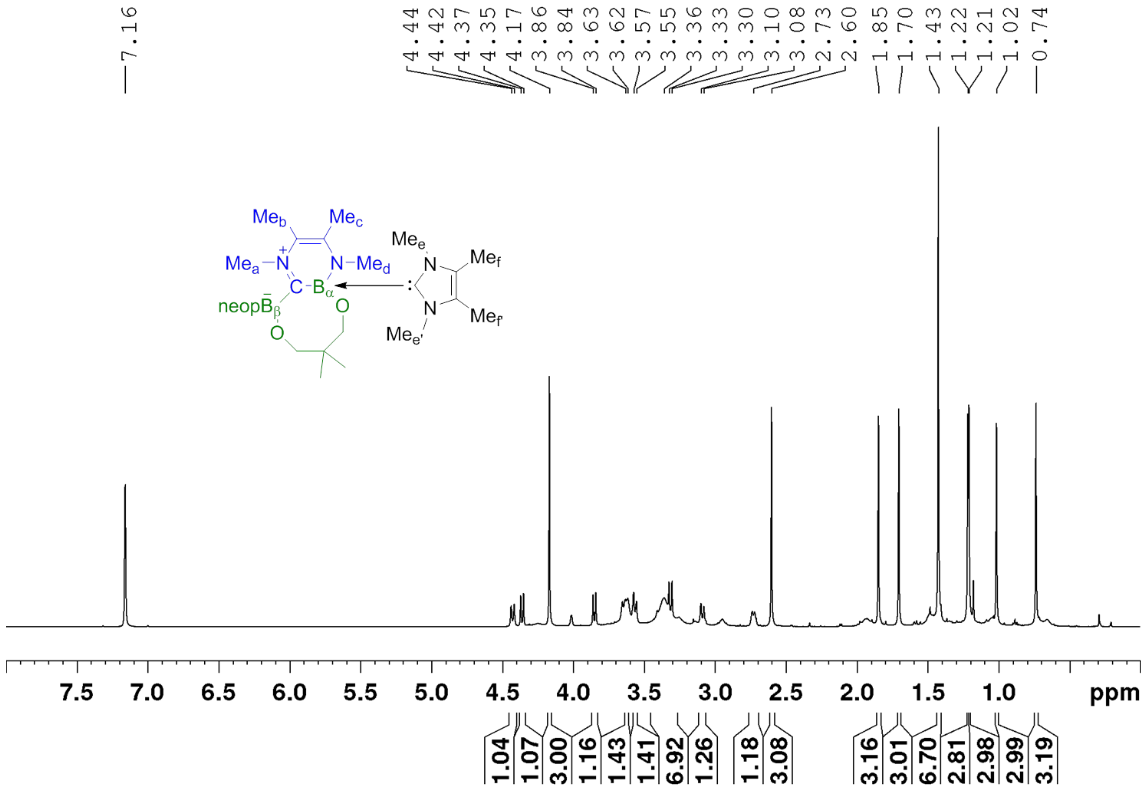

Figure S30: ^{1}H NMR spectrum of compound **13** in C$_6$D$_6$ (500 MHz, 25 °C).

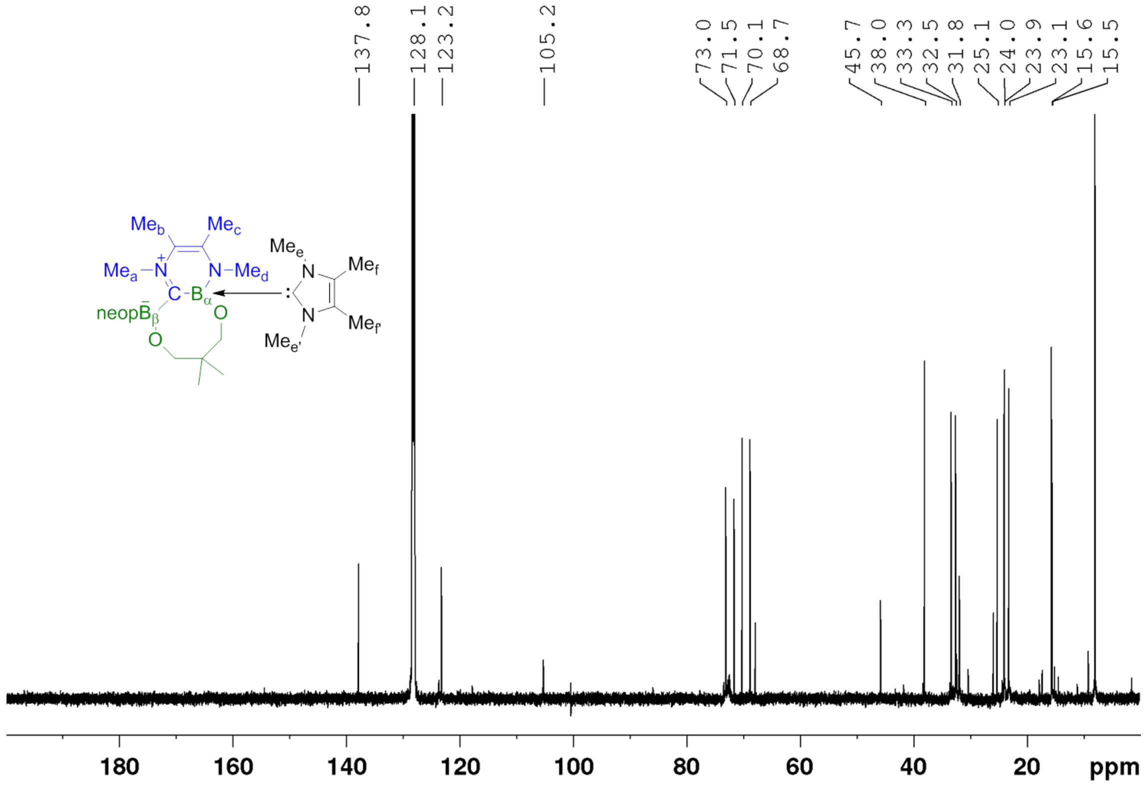

Figure S31: ^{13}C{^{1}H} NMR spectrum of compound **13** in C$_6$D$_6$ (125 MHz, 25 °C).

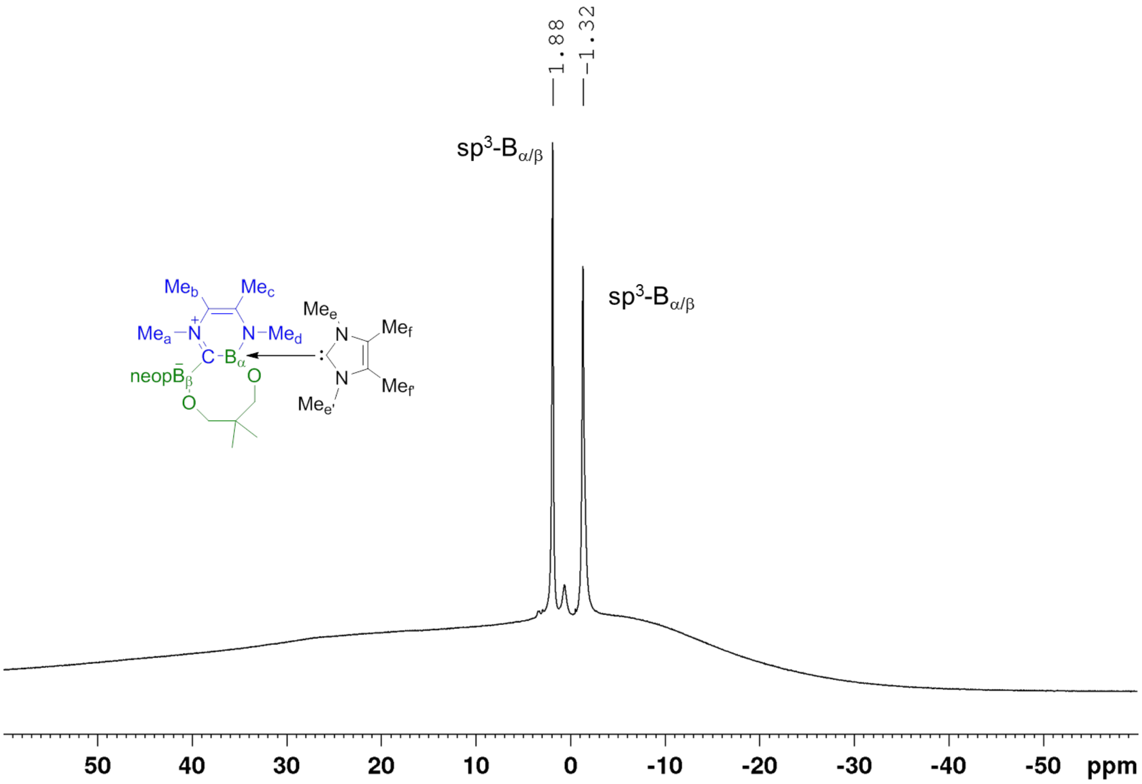

Figure S32: $^{11}B\{^{1}H\}$ NMR spectrum of compound **13** in C_6D_6 (160 MHz, 25 °C).

1.9 Solution NMR spectra of compound **14** mono-NHC adduct B_2eg_2•Mes_2Im

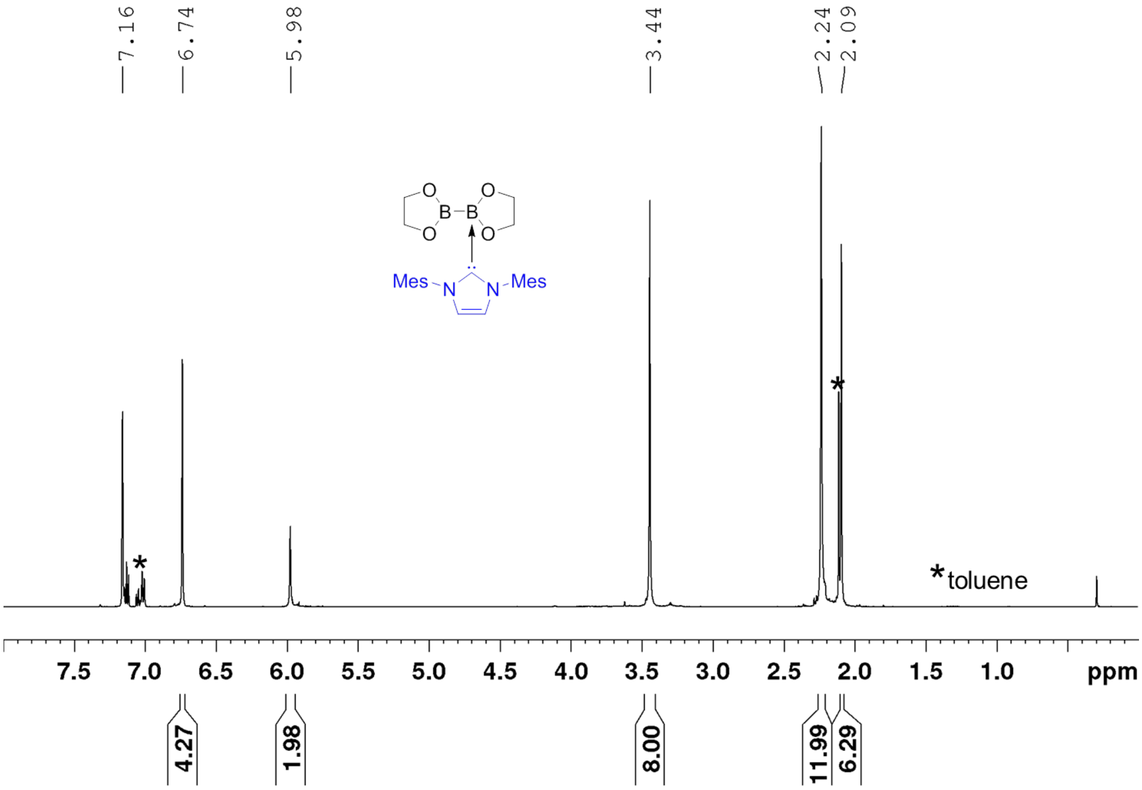

Figure S33: ^{1}H NMR spectrum of compound **14** in C_6D_6 (500 MHz, 25 °C).

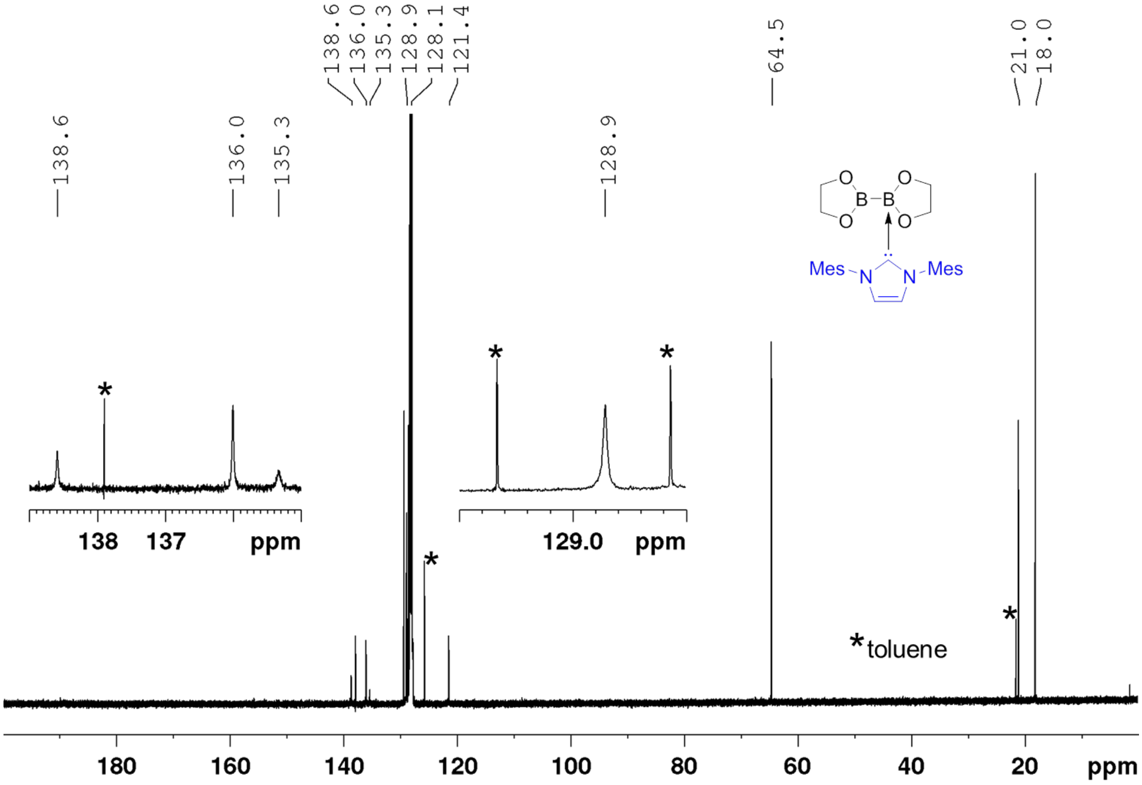

Figure S34: $^{13}C\{^1H\}$ NMR spectrum of compound **14** in C_6D_6 (125 MHz, 25 °C).

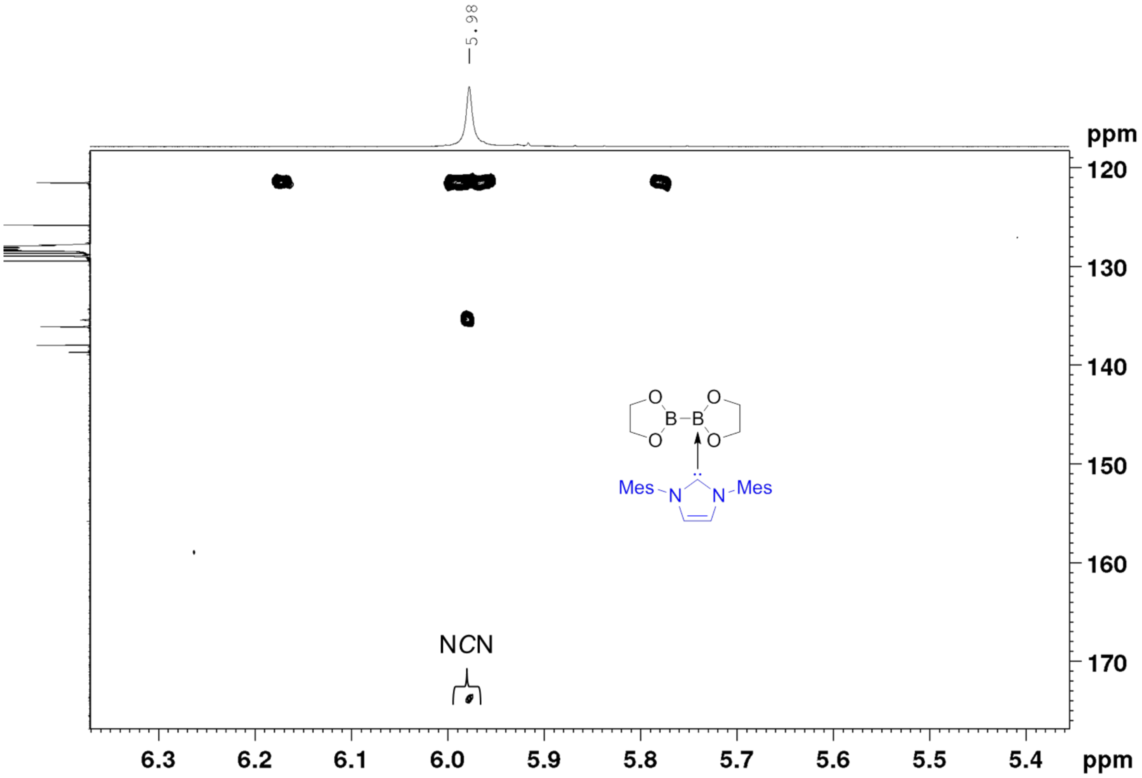

Figure S35: $^{13}C,^{1}H$ HMBC NMR spectrum of compound **14** in C_6D_6 (125 MHz, 25 °C).

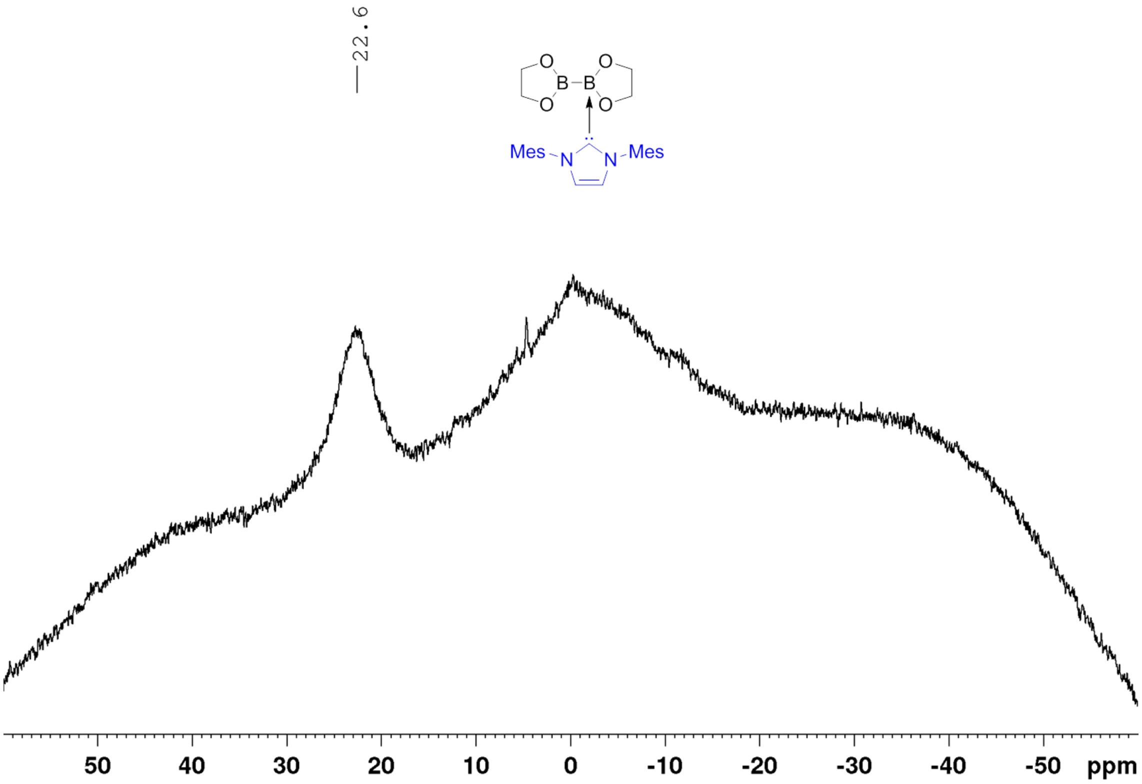

Figure S36: $^{11}B\{^{1}H\}$ NMR spectrum of compound **14** in C_6D_6 (96 MHz, 25 °C).

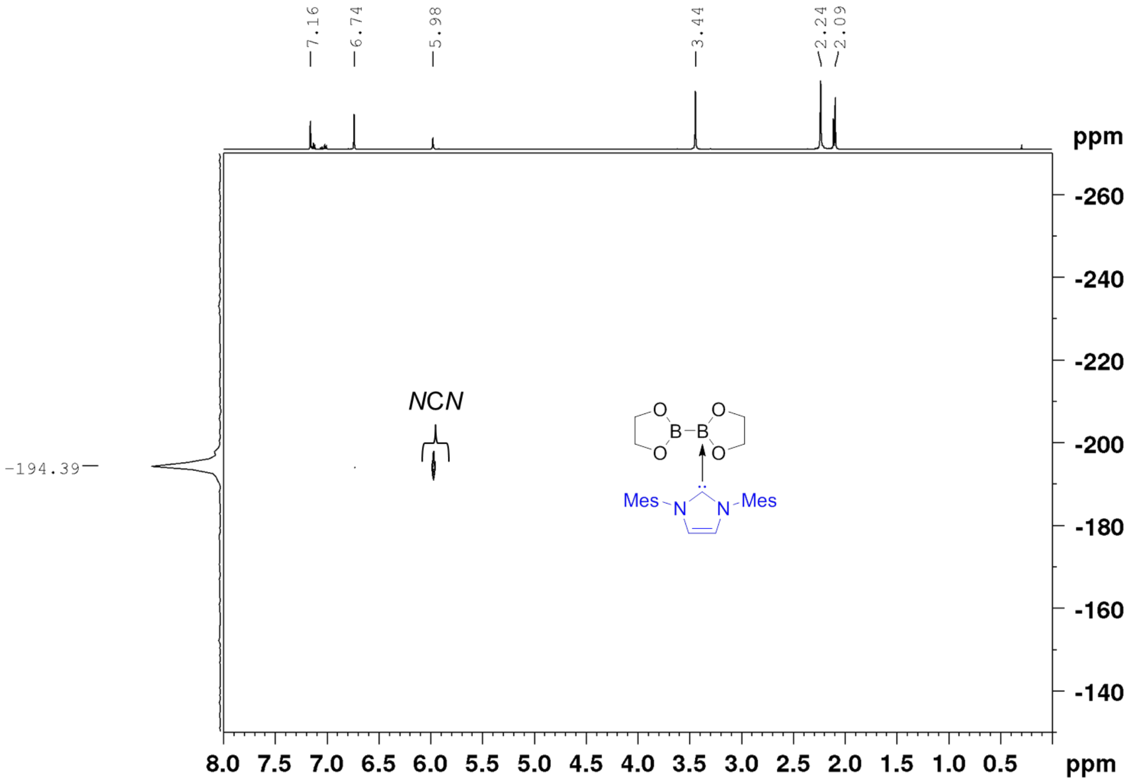

Figure S37: ^{15}N,^{1}H HMBC NMR spectrum of compound **14** in C_6D_6 (51 MHz, 25 °C).

1.10 Solid state NMR spectra of compound **14** mono-NHC adduct B_2eg_2•Mes_2Im

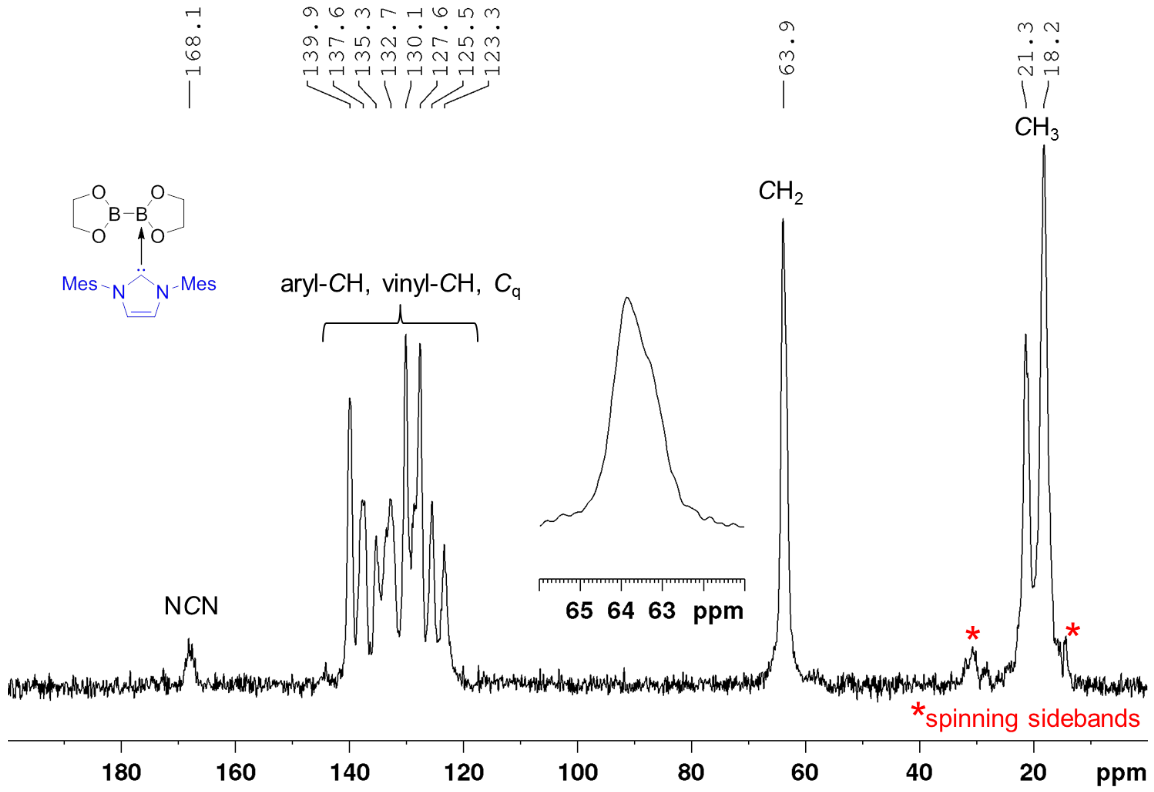

Figure S38: ^{13}C CP/MAS NMR spectrum of compound **14** (101 MHz, 22 °C, v rot = 11000 Hz).

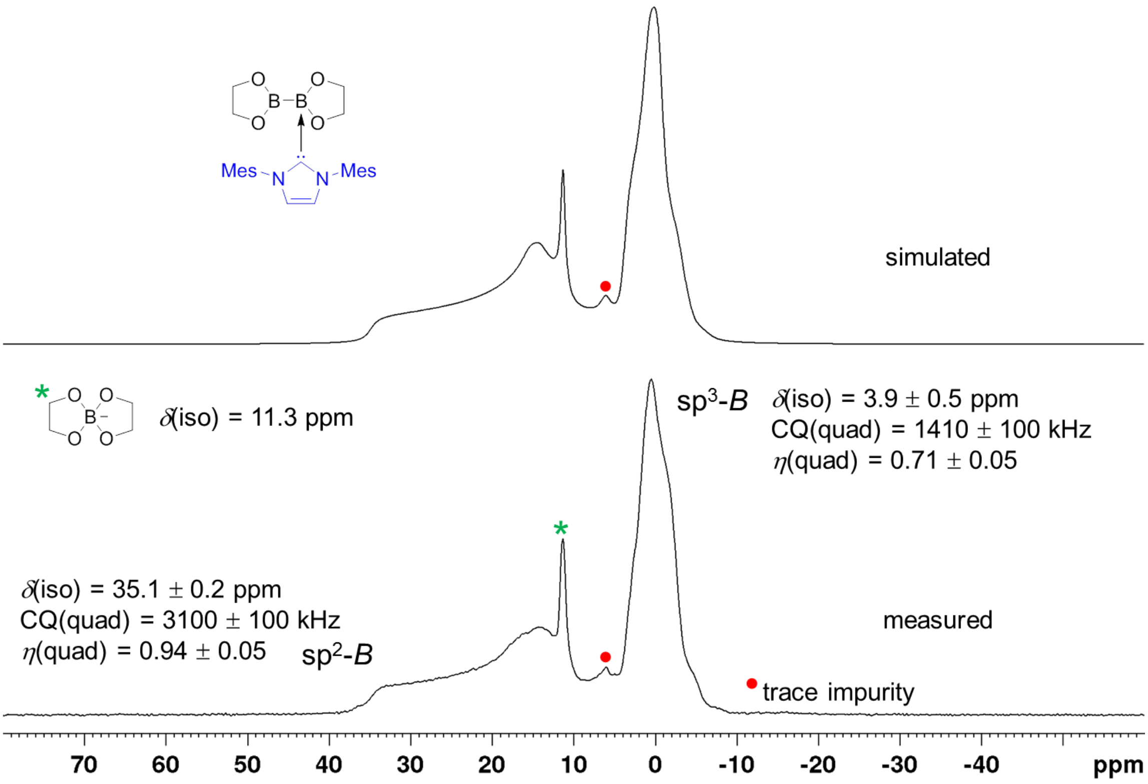

Figure S39: ^{11}B RSHE/MAS NMR spectrum of compound **14** (128 MHz, 22 °C, v rot = 15000 Hz).

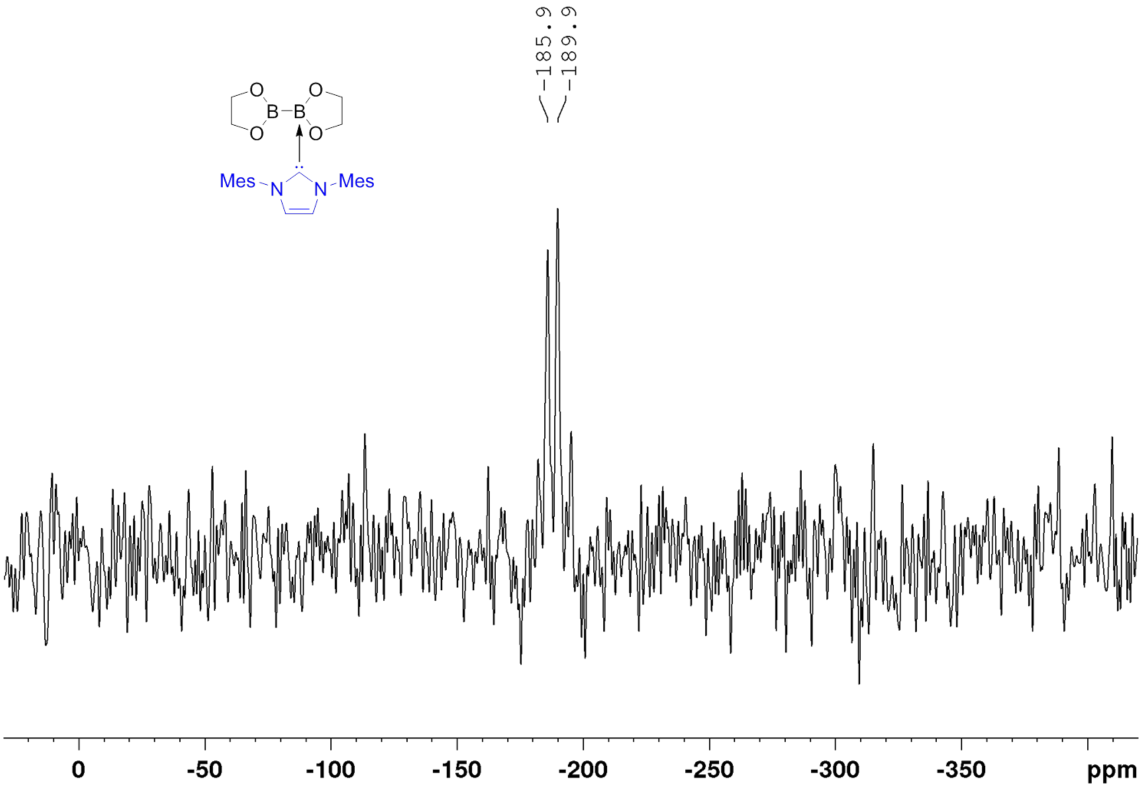

Figure S40: ^{15}N CP/MAS NMR spectrum of compound **14** (41 MHz, 22 °C, v rot = 7000 Hz).

1.11 Solution NMR spectra of compound **15** RER-B_2eg_2•(iPr$_2$Im)$_2$

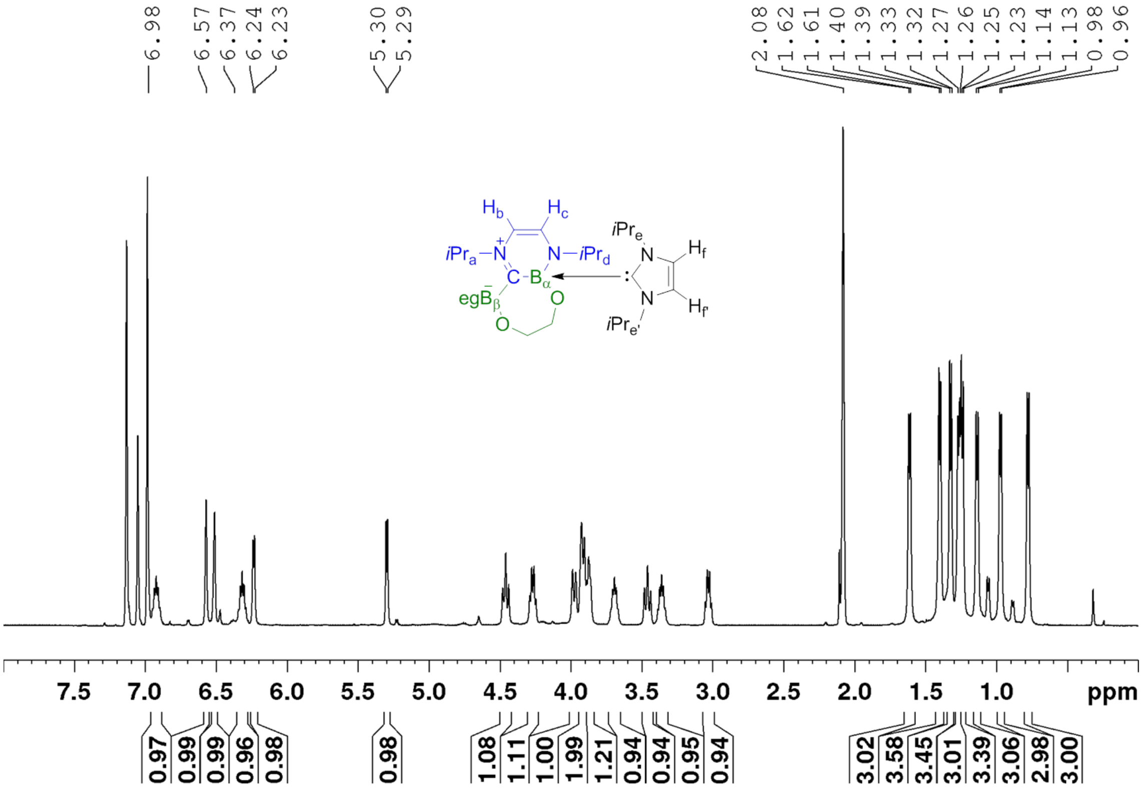

Figure S41: ^{1}H NMR spectrum of compound **15** in toluene-d_8 (500 MHz, -40 °C).

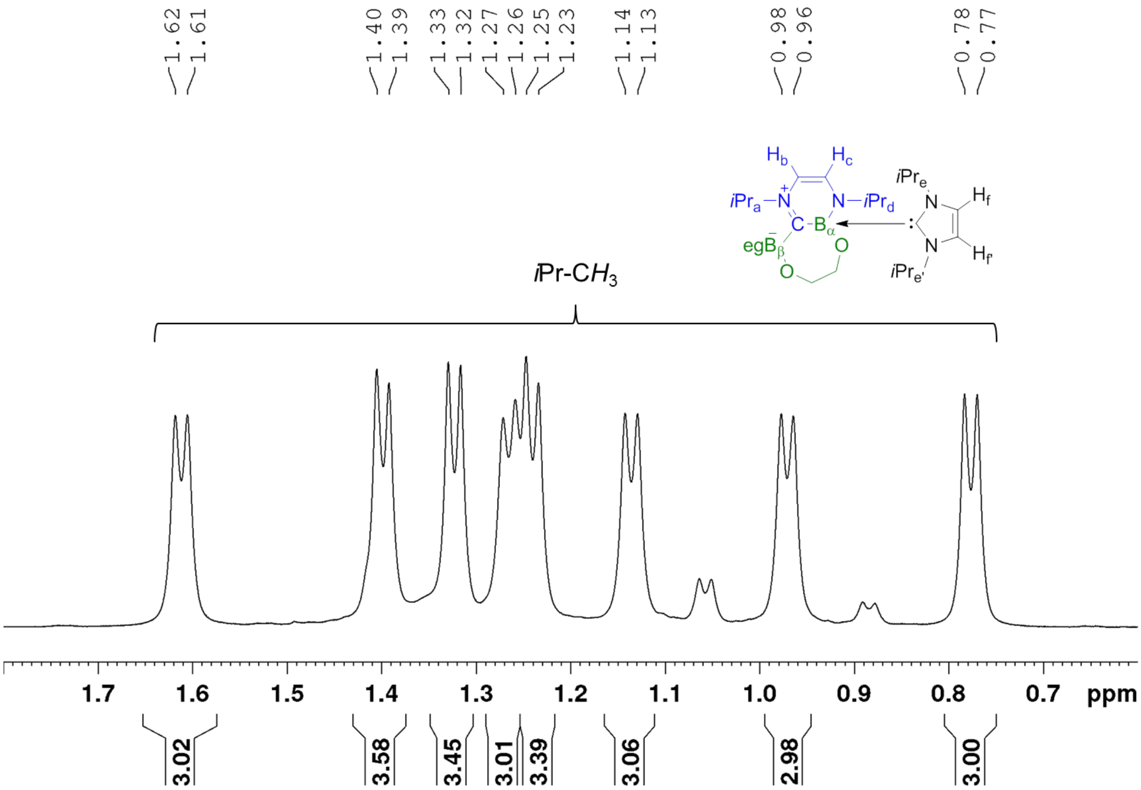

Figure S42: ^{1}H NMR spectrum of compound **15** in toluene-d_8 (500 MHz, -40 °C).

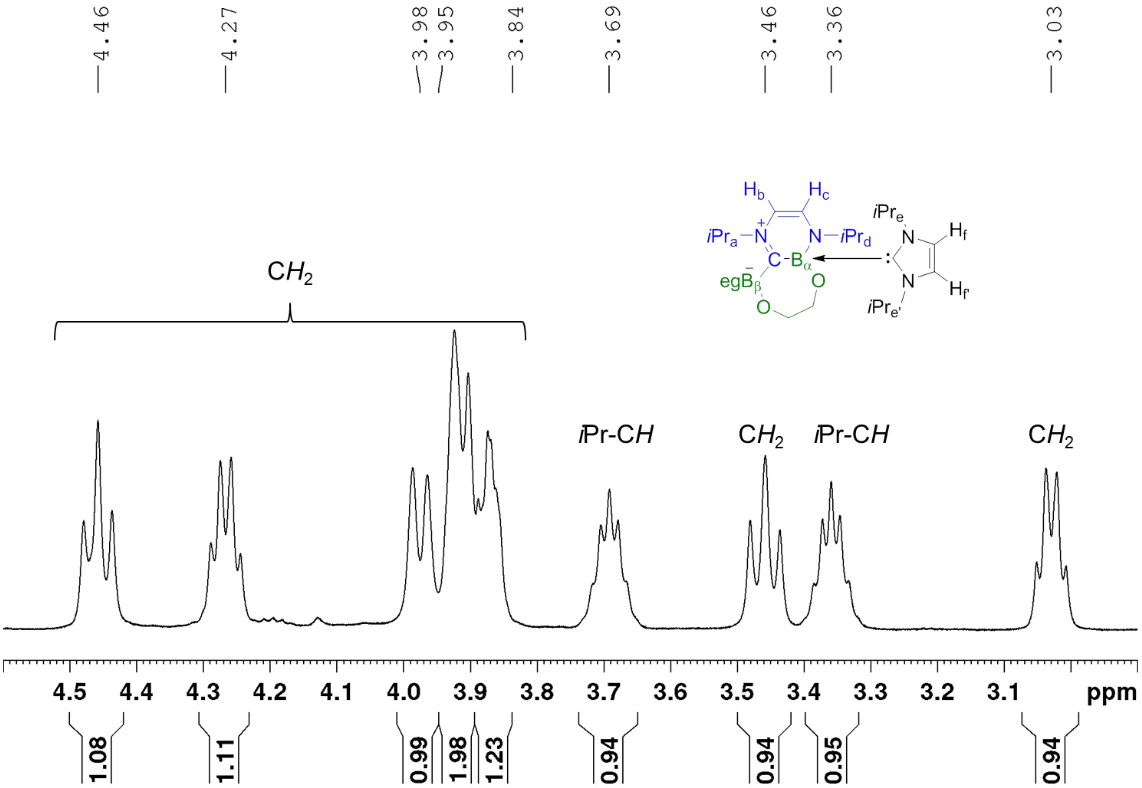

Figure S43: ^{1}H NMR spectrum of compound **15** in toluene-d_8 (500 MHz, -40 °C).

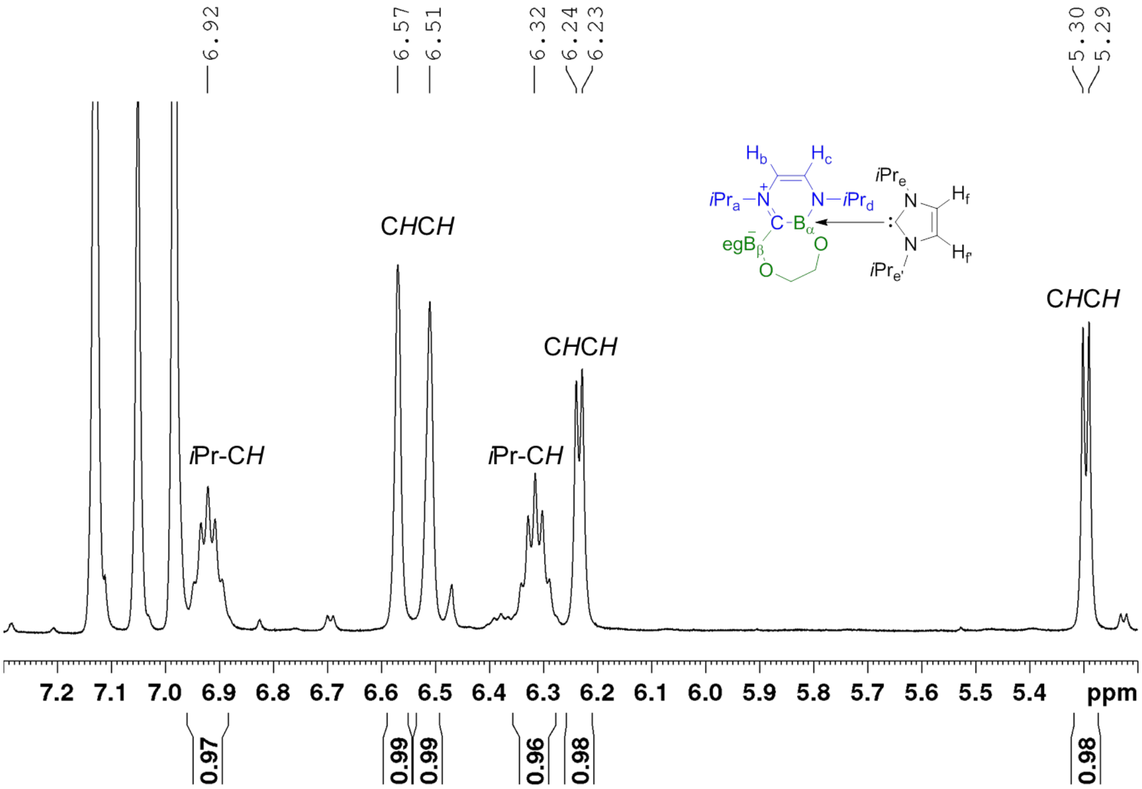

Figure S44: ^{1}H NMR spectrum of compound **15** in toluene-d_8 (500 MHz, -40 °C).

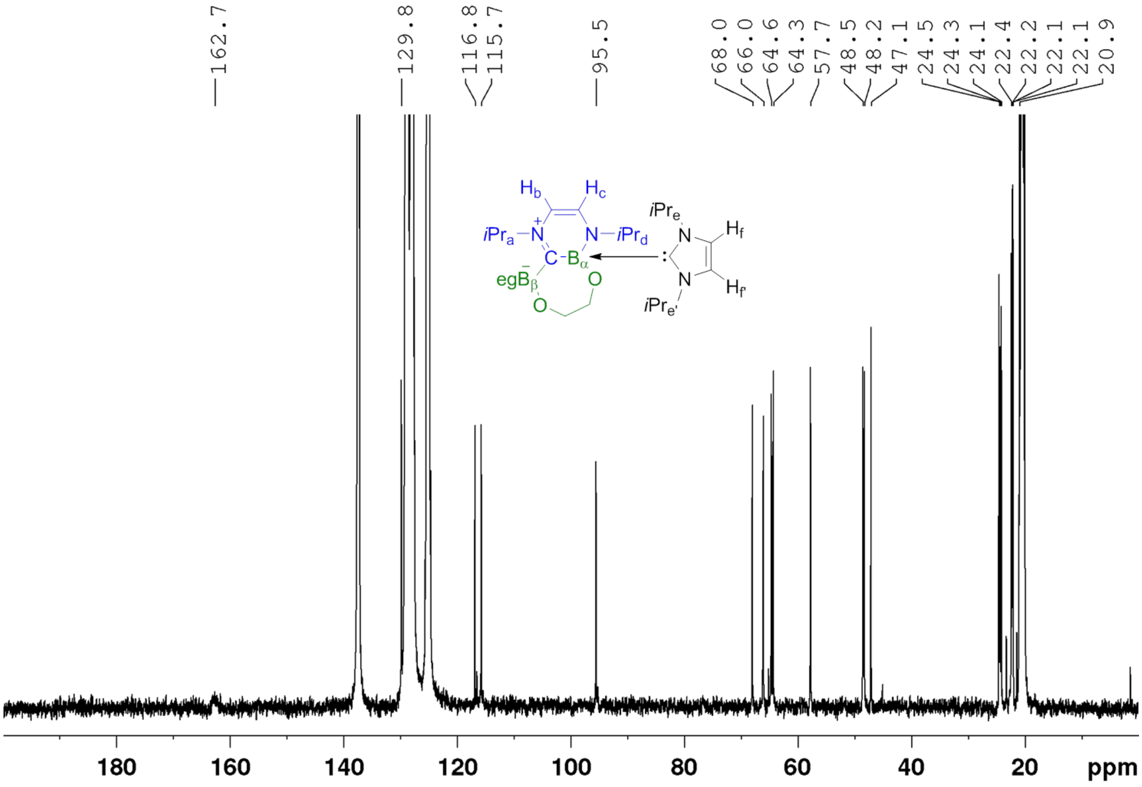

Figure S45: $^{13}C\{^1H\}$ NMR spectrum of compound **15** in toluene-d$_8$ (125 MHz, -40 °C).

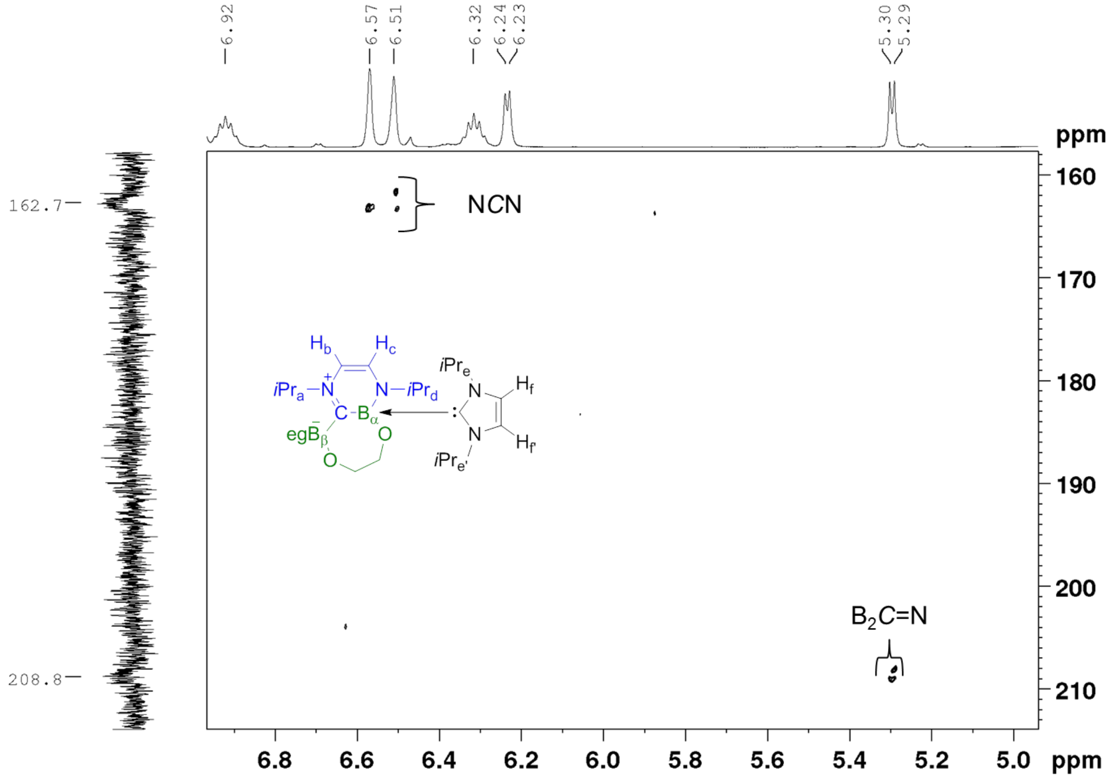

Figure S46: $^{13}C,^{1}H$ HMBC NMR spectrum of compound **15** in toluene-d$_8$ (125 MHz, -40 °C).

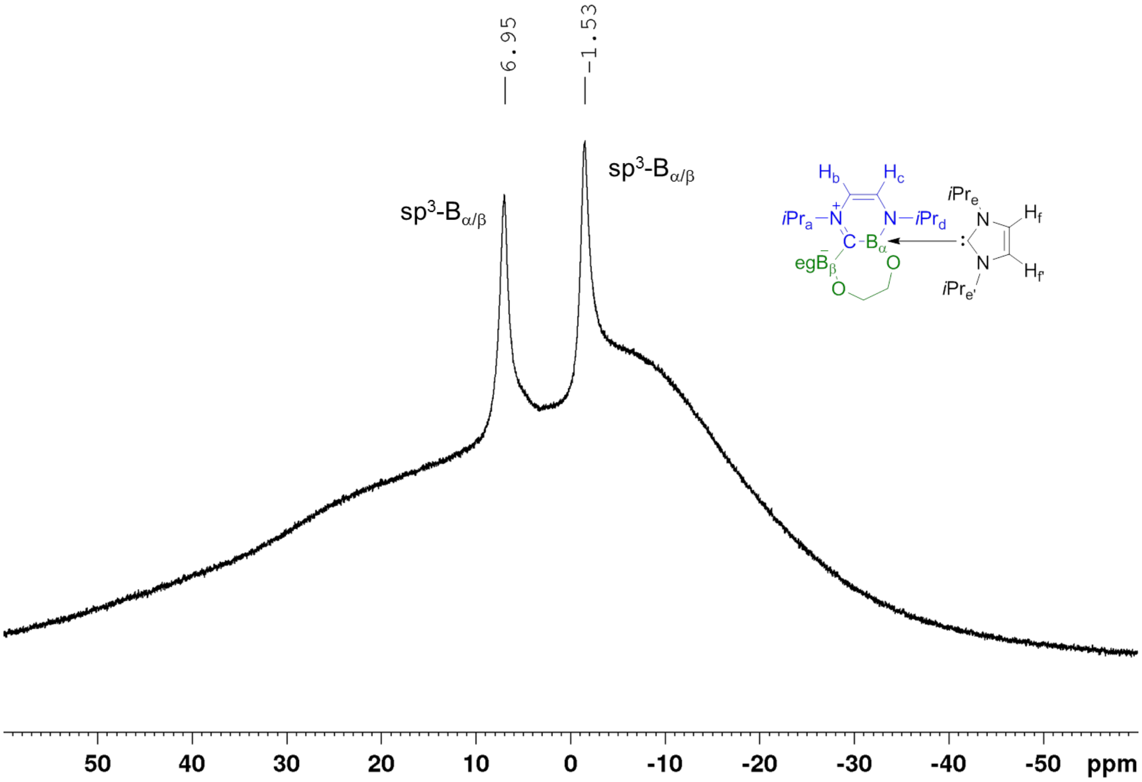

Figure S47: $^{11}B\{^{1}H\}$ NMR spectrum of compound **15** in toluene-d_8 (160 MHz, -40 °C).

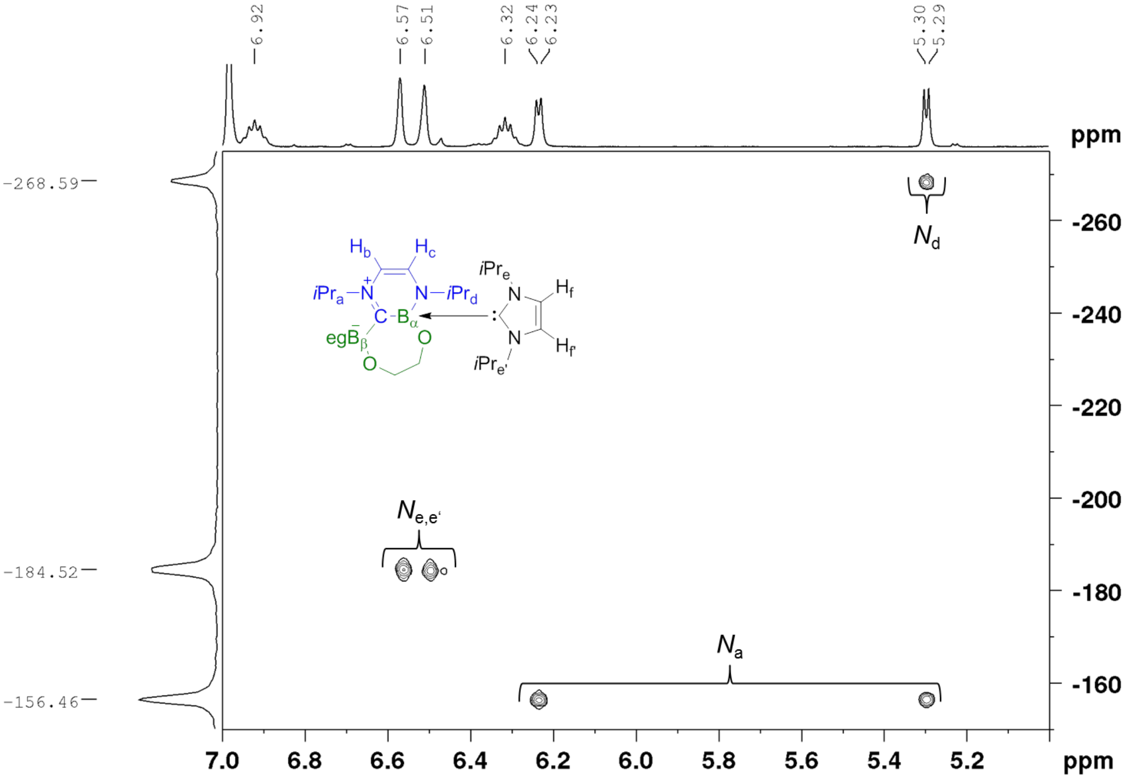

Figure S48: $^{15}N,^{1}H$ HMBC NMR spectrum of compound **15** in toluene-d_8 (51 MHz, -40 °C).

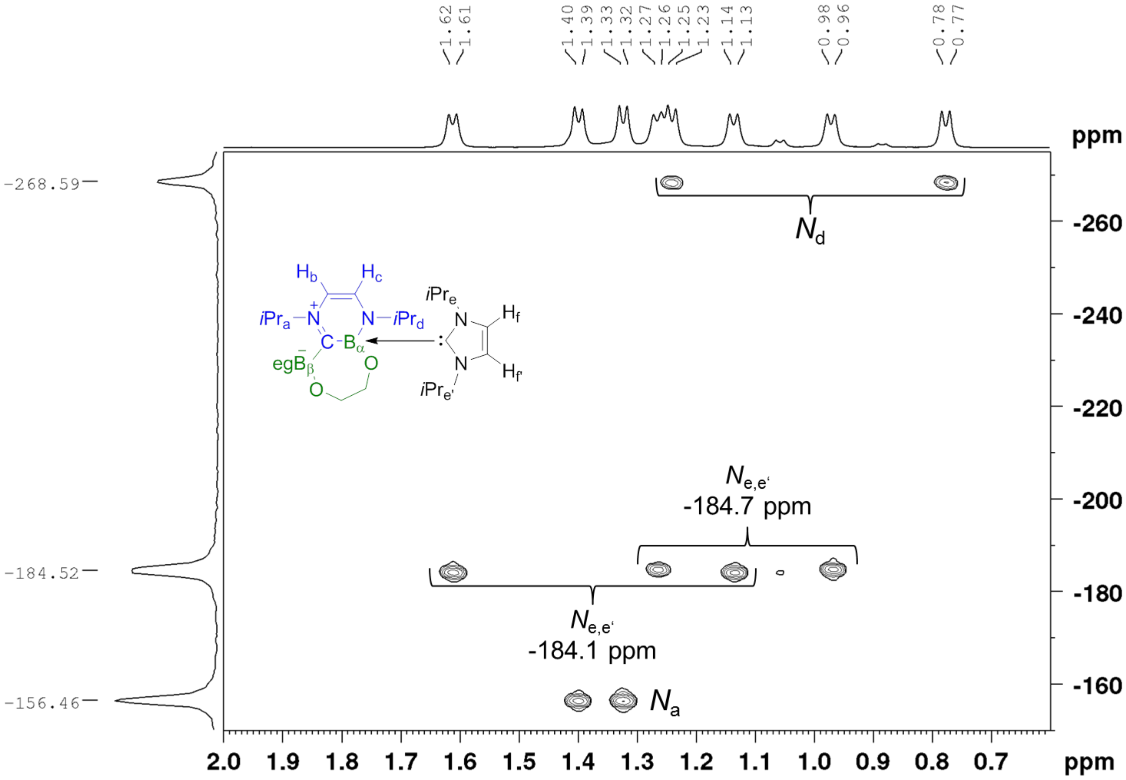

Figure S49: ^{15}N,^{1}H HMBC NMR spectrum of compound **15** in toluene-d$_8$ (51 MHz, -40 °C).

1.12 Solid state NMR spectra of compound **15** RER-B_2eg_2•(*i*Pr_2Im)$_2$

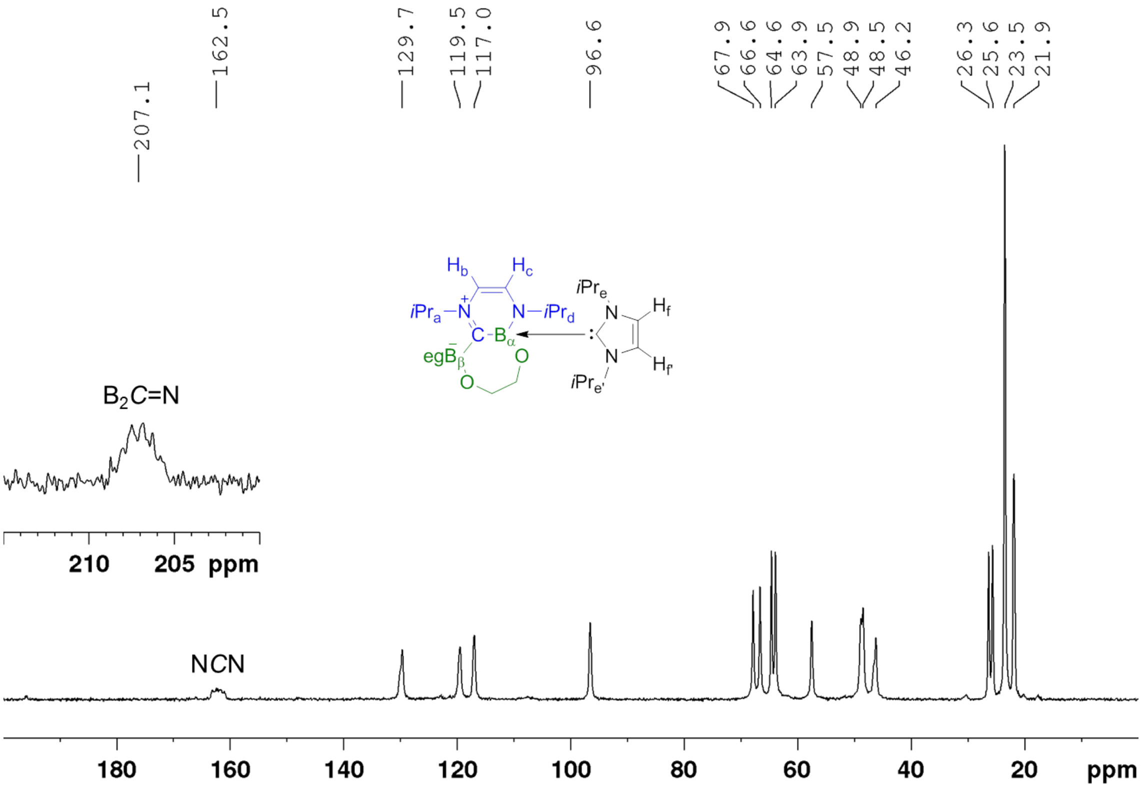

Figure S50: ^{13}C CP/MAS NMR spectrum of compound **15** (101 MHz, 22 °C, v rot = 10000 Hz).

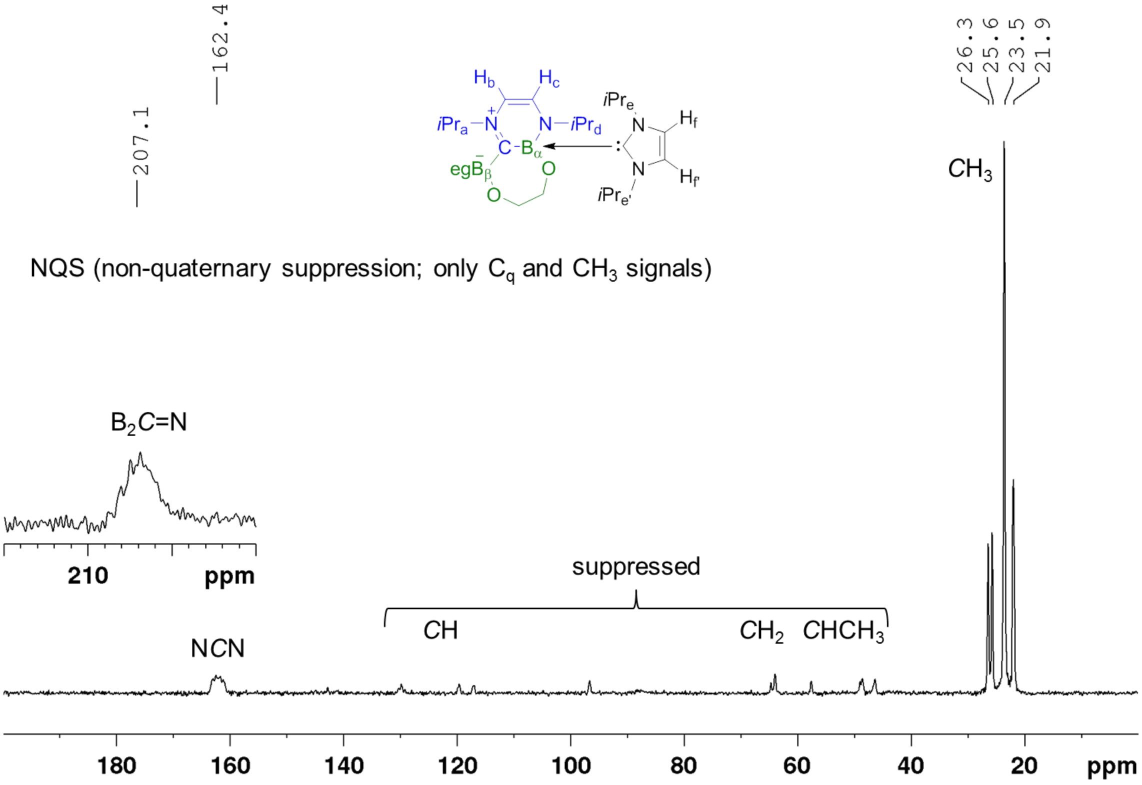

Figure S51: ^{13}C CP/NQS/MAS NMR spectrum of compound **15** (101 MHz, 22 °C, v rot = 12000 Hz).

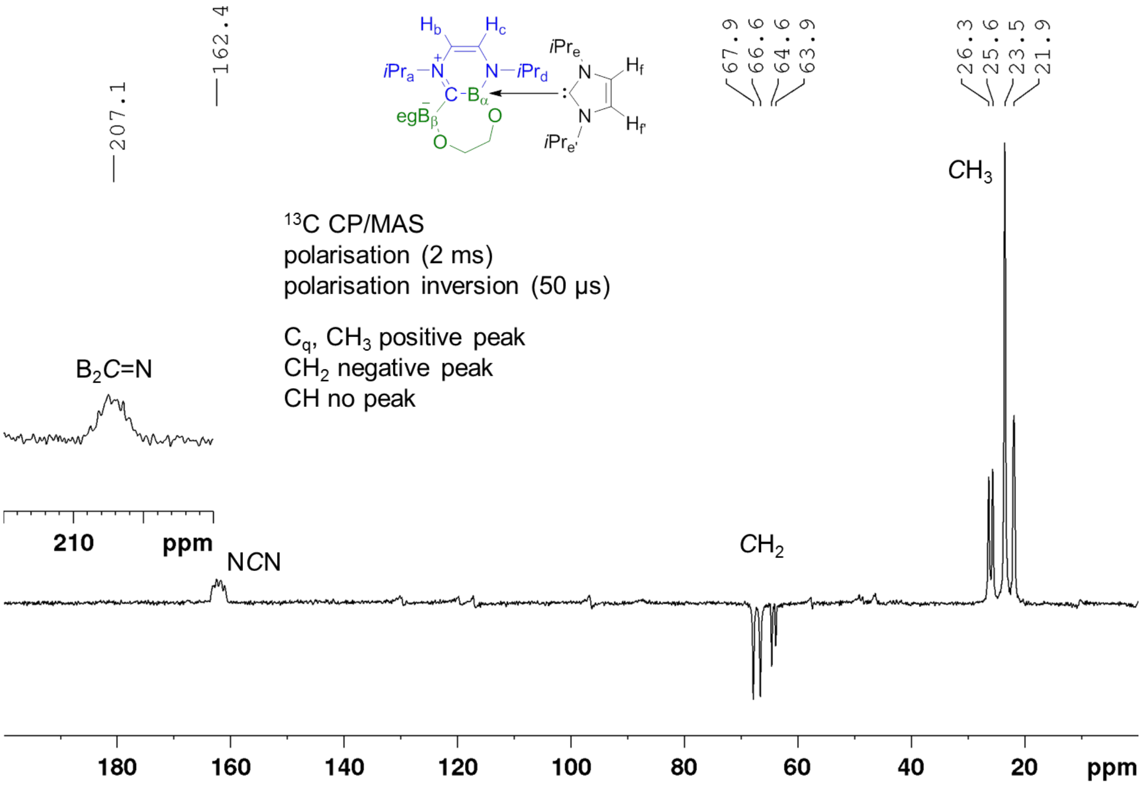

Figure S52: ^{13}C CP/PI/MAS NMR spectrum of compound **15** (101 MHz, 22 °C, v rot = 12000 Hz).

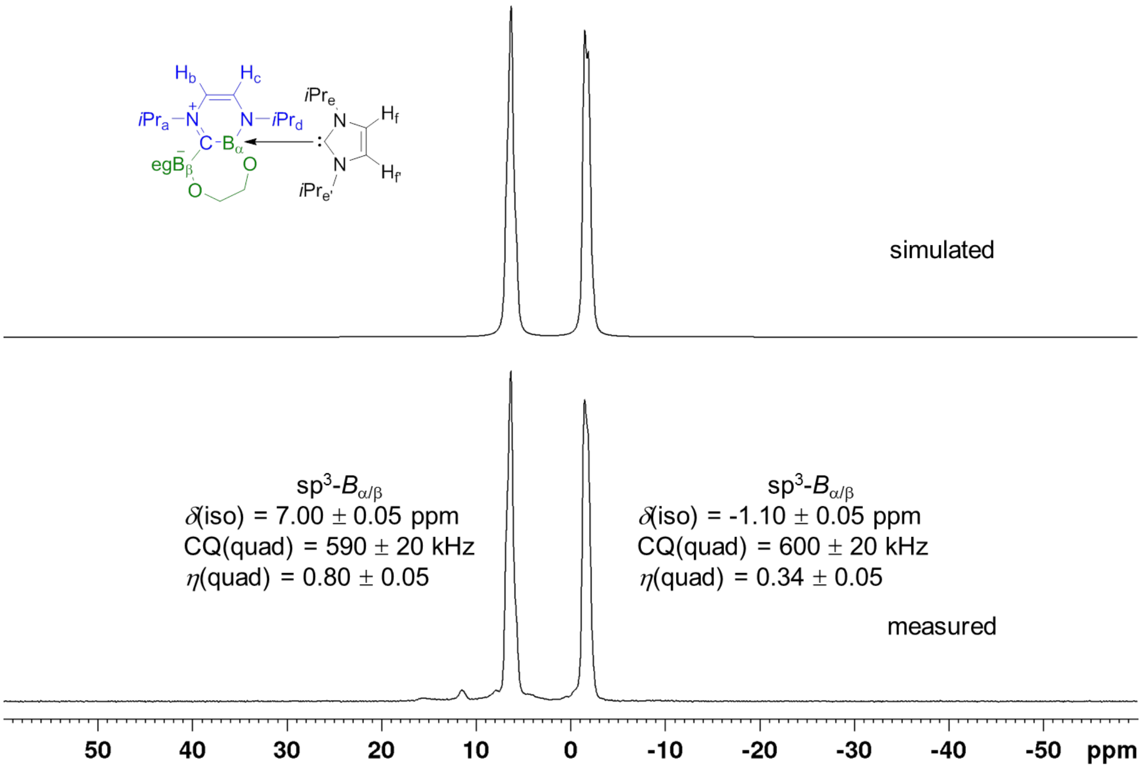

Figure S53: ^{11}B RSHE/MAS NMR spectrum of compound **15** (128 MHz, 22 °C, v rot = 15000 Hz).

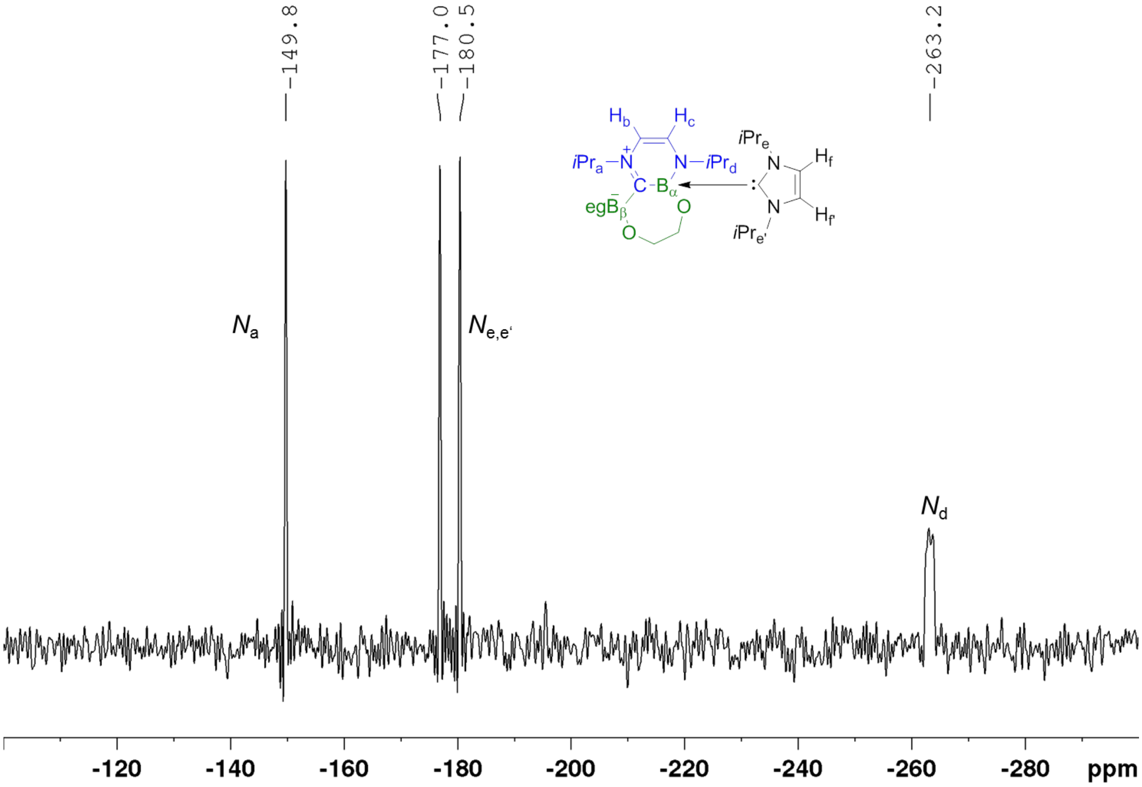

Figure S54: ^{15}N CP/MAS NMR spectrum of compound **15** (41 MHz, 22 °C, v rot = 8000 Hz).

1.13 Solution *in situ* NMR spectra of compound **16** RER-B_2eg_2•(Me_2Im^{Me})$_2$

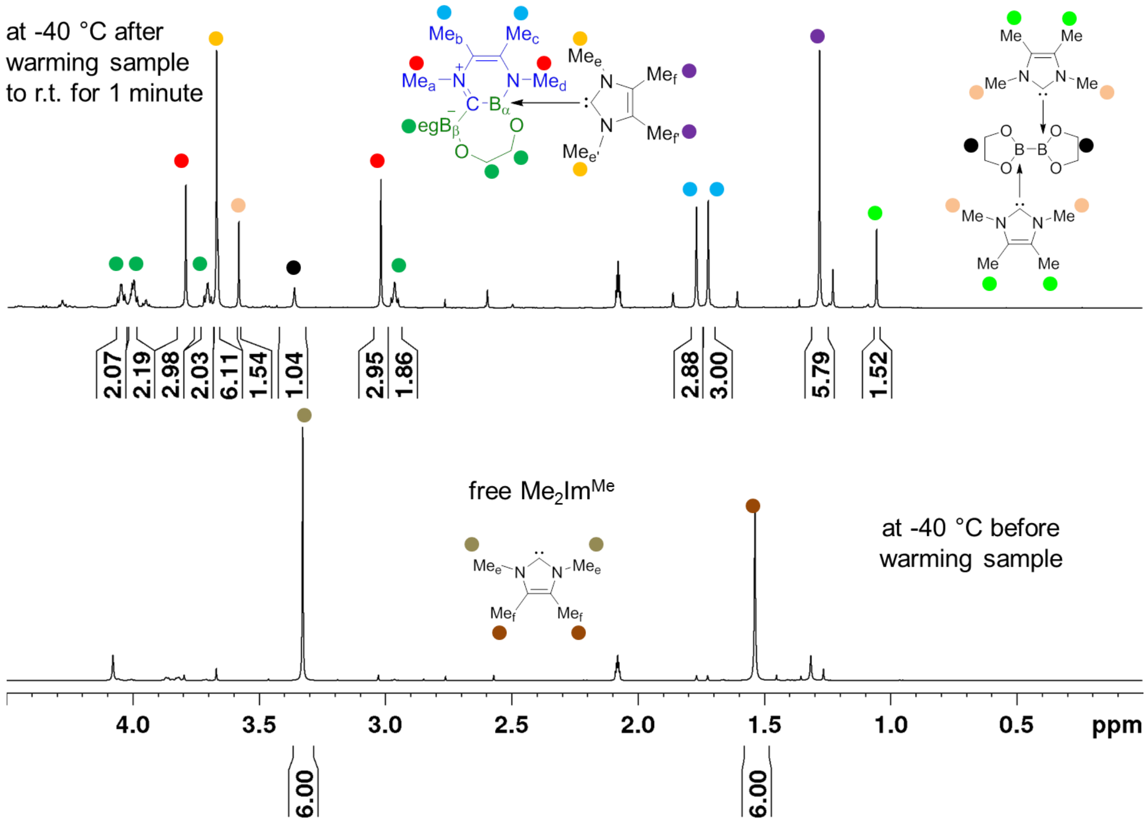

Figure S55: ^{1}H NMR *in situ* NMR spectra of compound **16** in toluene-d_8 (500 MHz, -40 °C).

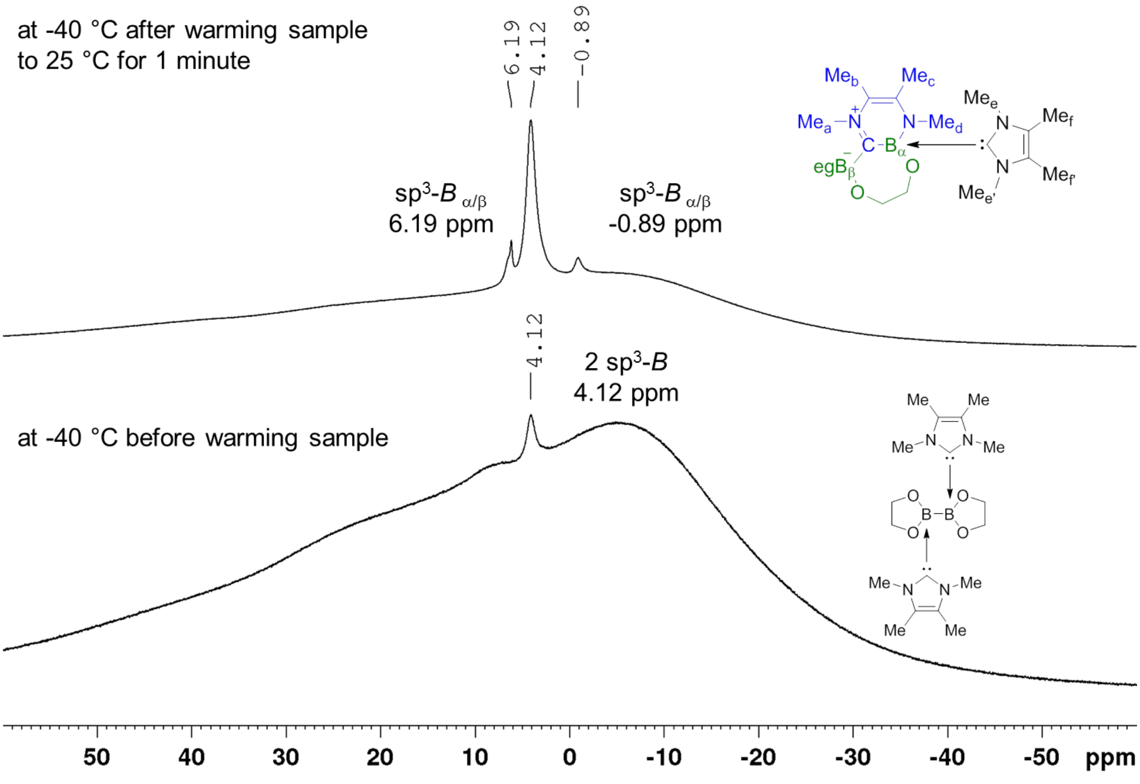

Figure S56: ^{11}B{^{1}H} NMR *in situ* spectra of compound **16** in toluene-d_8 (160 MHz, -40 °C).

1.14 Solid state NMR spectra of the product from the reaction of B_2eg_3 with *i*Pr_2Im

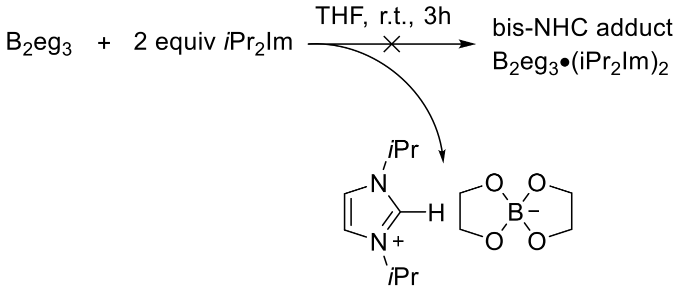

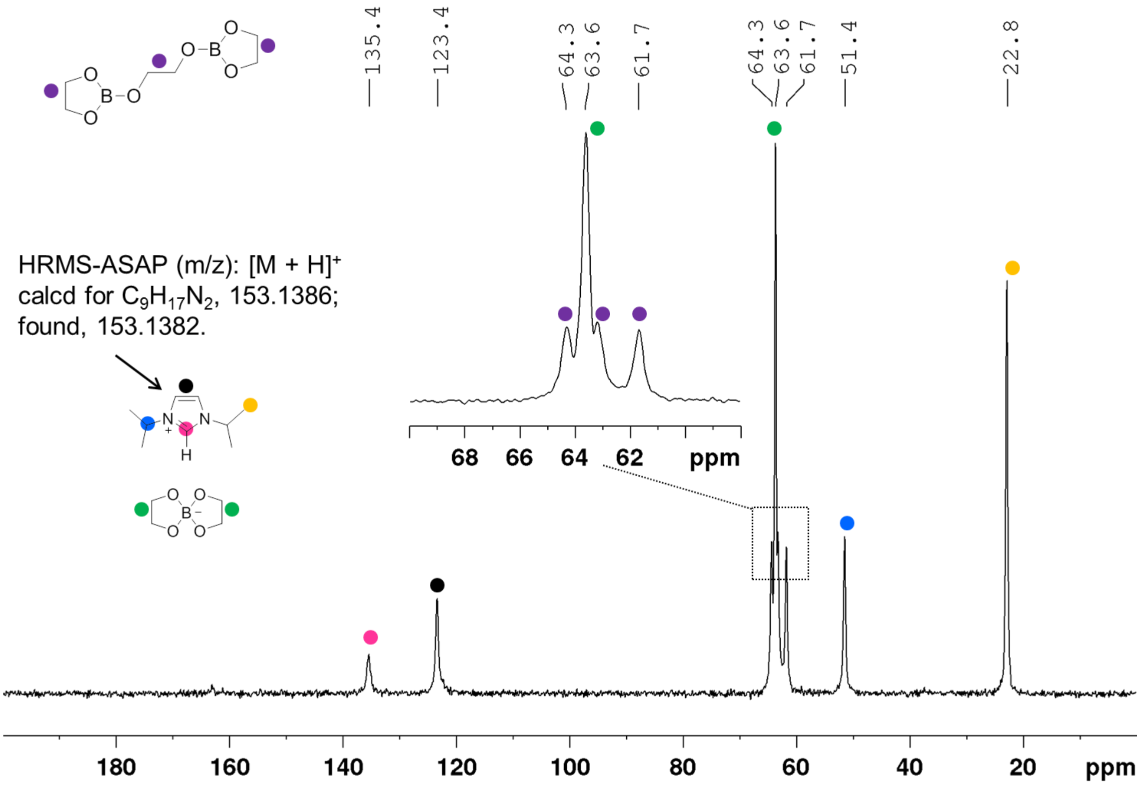

HRMS-ASAP (m/z): $[M + H]^+$ calcd for $C_9H_{17}N_2$, 153.1386; found, 153.1382.

Figure S57: ^{13}C CP/MAS NMR spectrum (101 MHz, 22 °C, v rot = 10000 Hz).

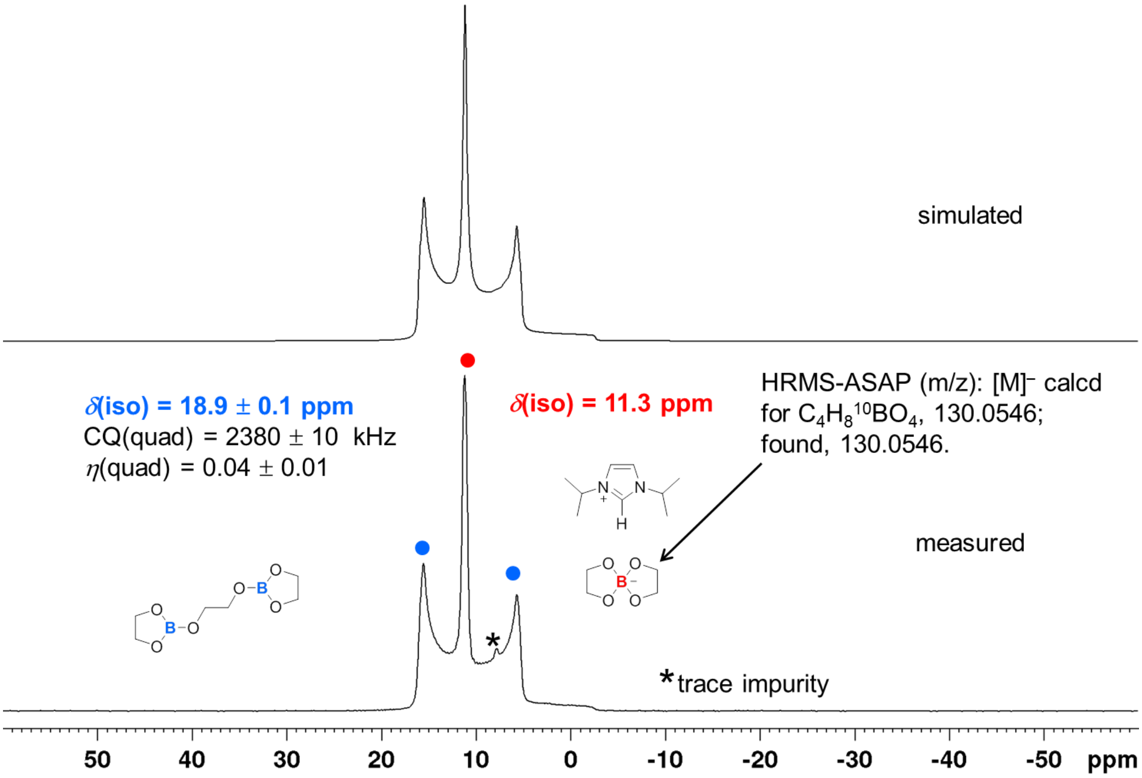

Figure S58: ^{11}B RSHE/MAS NMR spectrum (128 MHz, 22 °C, v rot = 15000 Hz).

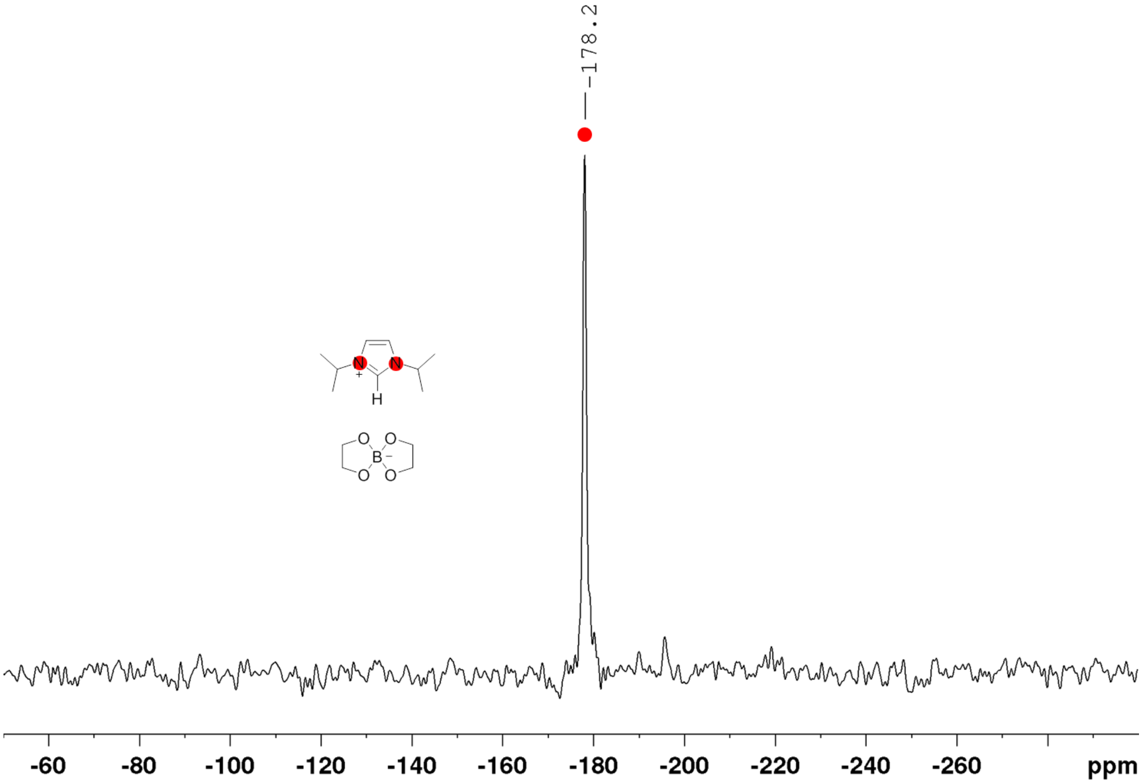

Figure S59: ^{15}N CP/MAS NMR spectrum (41 MHz, 22 °C, v rot = 8000 Hz).

1.15 High resolution mass spectra of the isolated solid from the reaction of B_2eg_3 with *i*Pr_2Im

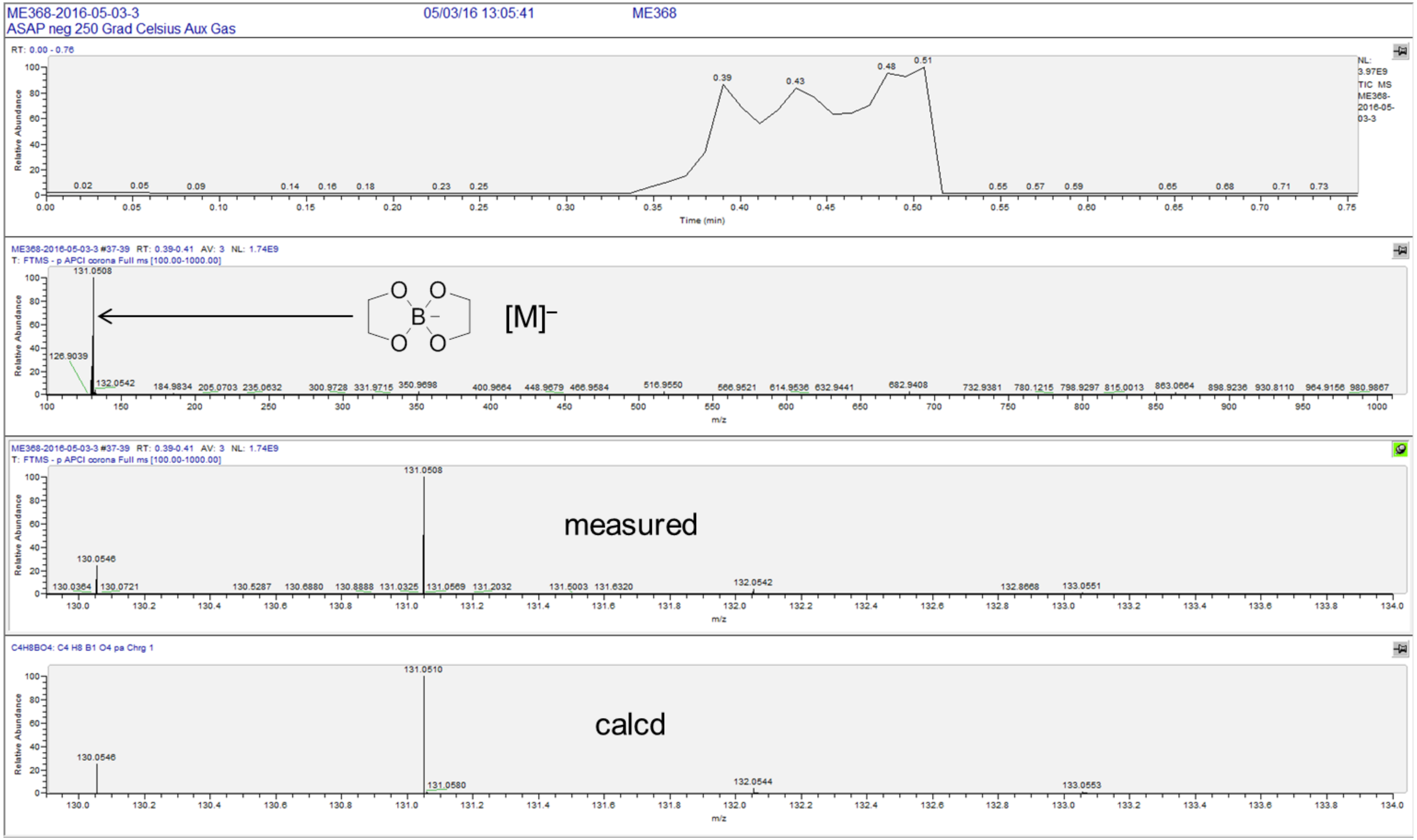

Figure S60: HRMS spectrum; ASAP negative at 250 °C.

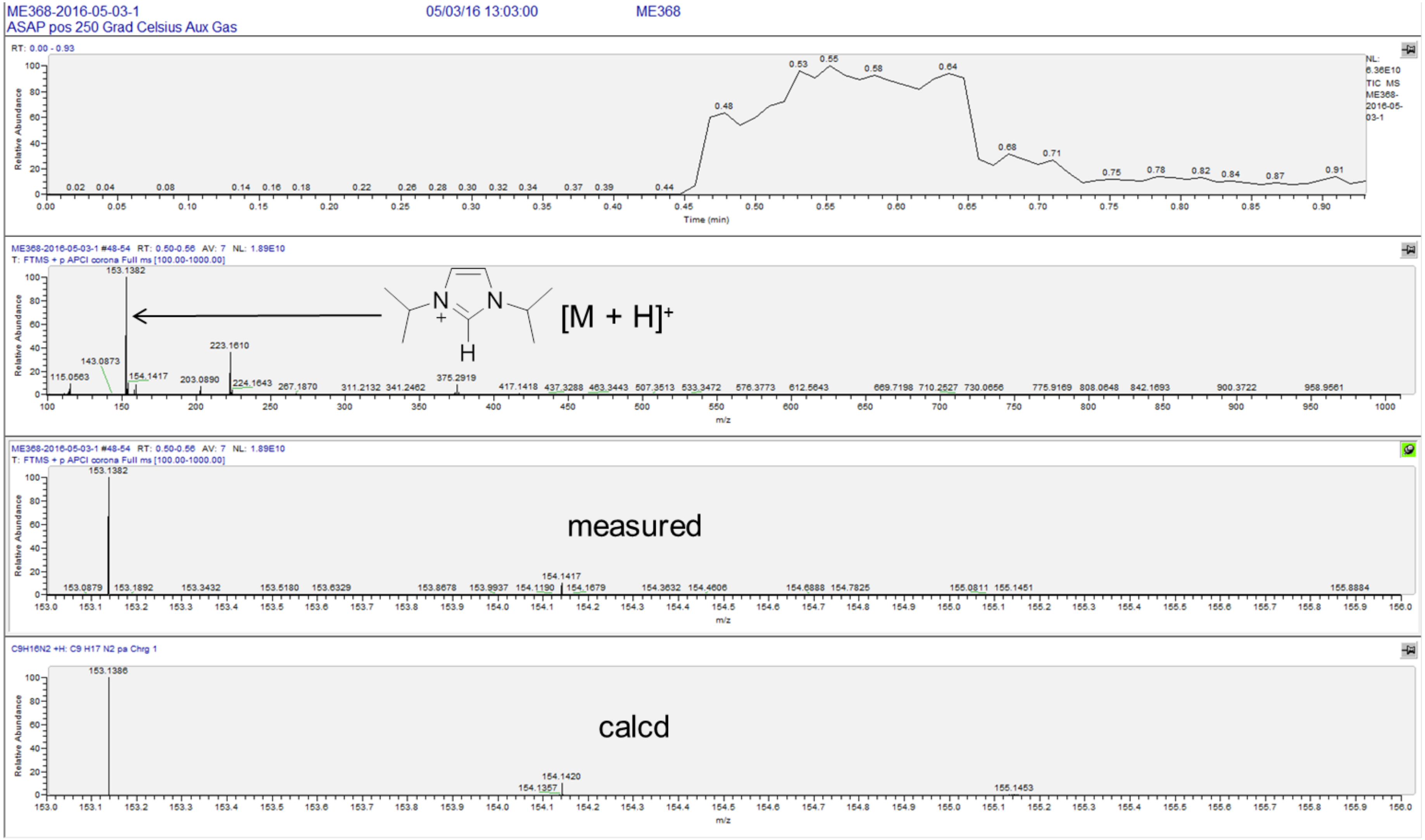

Figure S61: HRMS spectrum; ASAP positive at 250 °C.

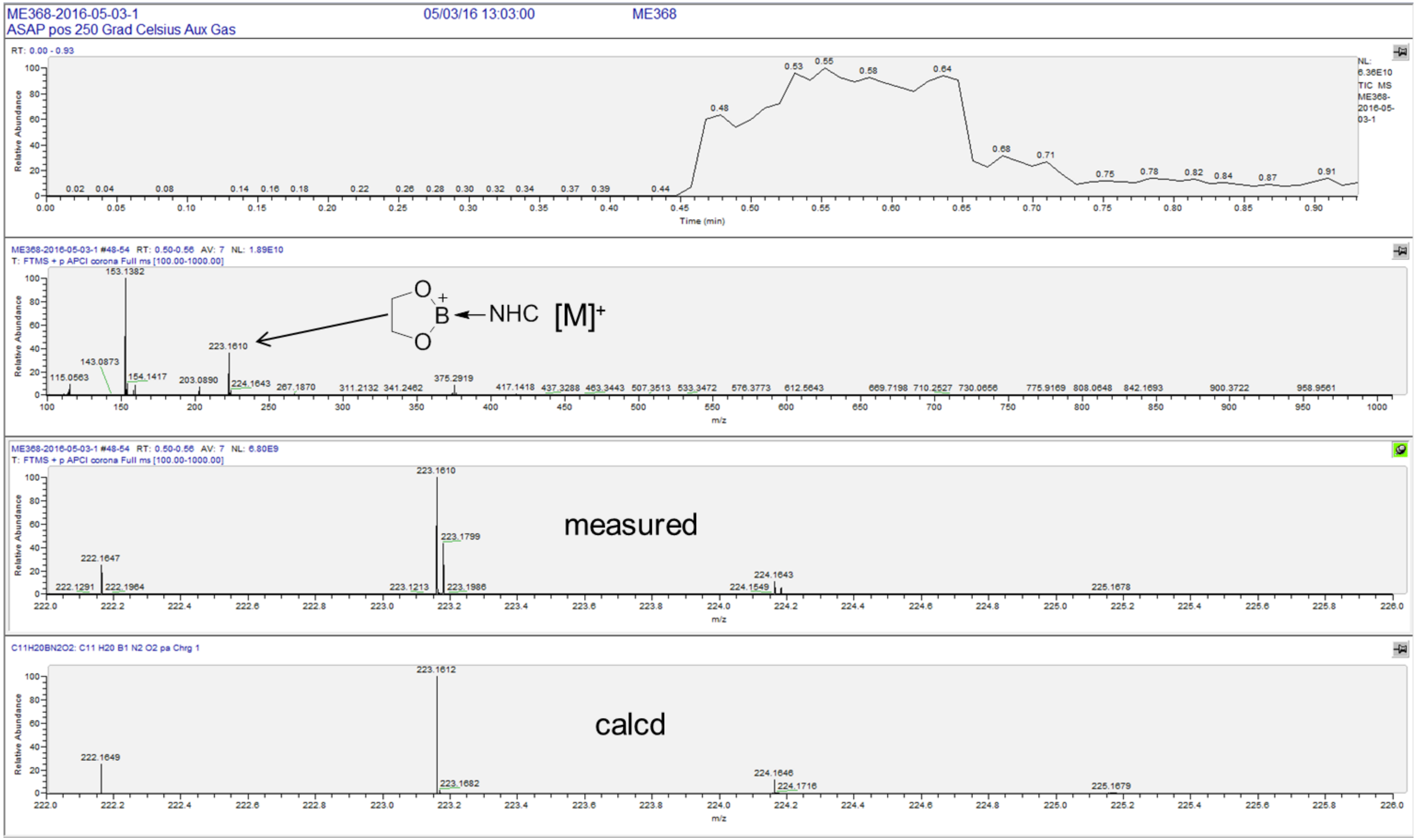

Figure S62: HRMS spectrum; ASAP positive at 250 °C.

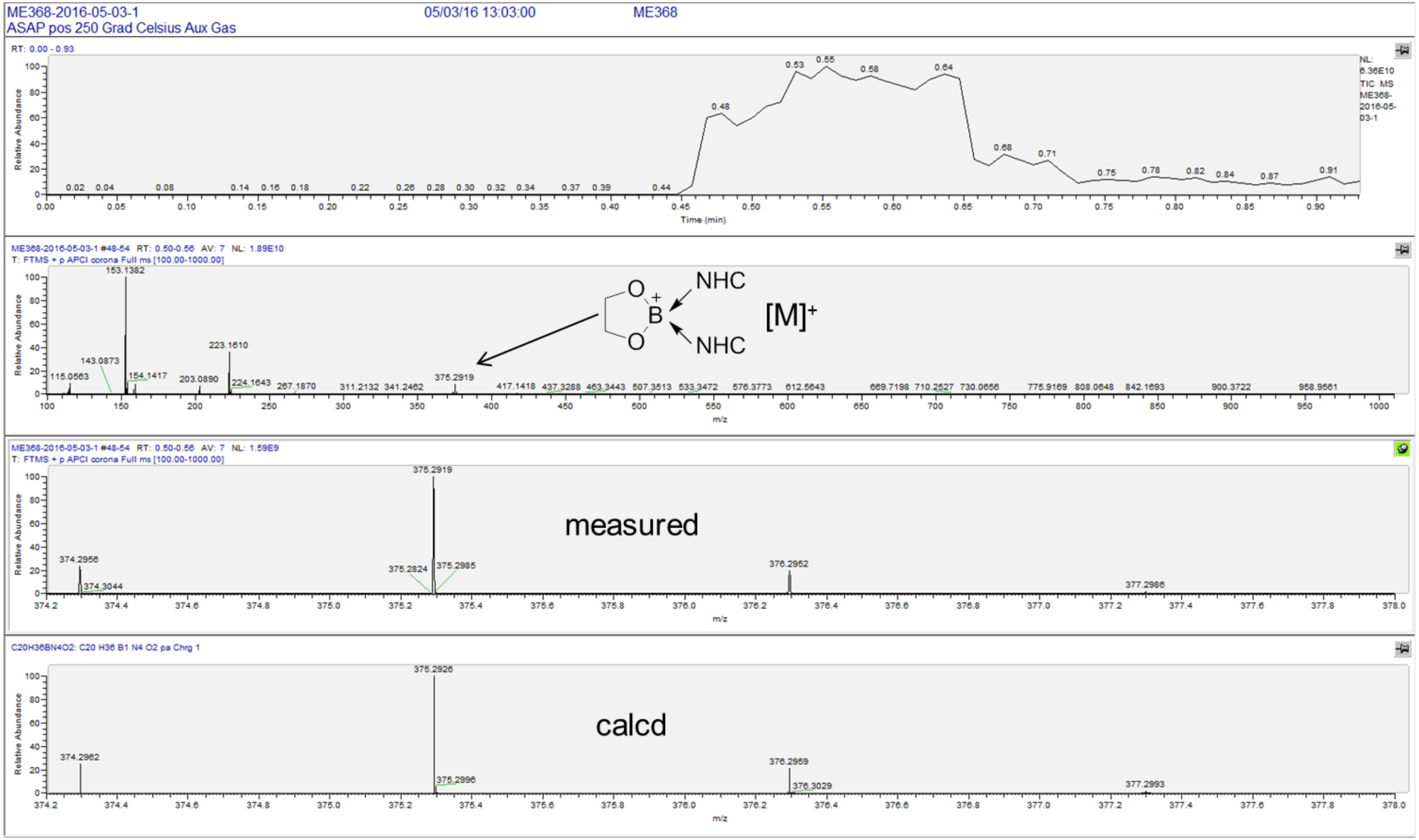

Figure S63: HRMS spectrum; ASAP positive at 250 °C.

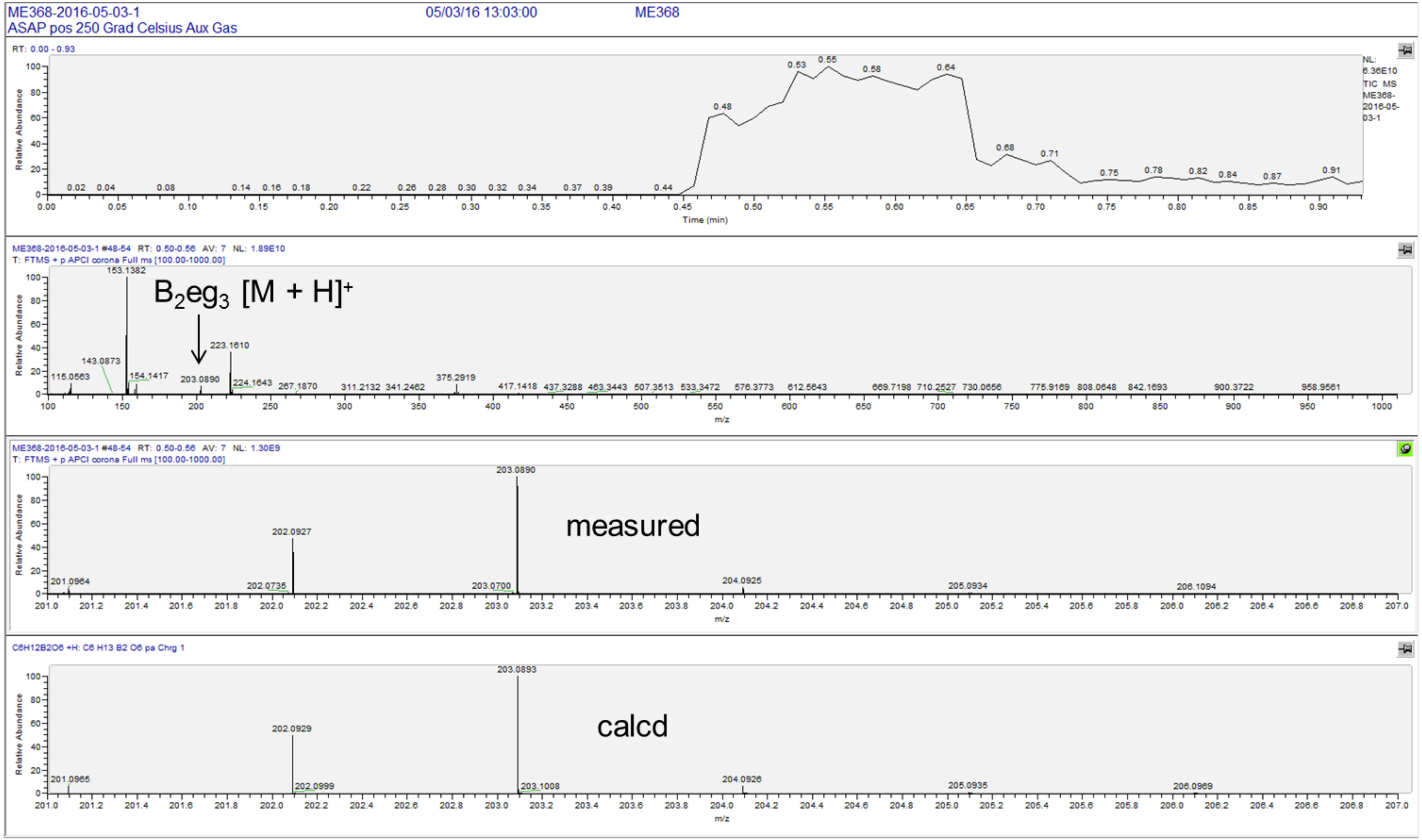

Figure S64: HRMS spectrum; ASAP positive at 250 °C.

1.16 Solid state NMR spectra of compound **18** tris(ethylene glycol) diborate (B_2eg_3)

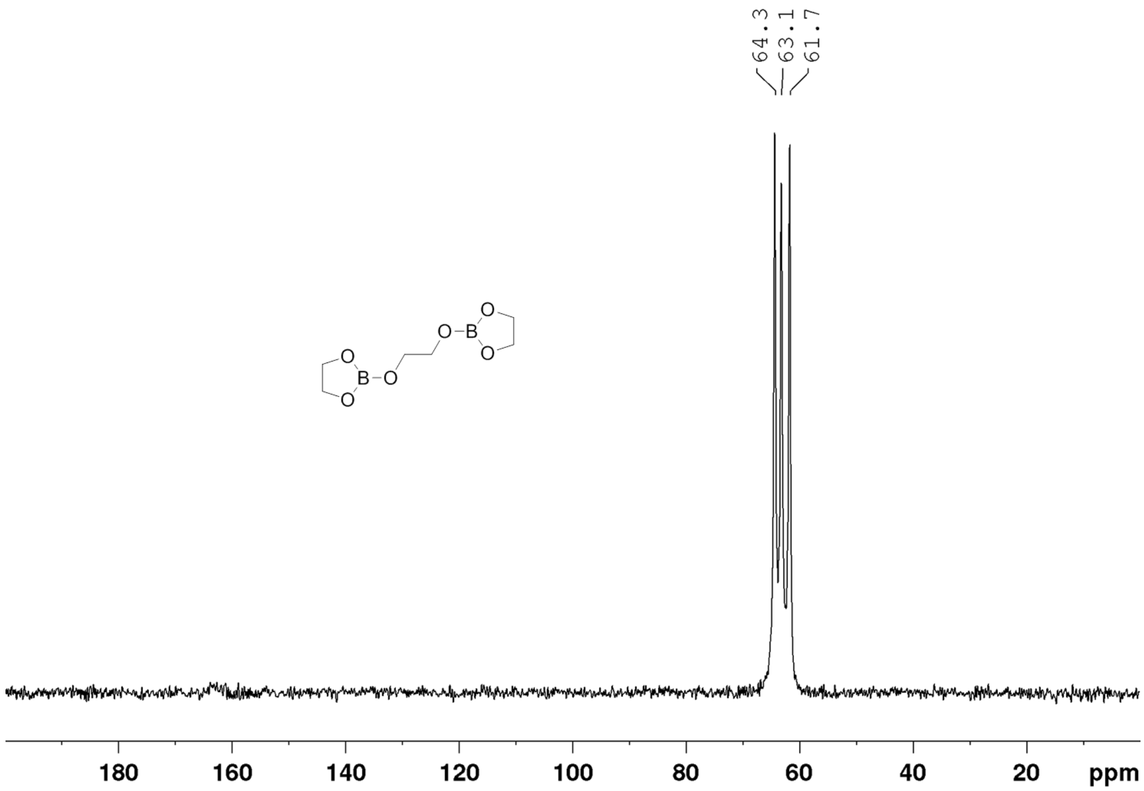

Figure S65: ^{13}C CP/MAS NMR spectrum of compound **18** (101 MHz, 22 °C, v rot = 10000 Hz).

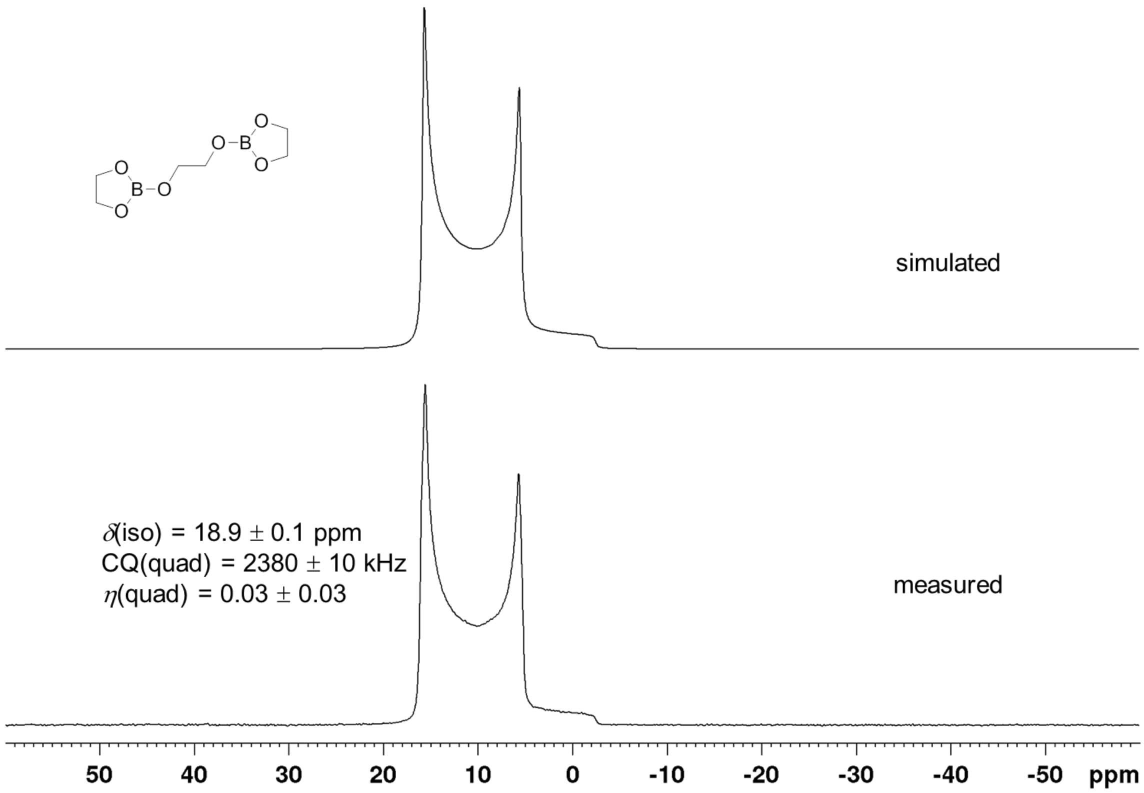

Figure S66: ^{11}B RSHE/MAS NMR spectrum of compound **18** (128 MHz, 22 °C, v rot = 15000 Hz).

1.17 Solid state NMR spectra of compound **19** bis-NHC adduct B_2eg_3•$(Me_2Im^{Me})_2$ + ($[Me_2Im^{Me}\text{-}H]^+[Beg_2]^-$)

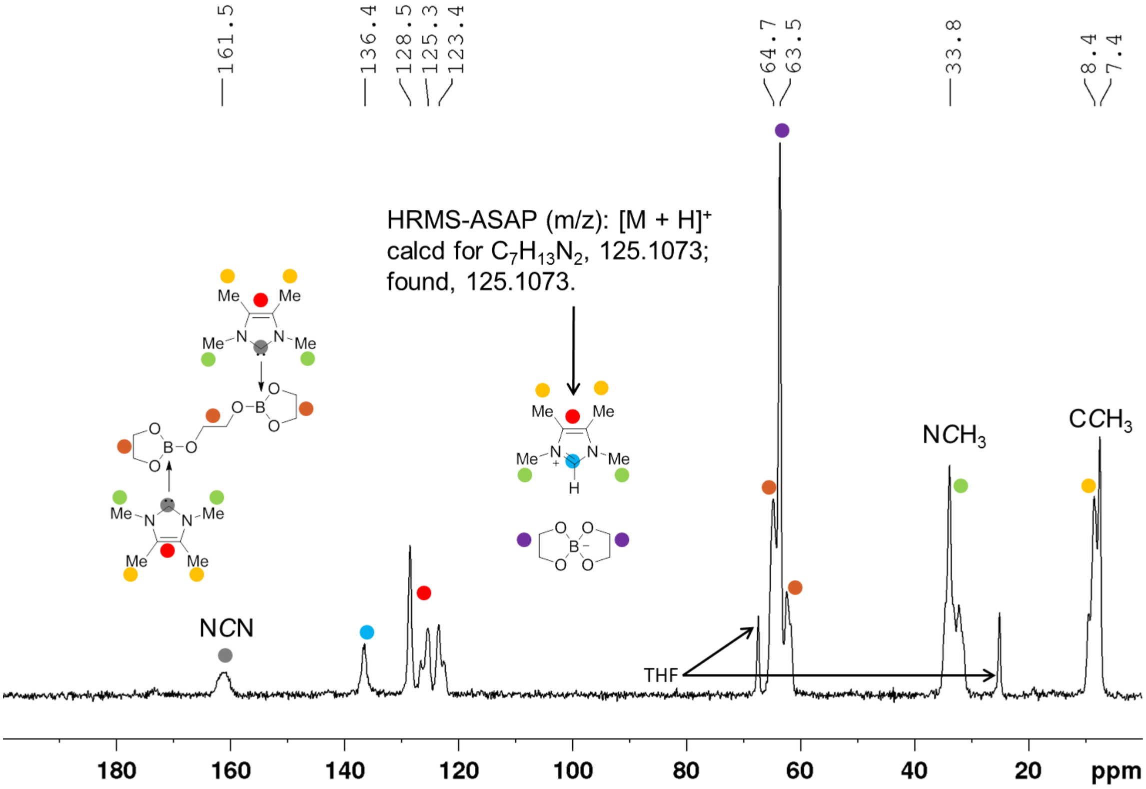

HRMS-ASAP (m/z): $[M + H]^+$ calcd for $C_7H_{13}N_2$, 125.1073; found, 125.1073.

Figure S67: ^{13}C CP/MAS NMR spectrum of compound **19** (101 MHz, 22 °C, v rot = 11000 Hz).

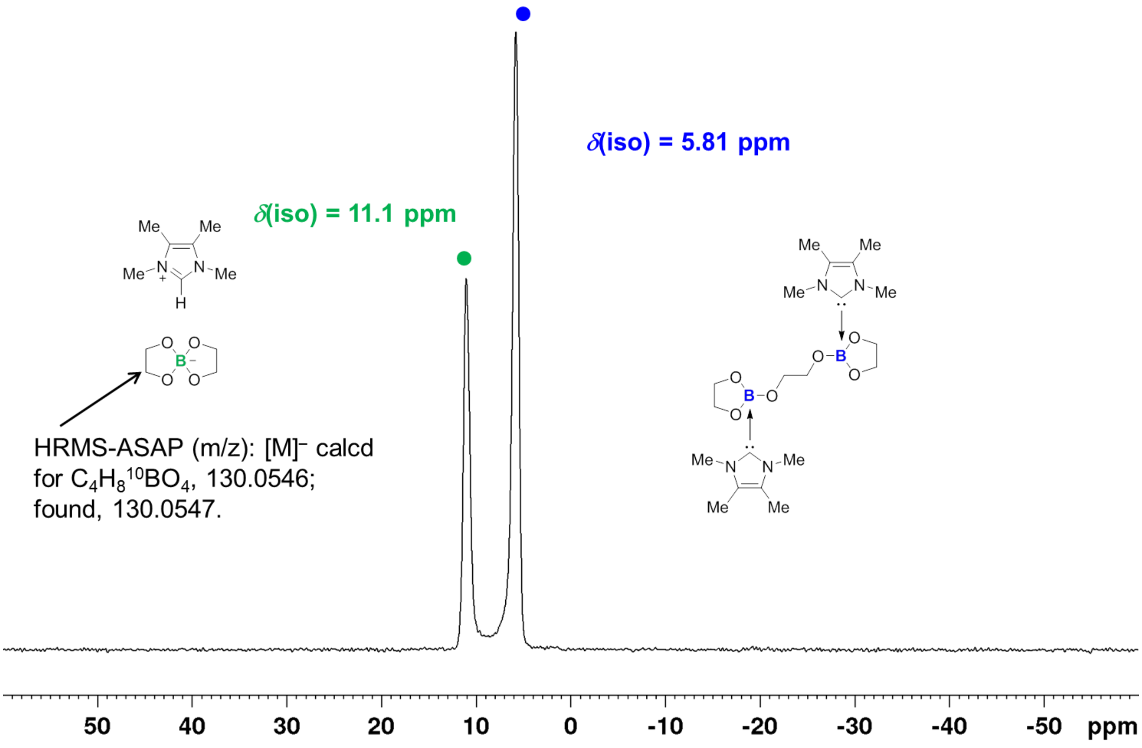

HRMS-ASAP (m/z): $[M]^-$ calcd for $C_4H_8{}^{10}BO_4$, 130.0546; found, 130.0547.

Figure S68: ^{11}B RSHE/MAS NMR spectrum of compound **19** (128 MHz, 22 °C, v rot = 15000 Hz).

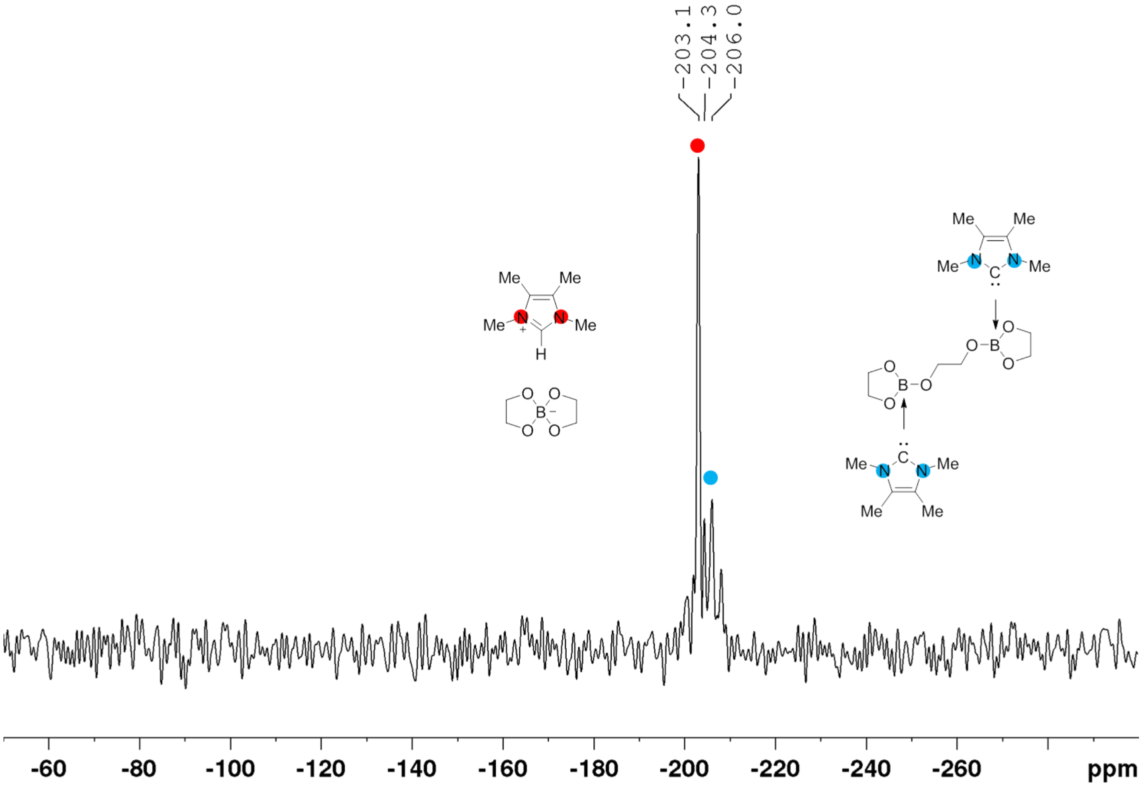

Figure S69: ^{15}N CP/MAS NMR spectrum of compound **19** (41 MHz, 22 °C, v rot = 8000 Hz).

1.18 High resolution mass spectra of the isolated solid from the reaction of B_2eg_3 with Me_2Im^{Me}

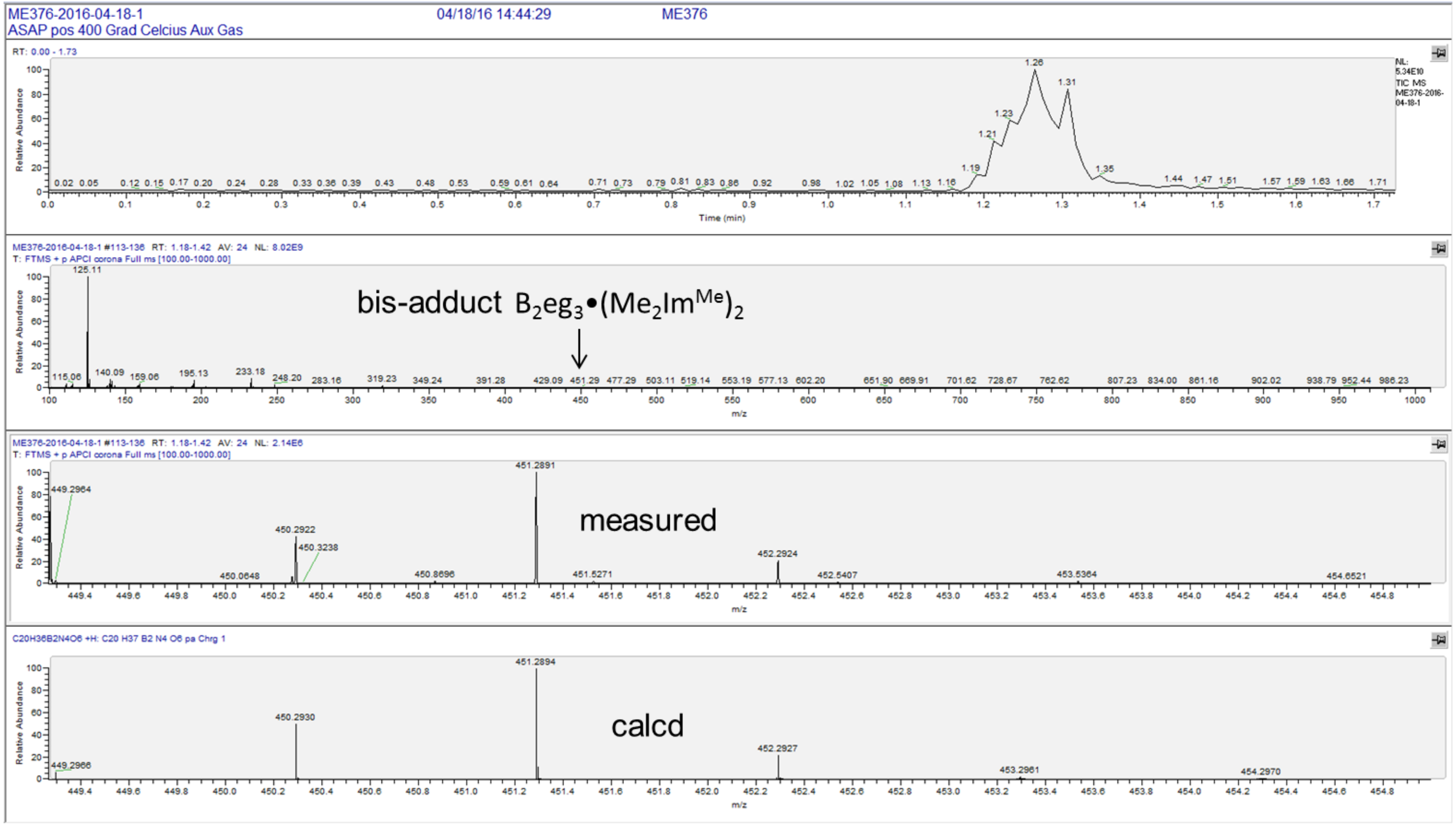

Figure S70: HRMS spectrum; ASAP positive at 400 °C.

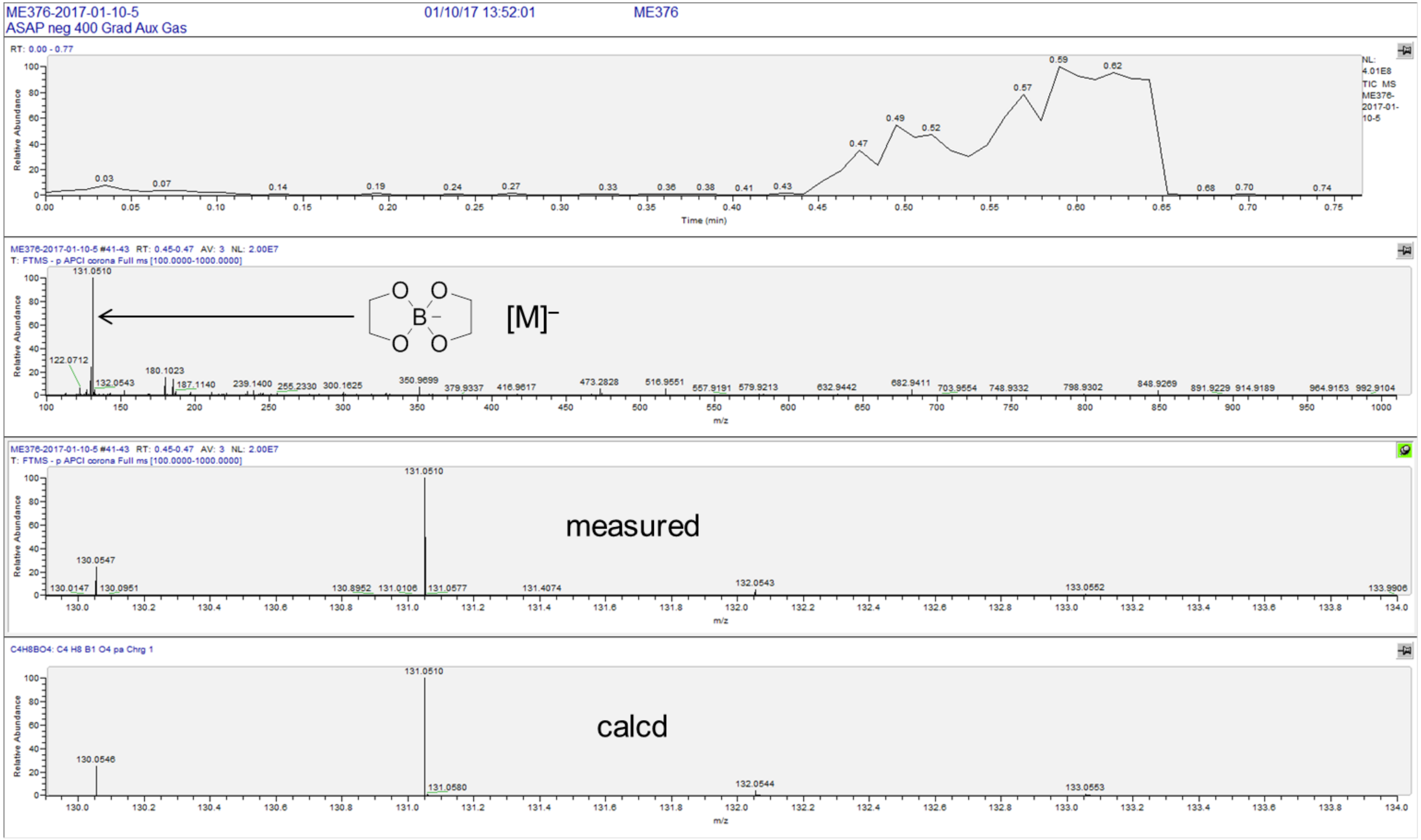

Figure S71: HRMS spectrum; ASAP negative at 400 °C.

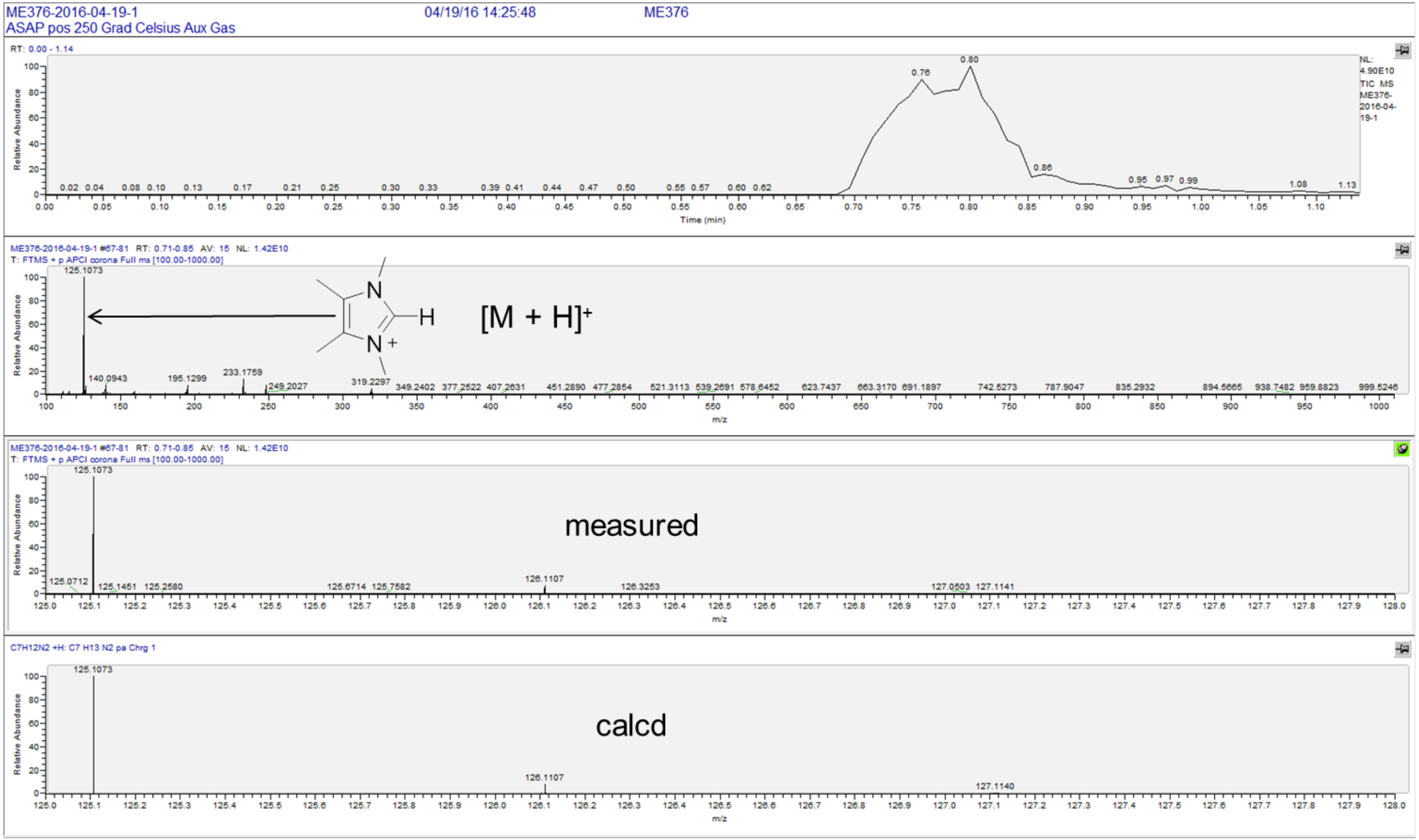

Figure S72: HRMS spectrum; ASAP positive at 250 °C.

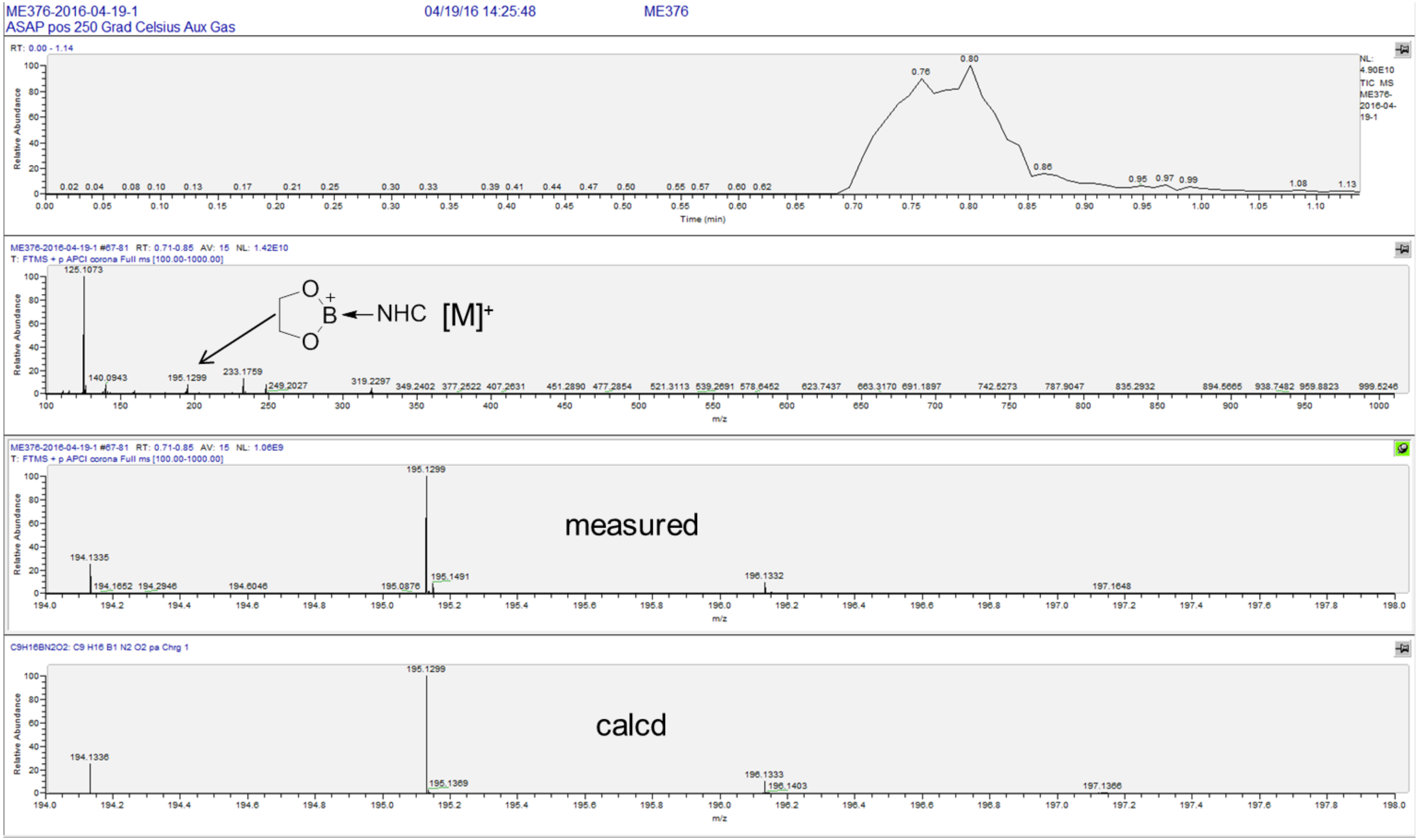

Figure S73: HRMS spectrum; ASAP positive at 250 °C.

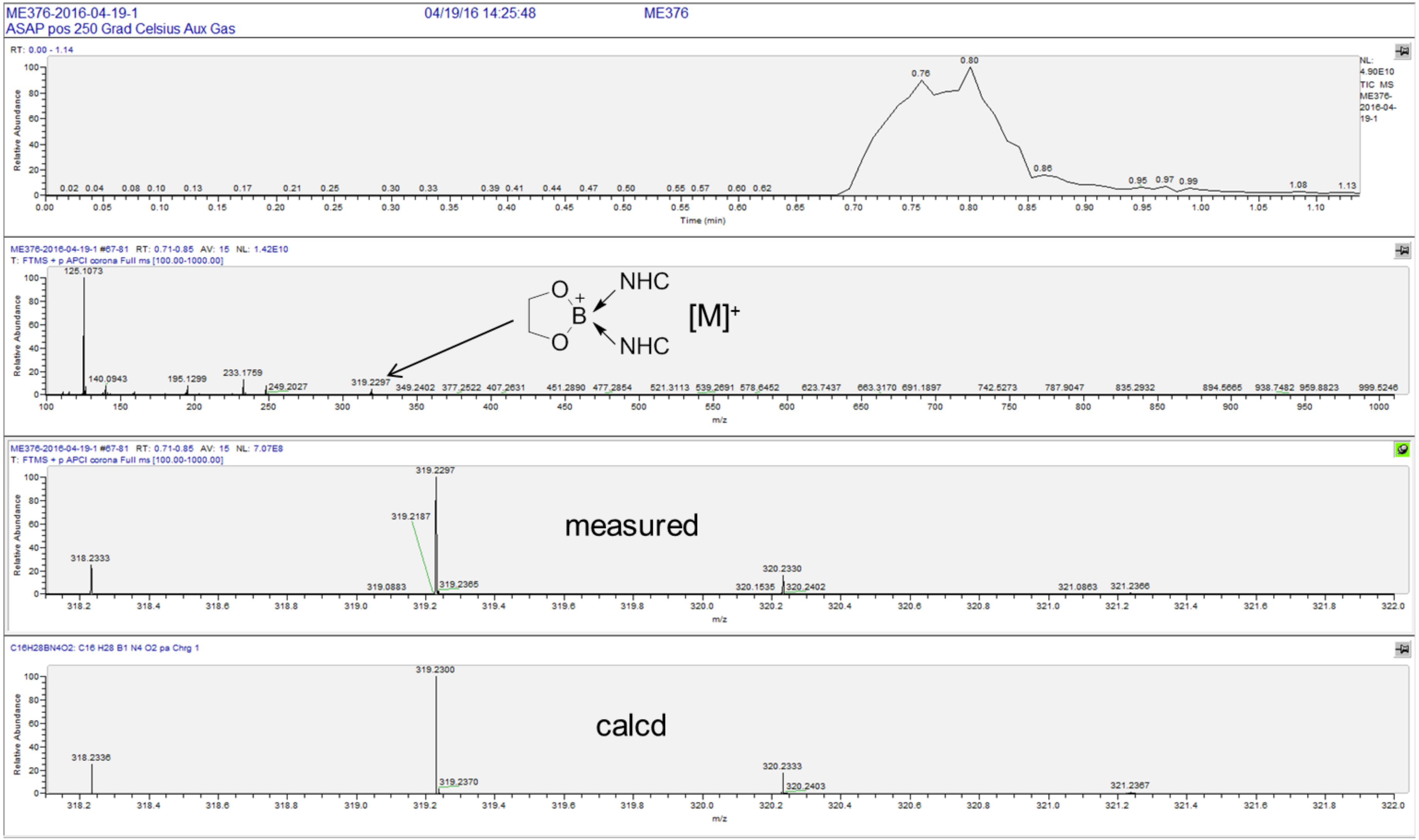

Figure S74: HRMS spectrum; ASAP positive at 250 °C.

1.19 Solution $^{11}B\{^{1}H\}$ NMR spectra of selected diboron(4) compounds (**1-5**)

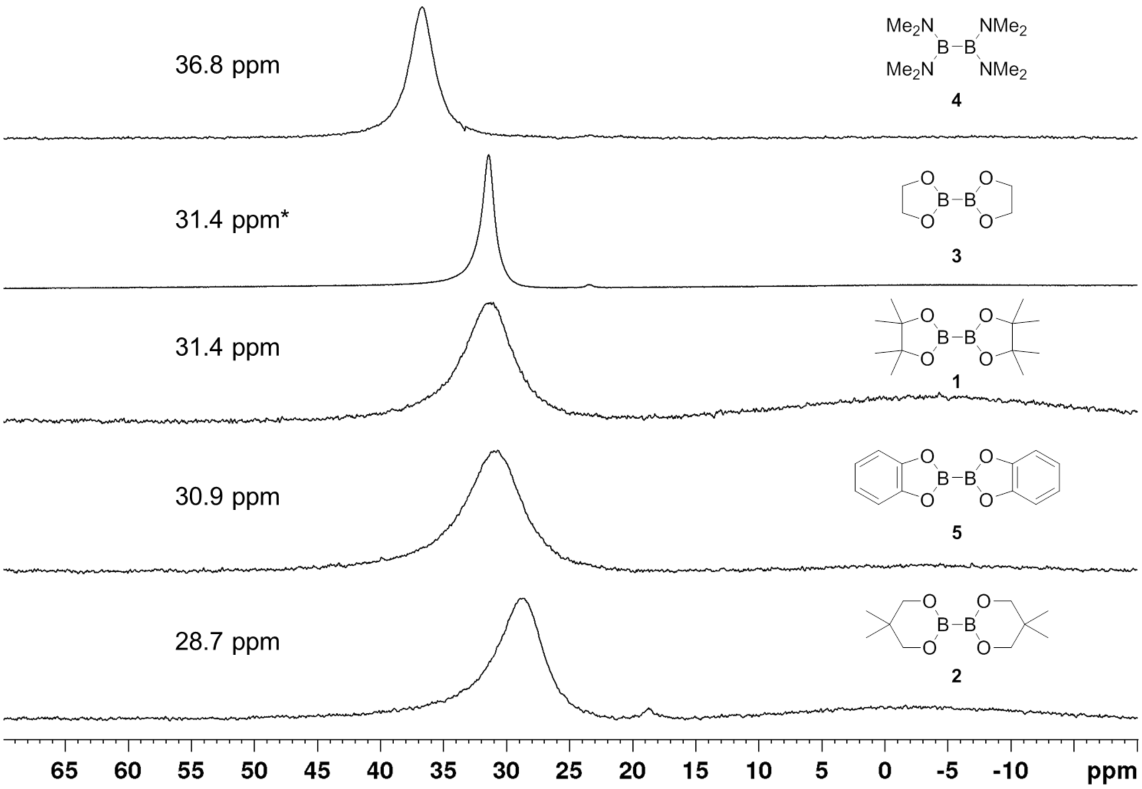

Figure S75: $^{11}B\{^{1}H\}$ NMR spectra of compound **1-5** in C_6D_6 (64 MHz, *96 MHz, 25 °C).

2 X-ray Structure Determination Data

2.1 Crystallographic data collection parameters for compound **1-4**

Table S1. Crystallographic data collection parameters for B_2pin_2, B_2neop_2, B_2eg_2 and $B_2(NMe_2)_2$

	B_2pin_2 (**1**)	B_2neop_2[a] (**2**)	B_2eg_2 (**3**)	$B_2(NMe_2)_2$[b] (**4**)
Chemical Formula	$C_{12}H_{24}B_2O_4$	$C_{10}H_{20}B_2O_4$	$C_4H_8B_2O_4$	$C_8H_{24}B_2N_4$
Formula mass ($g{\cdot}mol^{-1}$)	253.93	225.88	141.72	197.93
Crystal shape	fragment of prism	prism	column	conical[b]
Temp. (K)	100(2)	100(2)	120(2)	185(2)
μ (mm^{-1}), Radiation	0.082, MoK_α	0.088, MoK_α	0.123, MoK_α	0.060, MoK_α
Crystal system	monoclinic	monoclinic	monoclinic	monoclinic
Space group (no.)	*I*a (9)	$P2_1/n$ (14)	$P2_1/c$ (14)	$P2_1/c$ (14)
Z, Z'	8, 2	8, 2	2, ½	4, 1
a (Å)	10.1407(7)	15.2894(3)	3.9115(11)	9.4204(5)
b (Å)	14.8953(9)	8.7342(4)	8.015(3)	8.8439(6)
c (Å)	19.4745(10)	19.2066(10)	10.187(3)	16.0580(8)
α (°)	90	90	90	90
β (°)	98.798(5)	105.807(6)	99.939(11)	99.851(5)
γ (°)	90	90	90	90
Volume ($Å^3$)	2907.0(3)	2467.9(2)	314.57(17)	1318.12(13)
ρ_{calcd} ($g{\cdot}cm^{-3}$)	1.160	1.216	1.496	0.997
GooF on F^2	1.037	0.960	1.040	1.164
R_{int}	0.0593	0.0397[a]	0.0307	0.0440
R_1 [$I > 2\sigma(I)$]	0.0558	0.0430	0.0350	0.0589
wR_2 (all data)	0.1492	0.1373	0.0974	0.1587
Largest peak/hole ($e{\cdot}Å^{-3}$)	0.323/–0.349	0.530/–0.288	0.300/–0.209	0.214/–0.139
CCDC no.	1515555	1515553	1515550	1515554

[a] The crystal is non-merohedrally twinned; see below for further details. The R_{int} refers to the dataset that was used for structure solution. [b] The crystal was obtained by *in situ* crystallisation in a capillary on the diffractometer; see below for further details.

2.2 Structure determination of compound **1** B_2pin_2

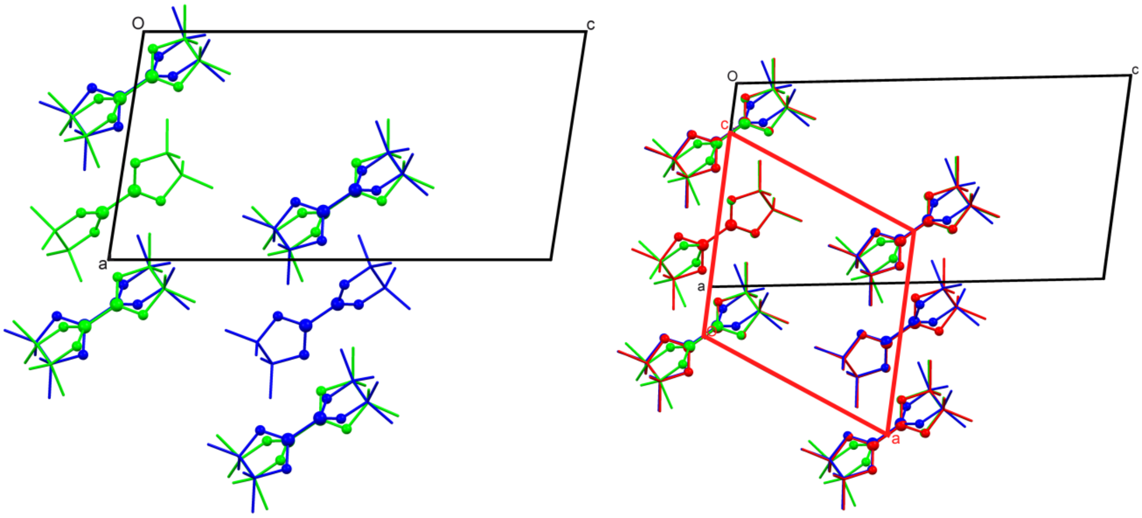

Figure S76. *left:* Detail of the packing pattern of the structure of B_2pin_2 in the *Ia* unit cell at 100 K; the two independent molecules are shown in blue and green. *right:* overlay of the structures of B_2pin_2 in the *Ia* unit cell at 100 K (blue and green) and of the structure at 120 K (red) in $P2_1/c$.[S1] Disorder omitted for clarity.

The single crystals of B_2pin_2 were obtained by cooling a solution in *n*-pentane to –40 °C.

B_2pin_2 undergoes a phase transition at about 103 K, at which the unit cell changes from a primitive monoclinic cell at higher temperatures to a monoclinic *I*-centred unit cell. During the phase transition the inversion symmetry of the sites of the B_2pin_2 molecules vanished. This reduction in symmetry is consequently accompanied by a change in the asymmetric unit. Above 103 K, the asymmetric unit consists of half a molecule of B_2pin_2, whereas at 100 K, two distinct sites are occupied by two inequivalent B_2pin_2 molecules (blue and green in Figure S75). However, during the phase transition the relative arrangement of the B_2pin_2 moieties does not change appreciably (Figure S75 right). Formally, the cell at lower temperatures in *Ia* can be deduced from the one at higher temperatures in $P2_1/c$ by the transformation

$P2_1/c$ at 120 K[S1]	**transformation (dir. axes)**	***Ia* at 100 K**
a = 10.2834(9) Å	a´ = – c	a´= 10.1407(7) Å
b = 7.4809(6) Å	b´ = 2 b	b´= 14.8953(9) Å
c = 10.1672(8) Å	c´ = 2 a + c	c´= 19.475(1) Å
γ = 110.48(1)°		γ´= 98.798(5)°

along with a shift of the origin.

One of the Bpin moieties in each molecule of B_2pin_2 shows positional disorder that was refined by applying split-atom models. The occupancy factors refined to 0.47(2) (Bpin moiety containing B2) and 0.52(1) (Bpin moiety containing B2A), respectively. Note that for several other crystals studied under identical conditions, the here not-disordered Bpin moieties also showed some disorder; typically in a ratio of <1:5.

2.3 Structure determination of compound **2** B_2neop_2

R3m **at 140 K** (CCDC no. 1515551)

a = 8.8506(11) Å
b = 8.8506(11) Å
c = 13.791(2) Å
V = 935.6(3) Å^3
R_{int} = *0.0282*
wR_2 = *0.1121*
R_1 = *0.0459*

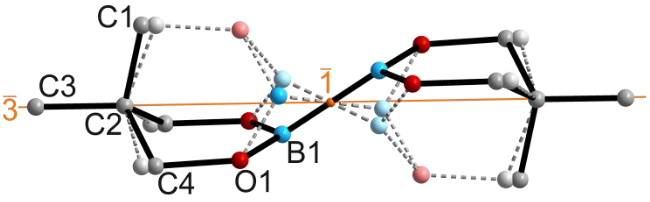

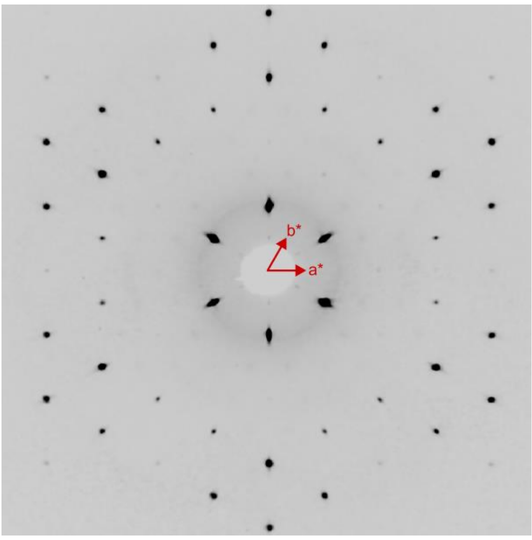

R3c **at 115 K** (CCDC no. 1515552)

a = 8.8311(5) Å
b = 8.8311(5) Å
c = 27.5396(16) Å
V = 1860.0(2) Å^3
R_{int} = *0.0327*
wR_2 = *0.1239*
R_1 = *0.0510*

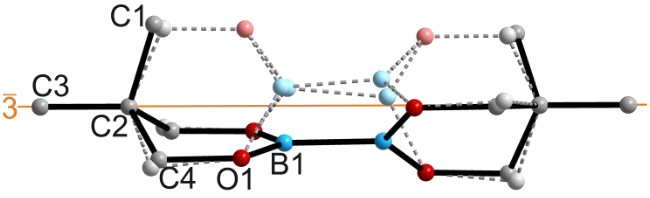

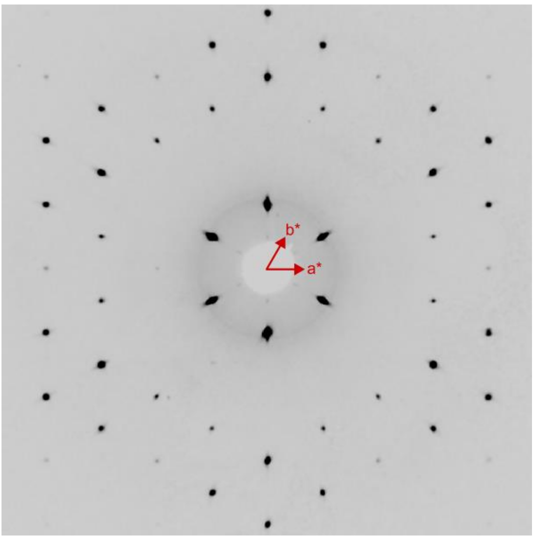

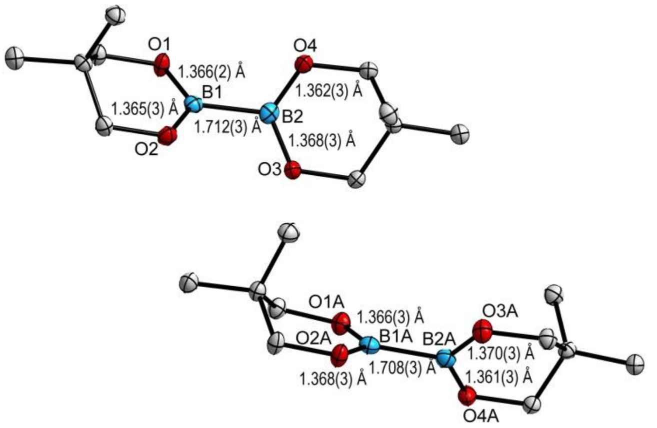

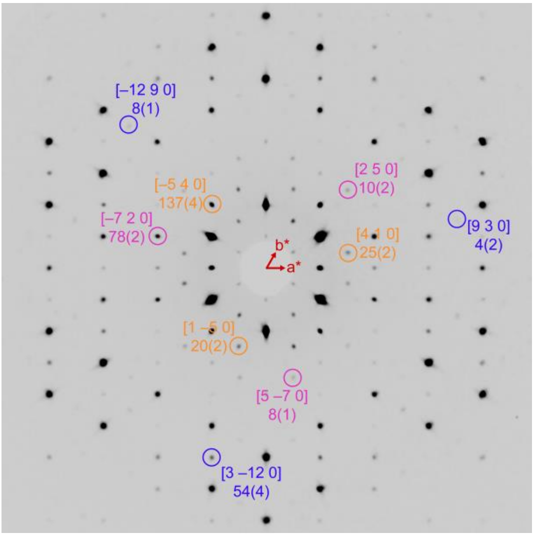

Figure S77. *top:* Apparent molecular structure of B_2neop_2 and reconstructed hk0 plane at 140 K. *middle:* Apparent molecular structure of B_2neop_2 and reconstructed hk0 plane at 115 K. Hydrogen atoms are omitted for clarity; atoms displayed as spheres with arbitrary radii. *bottom:* Molecular structure of B_2neop_2 and reconstructed hk0 plane at 100 K (trigonal cell setting). Hydrogen atoms are omitted for clarity; thermal ellipsoids drawn at the 50% probability level.

The single crystals of B_2neop$_2$ were obtained by gas-phase diffusion of *n*-hexane into a solution in C_6H_6 at ambient temperature.

B_2neop$_2$ undergoes two phase transitions upon cooling from 140 K to 100 K. At 140 K, a structure in $R\bar{3}m$ is found, identical to the one reported at 160 K.[S2] The molecular structure suffers from severe disorder over three sites due to the B_2neop$_2$ being situated on a 3-fold axis and on an inversion centre, hence, on positions with a site symmetry of $\bar{3}$ (Figure S76 top). This high imposed symmetry results in severe disorder and finally an implausible apparent conformation of the B_2neop$_2$ molecule reflected in pyramidalisation at the boron atoms and unexpected bond lengths (see main text).[S2]

Upon lowering the temperature to 115 K, the unit cell changes by doubling of the c axis, associated with this is a change in the space group type from $R\bar{3}m$ to $R\bar{3}c$ and, with that, the site symmetry of the positions of the B_2neop$_2$ is accordingly reduced to 3. As a consequence, a more plausible conformation of the B_2neop$_2$ molecules is now found, albeit still disordered over three sites (Figure S76 middle).

Finally, upon cooling to 100 K, the cell axes *a*, *b* and *c* are doubled resulting in a metrically trigonal cell:

a = 17.6263(4) Å
b = 17.4821(5) Å
c = 55.388(1) Å
$\alpha = \beta = 90°$
$\gamma = 120°$
V = 14818.3(5) Å

However, closer inspection of the diffraction pattern shows that the intensity of – assuming a Laue group of $\bar{3}m1$ – equivalent reflections agree poorly (Figure S76 bottom right). This supports an alternative description of the diffraction pattern as a 3-component twin by 120° and 240° rotation about the reciprocal c* axis of a monoclinic cell:

P*2$_1$/*n	**transformation (rec. axes)**
a' = 15.2894(8) Å	$a^{*\prime} = -2a^* - c^*$
b' = 8.7342(4) Å	$b^{*\prime} = 2b^* - a^*$
c' = 19.207(1) Å	$c^{*\prime} = 3c^*$
β = 105.807(6)°	
V = 2467.9(2) Å	

This description allows a well-behaved refinement of the structure of B_2neop$_2$ without any disorder; bond lengths and angles are now in the expected ranges (see main text). The twin factors refined to 0.1576(8) and 0.1083(7); for further refinement parameters see Table S1. Note that the twin factors change depending on the treatment of the particular crystal. Annealing by repeated heating and cooling in a temperature range of 110 K to 100 K (three cycles, 5 K/30 min) was found to give the most favourable twin ratios.

2.4 Structure determination of compound **4** $B_2(NMe_2)_4$

$B_2(NMe_2)_4$, a liquid at ambient temperature, was crystallised within a capillary *in situ* on the diffractometer. Pure, freshly distilled $B_2(NMe_2)_4$ (ca. 0.1 μL) was filled into a glass capillary of 1.0 mm outer diameter that narrows at one end into a cone. The capillary was flame sealed and glued onto a brass pin that was mounted on the goniometer head. A part of the conical section of the capillary was centred in the X-ray beam (0.5 mm diameter), so that a conical section of the capillary filled with $B_2(NMe_2)_4$ was exposed to the X-ray beam (bottom diameter: 0.42 mm, top diameter: 0.19 mm).

The temperature was gradually (within 3 h) lowered from r.t. to 200 K whereupon the $B_2(NMe_2)_4$ crystallised upon shock-cooling with a drop of liquid nitrogen; the poly-crystalline mass was found to melt at approximately 205 K. Sequences of cooling to 200 - 195 K, annealing, shock-cooling, and reheating to 210 K were performed until the diffraction pattern indicated that a single crystalline sample had formed. Finally, the temperature was lowered to 185 K.[S3]

The diffraction data were collected employing only ϕ scans in order to maintain the sample parallel to and fully immersed in the nitrogen gas stream and to ensure that the same part of the sample was measured during the entire measurement. Mechanical restrictions of the instrument used resulted in a data collection strategy using four sets of ϕ scans around 360° (each 1° in ϕ) at four different detector positions (at positive and negative angles). Each frame was exposed for 15 s at a nominal crystal to detector distance of 75 mm. To improve the statistics, this set of measurements was repeated more than twice. However, due to these restrictions, only a completeness of 92% could be reached.

Indexing was conducted considering only reflections above a resolution of 2.56 Å, where 70% of all reflections could be indexed with a single cell. Multi-component indexing with three identical cells allowed indexing of 91% of the reflections. However, a refinement including these three components did not improve the quality of the structure and was finally abandoned; only the major component was integrated and used in structure solution and refinement.

2.5 Crystallographic data collection parameters for compounds **6**, **7b**, **8**, **10**, **11**, **14**, **15**, **15'**, **17**

Table S2. Crystallographic data collection parameters for compounds **6**, **7b**, **8**

	compound **6**	compound **7b**	compound **8**
Chemical Formula	$C_{42}H_{80}B_4N_4O_8$	$C_{78}H_{92}B_4N_4O_8•C_7H_8$	$C_{39}H_{46}B_2N_2O_4•2(C_6H_6)$
Formula mass (g·mol^{-1})	812.34	1348.92	784.61
Crystal shape	block	block	needle
Temp. (K)	100(2)	100(2)	100(2)
μ (mm^{-1}), Radiation	0.073, MoK$_\alpha$	0.069, MoK$_\alpha$	0.073, MoK$_\alpha$
Crystal system	monoclinic	triclinic	orthorhombic
Space group (no.)	$P2_1/c$	$P\bar{1}$	$P2_12_12_1$
Z	4	2	4
a (Å)	19.0612(13)	12.395(2)	14.1863(9)
b (Å)	15.4007(10)	14.186(2)	16.4798(10)
c (Å)	17.5352(12)	23.450(4)	18.9462(13)
α (°)	90	90.354(4)	90
β (°)	108.309(2)	96.904(4)	90
γ (°)	90	98.937(4)	90
Volume (Å^3)	4887.0(6)	4042.6(11)	4429.4(5)
ρ_{calcd} (g·cm^{-3})	1.104	1.108	1.177
GooF on F^2	1.031	1.016	1.027
R_{int}	0.0321	0.0207	0.0502
R_1 [$I > 2\sigma(I)$]	0.0508	0.0413	0.0288
wR_2 (all data)	0.1345	0.1096	0.0689
Largest peak/hole (e·Å^{-3})	0.722/-0.338	0.395/-0.307	0.200/-0.185
CCDC no.	1529578	1529576	1529580

Table S3. Crystallographic data collection parameters for compounds **10**, **11**, **14**

	compound **10**	compound **11**	compound **14**
Chemical Formula	$C_{24}H_{37}BN_4O_2$	$C_{36}H_{44}B_2N_4O_6•2(C_6H_6)$	$C_{25}H_{32}B_2N_2O_4$
Formula mass (g·mol^{-1})	424.38	806.58	446.14
Crystal shape	block	block	block
Temp. (K)	100(2)	100(2)	100(2)
μ (mm^{-1}), Radiation	0.074, MoK$_\alpha$	0.078, MoK$_\alpha$	0.084, MoK$_\alpha$
Crystal system	triclinic	monoclinic	monoclinic
Space group (no.)	$P\bar{1}$	$P2_1/n$	$P2_1/c$
Z	2	4	4
a (Å)	9.4793(8)	13.6001(9)	8.3809(3)
b (Å)	9.8725(9)	15.4857(10)	18.6842(6)
c (Å)	13.4421(11)	21.2461(16)	15.0663(5)
α (°)	79.620(2)	90	90
β (°)	78.062(2)	91.861(2)	99.245(2)
γ (°)	87.549(2)	90	90
Volume (Å^3)	1210.6(18)	4472.2(5)	2328.59(14)
ρ_{calcd} (g·cm^{-3})	1.164	1.198	1.273
GooF on F^2	1.054	1.033	1.022
R_{int}	0.0252	0.0345	0.0367
R_1 [$I > 2\sigma(I)$]	0.0403	0.0615	0.0422
wR_2 (all data)	0.0999	0.1723	0.1103
Largest peak/hole (e·Å^{-3})	0.293/-0.202	0.378/-0.266	0.386/-0.251
CCDC no.	1529581	1529579	1529575

Table S4. Crystallographic data collection parameters for compounds **15**, **15'**, **17**

	compound **15**	compound **15'**	compound **17**
Chemical Formula	$C_{22}H_{40}B_2N_4O_4$	$C_{44}H_{80}B_4N_8O_8\bullet3(C_7H_8)$	$C_{24}H_{44}B_2N_4O_6\bullet2(C_6H_6)$
Formula mass (g·mol^{-1})	446.20	1168.80	662.46
Crystal shape	block	block	plate
Temp. (K)	100(2)	100(2)	100(2)
μ (mm^{-1}), Radiation	0.080, MoK$_\alpha$	0.075, MoK$_\alpha$	0.079, MoK$_\alpha$
Crystal system	monoclinic	triclinic	triclinic
Space group (no.)	$P2_1/c$	$P\bar{1}$	$P\bar{1}$
Z	4	2	2
a (Å)	9.9858(3)	14.7679(15)	7.5233(13)
b (Å)	15.1342(19)	14.7780(15)	12.070(2)
c (Å)	16.5840(2)	17.5940(18)	21.443(4)
α (°)	90	81.875(3)	94.556(5)
β (°)	91.132(4)	81.666(3)	92.752(5)
γ (°)	90	62.615(2)	106.214(5)
Volume (Å^3)	2505.8(6)	3359.5(6)	1858.7(5)
ρ_{calcd} (g·cm^{-3})	1.183	1.155	1.184
GooF on F^2	1.018	1.021	1.097
R_{int}	0.0849	0.0358	0.0517
R_1 [$I > 2\sigma(I)$]	0.0757	0.0380	0.0696
wR_2 (all data)	0.1541	0.0887	0.1513
Largest peak/hole (e·Å^{-3})	0.241/-0.247	0.299/-0.205	0.266/-0.337
CCDC no.	1529582	1529574	1529577

3 References

S1 (a) C. Kleeberg, A. G. Crawford, A. S. Batsanov, P. Hodgkinson, D. C. Apperley, M. S. Cheung, Z. Lin and T. B. Marder, *J. Org. Chem.* 2012, **77**, 785. (b) H. Nöth, *Z. Naturforsch., Teil B*, 1984, **39**, 1463. (c) H. Asakawa, K.-H. Lee, Z. Lin and M. Yamashita, *Nat. Commun.* 2014, **5**, 4245.

S2 W. Clegg, M. R. J. Elsegood, F. J. Lawlor, N. C. Norman, N. L. Pickett, E. G. Robins, A. J. Scott, P. Nguyen, N. J. Taylor and T. B. Marder, *Inorg. Chem.* 1998, **37**, 5289.

S3 For a helpful introduction to *in situ* crystallisation see: (a) D. S. Yufit and J. A. K. Howard, *CrystEngComm* 2010, **12**, 737. (b) D. S. Yufit and J. A. K. Howard, *CrystEngComm* 2012, **14**, 2003.